FLUORIDE REMOVAL FROM BRINE WITH ION EXCHANGE RESIN

by

EUNSEO SHIN

B.A.Sc., The University of British Columbia, 2018

A THESIS SUBMITTED IN PARTIAL FULFILLMENT OF

THE REQUIREMENTS FOR THE DEGREE OF

MASTER OF APPLIED SCIENCE

in

THE FACULTY OF GRADUATE AND POSTDOCTORAL STUDIES

(Materials Engineering)

THE UNIVERSITY OF BRITISH COLUMBIA

(Vancouver)

August 2020

The following individuals certify that they have read, and recommend to the Faculty of Graduate and Postdoctoral Studies for acceptance, the thesis entitled:

Fluoride removal from brine with ion exchange resin

submitted by Eunseo Shin in partial fulfillment of the requirements for

the degree of Master of Applied Science

in Materials Engineering

Examining Committee:

David Dreisinger, Materials Engineering
Supervisor

Wenying Liu, Materials Engineering
Supervisory Committee Member

Berend Wassink, Materials Engineering
Supervisory Committee Member

Additional Supervisory Committee Members:

Tom Troczynski (Chair), Materials Engineering
Supervisory Committee Member

Abstract

The presence of fluoride has caused a number of complications in various industrial applications. In the sodium sulfate salt splitting technology developed by NORAM Engineering and Constructors, the undesirable fluoride ions in brine solution could cause the breakdown of the protective passivation layer on the titanium anode, resulting in pit corrosion or spalling of the coating on the dimensionally stable anode (DSA). Conventionally, adsorbents such as activated alumina (AA), coagulation including calcium fluoride precipitation method, ion-exchange (IX), solvent extraction (SX), and reverse osmosis (RO) have been used to remove fluoride from solution. Of all the options, CaF_2 precipitation method is the most commonly used to remove fluoride from solution. However, along with its slow nucleation, CaF_2 has a theoretical solubility limit of 8 ppm F^- at stoichiometric concentration of calcium in wastewater [1]. Therefore, a different approach for a robust fluoride removal system is required. In this work, aluminum or zirconium was pre-loaded onto LANXESS Lewatit Monoplus TP 260 amino phosphonic acid functional group cation chelating resin. These resins were then used to selectively load fluoride from Na_2SO_4 brine solution. Preliminary batch isotherm studies revealed that aluminum can be readily loaded onto this resin type; however, the zirconium loading capacity was poor due to the solubility limit of zirconium where low pH inhibits an effective loading process. Subsequently, fluoride batch isotherm studies revealed that the maximum fluoride loading capacity of Al pre-loaded and Zr pre-loaded resin were 1.30 mol/kg Al-resin and 0.70 mol/kg Zr-resin from 12 wt.% Na_2SO_4 brine, respectively. However, in the column loading trials, an increase in fluoride loading capacity was recorded with Zr pre-loaded resin as the cycles of loading and regeneration continued.

Most notably, Zr pre-loaded resin provided minimal metal leakage (Zr) during the sorption process while reducing the fluoride concentration below 0.5 mg/L throughout all the loading cycles.

Lay Summary

In the chemical and metallurgical industry, an undesirable impurity in chemical process solutions can adversely impact the quality and efficiency of the process. Fluoride is an element that is frequently found in small concentrations in chemical solutions and may have a deleterious effect. In order to remove fluoride from solution, calcium fluoride precipitation is frequently employed for industrial solutions. Ion exchange resin technology, on the other hand, has been commonly used for water filtration. Therefore, this work investigated the use of ion exchange resins preloaded with metals for the removal of fluoride from a concentrated brine solution. The purpose of the purification was to remove any negative impacts of fluoride on a chemical process of salt splitting.

Preface

This thesis is the original and independent work by the author, Martin Eunseo Shin. The foundation of this project was constructed based on consultations with the principal investigator and UBC Hydrometallurgy Chair, Prof. David Dreisinger and process engineer from NORAM Engineering and Constructors, Dr. Alexander Burns. The development and validation of analytical methods for fluoride analysis and experimental design were carried out by Martin Eunseo Shin. The batch isotherm studies reported in this work were conducted at BC Research Inc., and the column resin-loading trials were performed at UBC Department of Materials Engineering. General experimental direction and safety measures were guided by Dr. Bé Wassink. ICP-OES analysis for cation analysis in solution were conducted by Maureen Soon at UBC Department of Earth, Ocean and Atmospheric Sciences.

Table of Contents

Abstract ..... **iii**

Lay Summary ..... **v**

Preface ..... **vi**

Table of Contents ..... **vii**

List of Tables ..... **xi**

List of Figures ..... **xiii**

Nomenclature ..... **xvii**

Acknowledgements ..... **xviii**

Chapter 1: Introduction **1**

Chapter 2: Literature Review **3**

2.1 Brine Treatment 3

2.1.1 Applications 3

2.1.2 Salt splitting Technology 4

2.1.3 Effect of Impurities 6

2.2 Fluoride Background 7

2.2.1 Source 7

2.2.2 Characteristics 9

2.2.3 Eh-pH diagrams 10

2.3 Fluoride Removal Technologies 16

2.3.1 Overview 16

2.3.2 Activated Alumina Adsorbents 17

2.3.3 CaF_2 precipitation and coagulation 19

2.3.4 Solvent Extraction 21
2.3.5 Membranes 22
2.4 Ion Exchange 23
2.4.1 Principle 23
2.4.2 Resin Manufacturers 25
2.4.3 Applications 26
2.4.4 Resin Type 26
2.4.4.1 Strong acid cation resin 26
2.4.4.2 Weak acid cation resin 27
2.4.4.3 Anion resin 27
2.4.4.4 Chelating resin 28
2.4.5 LEWATIT Monoplus TP 260 resin 29
2.4.6 Isotherms 30
2.4.7 Kinetics 31
2.4.8 Error Analysis 32
2.5 Summary and Objectives 34
Chapter 3: Experimental Methods 37
3.1 Preparations 37
3.1.1 Materials 37
3.1.2 Apparatus 38
3.1.3 Resin Preparation 38
3.2 Procedures for Fluoride Removal with Ion Exchange Resin 40
3.2.1 Batch Isotherm Tests 40

3.2.2 Stripping Tests 42
3.2.3 Column Tests 44
3.3 Analysis Procedures 46
3.3.1 Fluoride Ion Selective Electrode (F-ISE) 46
3.3.2 Inductively Coupled Plasma Optical Emission Spectrometer (ICP-OES) 48
Chapter 4: Batch Fluoride Removal with Pre-loaded resins 49
4.1 Batch kinetics trial 49
4.2 Batch isotherm study on the resin in sodium form 52
4.2.1 Calcium and Magnesium 52
4.2.2 Aluminum and Zirconium 56
4.2.3 Stripping tests 59
4.3 Fluoride Batch isotherm study with Al-resin 60
4.3.1 Effect of Na_2SO_4 60
4.3.2 Effects of pH and temperature 63
4.4 Fluoride Batch isotherm study with Zr-resin 66
4.4.1 Effect of Na_2SO_4 66
4.4.2 Effect of pH and temperature 69
Chapter 5: Column Fluoride Removal with Pre-loaded Resins 72
5.1 Pre-loading Metal Regeneration Cycles 72
5.1.1 Aluminum pre-loaded resin 72
5.1.2 Zirconium pre-loaded resin 74
5.2 Acid Regeneration Cycles 76
5.2.1 Aluminum pre-loaded resin 76

5.2.2 Zirconium pre-loaded resin 77
5.3 Aluminum-Fluoride Co-loading Cycles 79
Chapter 6: Conclusion and Future Work 80
6.1 Summary 80
6.2 Conclusion 81
6.3 Future Work 83
Bibliography 86
Appendices 96
Appendix A Derivations for kinetic models 96
Appendix B Determination of fluoride example calculation 98
Appendix C Procedure for non-linear least square (NLLS) error analysis 100
Appendix D Error functions and isotherm parameters for the batch isotherms 101

List of Tables

Table 2. 1 Halogen bond energies (KJ/mol) [27] 9

Table 2. 2 Stability constant for Al-F-H_2O and Zr-F-H_2O system at 25 °C [28] 10

Table 2. 3 Fluoride removal technologies and their advantages and limitations [30, 31] 16

Table 2. 4 Solubility of alkaline earth metal fluorides in 25 ºC [39] 19

Table 2. 5 Ion exchange resin manufacturers and their brands 25

Table 2. 6 Lanxess' LEWATIT Monoplus TP 260 product information [58] 30

Table 2. 7 Non-linear least square (NLLS) error function for model fitting process [60] 33

Table 3. 1 Isotherm studies list for the baseline study 43

Table 3. 2 Fluoride isotherm studies list 43

Table 3. 3 ICP-OES Wavelengths for the elements 48

Table 4. 1 Experimental conditions and Non-linear least square (NLLS) kinetic model data for ion exchange of metals on TP 260 resin (303 K; pH 7; 80 mL of solution) 49

Table 5. 1 Cumulative formation constant for metal complexes [72] 77

Table A. 1 Non-linear least square (NLLS) analysis of Langmuir model for Ca^{2+} and Mg^{2+} equilibrium isotherm profiles in 0 , 12 and 24 wt.% Na_2SO_4 solution with Lewatit Monoplus TP 260 resin. Minimum error values are indicated with bold numbers. (303 K; Initial conc. ~150 ppm Ca^{2+} and Mg^{2+}; pH 7) 101

Table A. 2 Non-linear least square (NLLS) analysis of Langmuir model for Al^{3+} and Zr^{4+} equilibrium isotherm profiles in 0 - 24 wt.% Na_2SO_4 solution with Lewatit Monoplus TP 260 resin. Minimum error values are indicated with bold numbers. (303 K; Initial conc. ~150 ppm Al^{3+} and Zr^{4+}; pH 2.5 for Al^{3+} and pH 1.5 for Zr^{4+}) 102

Table A. 3 Non-linear least square (NLLS) analysis of D-R and Langmuir model for F^- equilibrium isotherm profiles in 6 - 24 wt.% Na_2SO_4 solution with Al^{3+} and Zr^{4+} pre-loaded Lewatit Monoplus TP 260 resin. Minimum error values are indicated with bold numbers. (303 K; Initial conc. ~25 ppm F^-; pH 7)..... 103

Table A. 4 Non-linear least square (NLLS) analysis of D-R and Langmuir model for F^- equilibrium isotherm profiles in temperature of 303 – 333 K with Al^{3+} and Zr^{4+} pre-loaded Lewatit Monoplus TP 260 resin. Minimum error values are indicated with bold numbers. (12 wt.% Na_2SO_4; Initial conc. ~25 ppm F^-; pH 7)..... 104

List of Figures

Figure 2. 1 A three compartments electrochemical cell with Na_2SO_4 electrolytes [15] 5

Figure 2. 2 Eh-pH diagram for F – H_2O system at 25.0 C, 1 atm, a) [F] = $1.3*10^{-3}$ M (25 mg/L), b) [F] = $1.3*10^{-3}$ M and [Na] = 1.69 M by HSC 6.0 software 11

Figure 2. 3 Eh-pH diagram for Al – H_2O system at 25.0 C, 1 atm, [Al] = 1 M by HSC 6.0 software 12

Figure 2. 4 Eh-pH diagram for Al – F – H_2O system at 25.0 C, 1 atm, [Al] = 1 M a) [F] = $1.3*10^{-3}$ M (25 mg/L), b) [F] = 1 M by HSC 6.0 software 13

Figure 2. 5 Eh-pH diagram for a) Zr – H_2O system at 25.0 C, 1 atm, [Zr] = 1 M by HSC 6.0 software 14

Figure 2. 6 Eh-pH diagram for Zr – F – H_2O system at 25.0 C, 1 atm, [Zr] = 1 M a) [F] = $1.3*10^{-3}$ M (25 mg/L), b) [F] = 1 M by HSC 6.0 software 15

Figure 2. 7 Conventional wastewater treatment flow for fluoride removal [41] 20

Figure 2. 8 Generic structural models of Al loaded chelating resin with iminodiacetate functional group [56] 29

Figure 2. 9 Process flow for fluoride removal from zinc sulfate electrolyte 34

Figure 3. 1 Column ion exchange apparatus 44

Figure 4. 1 Removal of a) Ca^{2+} or b) Mg^{2+} with respect to contact time (303 K; pH 7). Round markers and lines indicate the experimental values and Non-linear least square (NLLS) fitted pseudo second-order model, respectively. 51

Figure 4. 2 Removal of fluoride with respect to contact time (303 K; pH 7) 52

Figure 4. 3 Equilibrium isotherms of a) Ca^{2+} b) Mg^{2+} with Monoplus TP 260 AMPA chelating resin in 0, 12, and 24 wt.% Na_2SO_4 solution (303 K; Initial conc. ~150 ppm Ca^{2+} or Mg^{2+}; pH 7); • Experimental data, — Langmuir isotherm best fit 54

Figure 4. 4 Ca^{2+} and Mg^{2+} loading capacity with respect to Na^{+} addition in solution 56

Figure 4. 5 Equilibrium isotherms of a) Al^{3+} b) Zr^{4+} with Monoplus TP 260 AMPA chelating resin in 0 - 24 wt.% Na_2SO_4 solution (303 K; Initial conc. ~150 ppm Al^{3+} or Zr^{4+}; pH 2.5 for Al^{3+} and pH 1.5 for Zr^{4+}); • Experimental data, — Langmuir isotherm best fit 58

Figure 4. 6 Stripping analysis of Ca, Mg, Al, and Zr with 1.8 M HCl..... 59

Figure 4. 7 a) Equilibrium isotherms of F^- on Al^{3+} pre-loaded Monoplus TP 260 resin in 0 - 24 wt.% Na_2SO_4 solution (303 K; Initial conc. ~25 ppm F^-; pH 7), b) Aluminum leakage (%) during the sorption process from the Al^{3+} loaded resins; • Experimental data, — Dubinin-Radushkevich isotherm best fit 62

Figure 4. 8 a) Loading curves of F^- on Al^{3+} pre-loaded Monoplus TP 260 resin in solution pH of 3 - 11 (303 K; Initial conc. ~25 ppm F^-; 12 wt.% Na_2SO_4), b) Aluminum leakage (%) during the sorption process from the Al^{3+} loaded resins; • Experimental data 64

Figure 4. 9 a) Equilibrium isotherms of F^- on Al^{3+} pre-loaded Monoplus TP 260 resin in solution Temperature of 303 and 318 K (Initial conc. ~25 ppm F^-; 12 wt.% Na_2SO_4; pH 7), b) Aluminum leakage (%) during the sorption process from the Al^{3+} loaded resins; • Experimental data, — Dubinin-Radushkevich isotherm best fit 65

Figure 4. 10 a) Equilibrium isotherms of F^- on Zr^{4+} pre-loaded Monoplus TP 260 resin in 0 - 24 wt.% Na_2SO_4 solution (303 K; Initial conc. ~25 ppm F^-; pH 7), b) Zirconium leakage (%)

during the sorption process from the Zr^{4+} loaded resins; • Experimental data, — Langmuir isotherm best fit..... 68

Figure 4. 11 a) Loading curves of F^- on Zr^{4+} pre-loaded Monoplus TP 260 resin in solution pH of 3 - 11 (303 K; Initial conc. ~25 ppm F^-; 12 wt.% Na_2SO_4), b) b) Zirconium leakage (%) during the sorption process from the Zr^{4+} loaded resins; • Experimental data, — Langmuir isotherm best fit..... 70

Figure 4. 12 a) Equilibrium isotherms of F^- on Zr^{4+} pre-loaded Monoplus TP 260 resin in solution Temperature of 303, 318, and 333 K (Initial conc. ~25 ppm F^-; 12 wt.% Na_2SO_4; pH 7), b) Zirconium leakage (%) during the sorption process from the Zr^{4+} loaded resins; • Experimental data, — Langmuir isotherm best fit..... 71

Figure 5. 1 a) Column breakthrough curves of F^- on Al^{3+} pre-loaded Monoplus TP 260 with $Al_2(SO_4)_3$ regeneration cycles (Initial conc. ~25 ppm F^-; 12 wt.% Na_2SO_4; 303 K; pH 7; 5 BV/hr), b) Aluminum leakage during the sorption process..... 73

Figure 5. 2 a) Column breakthrough curves of F^- on Zr^{4+} pre-loaded Monoplus TP 260 with $Zr(SO_4)_2$ regeneration cycles (Initial conc. ~25 ppm F^-; 12 wt.% Na_2SO_4; 303 K; pH 7; 5 BV/hr), b) Zirconium leakage during the sorption process..... 75

Figure 5. 3 a) Column breakthrough curves of F^- on Al^{3+} pre-loaded Monoplus TP 260 with 0.1 M H_2SO_4 regeneration cycles (Initial conc. ~25 ppm F^-; 12 wt.% Na_2SO_4; 303 K; pH 7; 5 BV/hr)..... 76

Figure 5. 4 Column breakthrough curves of F^- on Zr^{4+} pre-loaded Monoplus TP 260 with a) 1.0 M H_2SO_4 b) 1.0 M NaOH regeneration cycles (Initial conc. ~25 ppm F^-; 12 wt.% Na_2SO_4; 303 K; pH 7; 5 BV/hr)..... 78

Figure 5. 5 Column loading of Al^{3+} and F^{-} on Na^{+} form Monoplus TP 260 (12 wt.% Na_2SO_4; 303 K; pH 5; 5 BV/hr) 79

Nomenclature

AA	Activated Alumina
C_0	Initial concentration
Ce	Equilibrium concentration
C_F	Final concentration
DI	Deionized
DSA	Dimensionally stable anode
E	Electrode reduction potential
ED	Electrodialysis
E°	Standard electrode reduction potential
HSC 6.0	HSC Chemistry 6.0
ICP-OES	Inductively coupled plasma – optical emission spectrometry
IX	Ion exchange
mV	millivolt
ppm	Parts per million
RO	Reverse Osmosis
Rpm	Revolutions per minute
SX	Solvent Extraction
TDS	Total Dissolved Solids

Acknowledgements

To the greatest extent, I would first like to thank my advisor, Dr. David Dreisinger for providing me the opportunity to undertake this exciting project and for giving me guidance and support throughout the Master's program at UBC. It was a privilege to work alongside him as he always patiently listens and provides the best course of action for my interest in any situation.

This project would never have been completed without Dr. Alexander Burns from NORAM Engineering and Constructors, whom I also want to express my sincere gratitude for patiently guiding the research project throughout the term. His expertise and assistance were freely offered throughout my program and helped me advance in technical knowledge, become more familiar with industry and meet a lot of research and development personnel in industry.

I would also like to sincerely thank Dr. Bé Wassink for his kind assistance in my lab work and unconditional willingness to help and consult whenever problem arose during the course of the Master's program. This also extends to all my precious peers in the Hydrometallurgy group, Jianming, Chihwei, Chulho, Fei, Jackie, Maryam, Mary, Hiroki, and Brighty for their friendship and help. I also thank Maureen Soon for her support in conducting ICP-OES analysis.

I also had a great opportunity to work at BC Research Inc., so I first want to thank James Lockhart for providing the resources and technical expertise. I also really appreciate the splendid support from Tsuki, Onyinye, Ruben, Brian, Gabe, Jun, Ziliang, and Maggie.

Lastly, I appreciate my family, friends in Canada, and Hannah for their unconditional support and love.

Chapter 1: Introduction

Salt splitting electrodialysis has gained growing interest in the past few decades for its desirability in minimizing chemical consumption, effluent treatment costs, and facilitating acid and caustic recovery [2]. Of particular interest is the treatment of sodium sulfate brine solutions with salt splitting electrodialysis technology for various industrial applications. Sodium sulfate (Na_2SO_4), recovered from black liquor, a byproduct of pulp mills, can be treated to regenerate acid and caustic soda [3]. Industrial Na_2SO_4 waste solution generated from organic synthetic processes can be treated with this technology to meet environmental standards for discharge of salts [4]. A number of studies have also been conducted in relation to the application of electrodialysis in the mining and chemical industry to mitigate such problems noted above [5, 6]. Likewise, NORAM Engineering and Constructors has proprietary electrochemical technology for salt splitting, where the undesirable presence of fluoride in electrolytic cells could cause the breakdown of the protective passivation layer on the titanium anode, resulting in pitting corrosion or spalling of the coating [7]. As replacing these anodes can incur significant costs, pre-treatment of brine solutions to reduce fluoride concentration is imperative. Therefore, removal of such undesirable ions from brines prior to injecting into an electrolytic cell is critical in maintaining the cell performance.

A large number of research works on removal of fluoride have been conducted. Many studies relate to the water treatment industry with technologies, such as activated alumina, coagulation, solvent extraction, reverse osmosis, and ion exchange resin. Many of these technologies have clear drawbacks in efficiency and scaling up of the process. Ion exchange resin removal of fluoride is expected to be an attractive option for the pre-treatment of the brine solutions. In this

work, metal-loaded amino methyl phosphonic acid (AMPA) chelating weak acid cation exchange resin was investigated to remove fluoride from brine solutions.

Chapter 2: Literature Review

2.1 Brine Treatment

2.1.1 Applications

With growing demand for technologies that brings an environmentally and economically sustainable means of producing chemicals, salt splitting electrodialysis (ED) has received significant attention within various industries. This technology offers minimization of the environmental impact by the recovery of chemical waste and avoiding disposal. This has resulted in a number of applications around the world. The electrodialysis of sodium chloride solution, commonly known as the chlor-alkali process, is widely used to produce chlorine and sodium hydroxide. In recent years, the use of electrodialysis has also been investigated with a number of different industrial solution feedstocks. Electrodialysis technology was tested with acid mine drainage (AMD), one of the major impacts caused by coal mining activities, for water recovery. Buzzi et al. [8] particularly evaluated electrodialysis for the treatment of AMD in Brazil and confirmed that it could remove 97% of the contaminants in AMD and recover water. Likewise, ED technology was investigated with gold mine effluent, containing various kinds of cyanide species, where Zheng et al. [9] used a five compartment ED apparatus with homogenous ion exchange membranes to achieve a cyanide removal rate of 98% from gold mine effluent. More recently, the booming market for lithium ion batteries has triggered the mineral processing industry to consider the use of electrodialysis to concentrate lithium brine solution, instead of using the conventional lithium precipitation method [10, 11, 12].

Treatment of sodium sulfate brine solution by electrodialysis can also be applied. Pisarska et al. [13] studied the treatment of industrial waste sodium sulfate solution from cyclohexanone manufacture by applying the electrodialysis method. This author emphasized that this process

can not only significantly reduce the discharged salts to the environment, but also produced solutions of NaOH and H_2SO_4 that are free of impurities. They confirmed that the sodium sulfate salt splitting method can be effectively utilized within the originating cyclohexanone processing plant. In the pharmaceutical industry, the ED process was studied for the removal of sodium sulfate from magnesium stearate (MgSt) aqueous slurry, a widely used lubricant for tablet formations, in which a byproduct sodium sulfate is created during magnesium stearate production as illustrated in Equation (2.1) and (2.2) [14].

$$C_{17}H_{33}COOH + NaOH \rightarrow Na(C_{17}H_{35}COO) + H_2O \quad (2.1)$$

$$2Na(C_{17}H_{35}COO) + H_2O + MgSO_4 \rightarrow Mg(C_{17}H_{35}COO)_2 + Na_2SO_4 + H_2O \quad (2.2)$$

The author demonstrated that the ED process efficiently converted sodium sulfate into NaOH and H_2SO_4 from the MgSt slurry and confirmed it as a promising process for MgSt slurry purification. Electrodialysis has therefore been applied in various industries with its unique benefits over other available technologies. NORAM Engineering and Constructors Ltd. also provides an electrodialysis technology that treats Na2SO4 brine solution having high concentration in the range of 12 – 24 wt.% In this thesis, purification of high concentrations of Na_2SO_4 in brine solution that would enter into the ED cells is the target of investigation.

2.1.2 Salt splitting Technology

The term “salt splitting” represents the decomposition of chemical compounds by electrodialysis using direct electric current. Electrodialysis is performed through applying a current into a cell comprising of an anode and a cathode. The positive electrode, anode, attracts anions and is the site of the oxidation process; whereas, the cathode is the negative electrode that attracts cations and is the site of the reduction process. In between these electrodes, various ion exchange membranes are placed to allow either cations or anions to pass. The cell is fed

with salt solution, in which Na_2SO_4 electrolytes is of particular interest in this work. For this application, sodium ions pass through a cation exchange membrane and sulfate ions pass through an anion exchange membrane. A general three compartment salt splitting cell can be seen in **Fig. 2.1**.

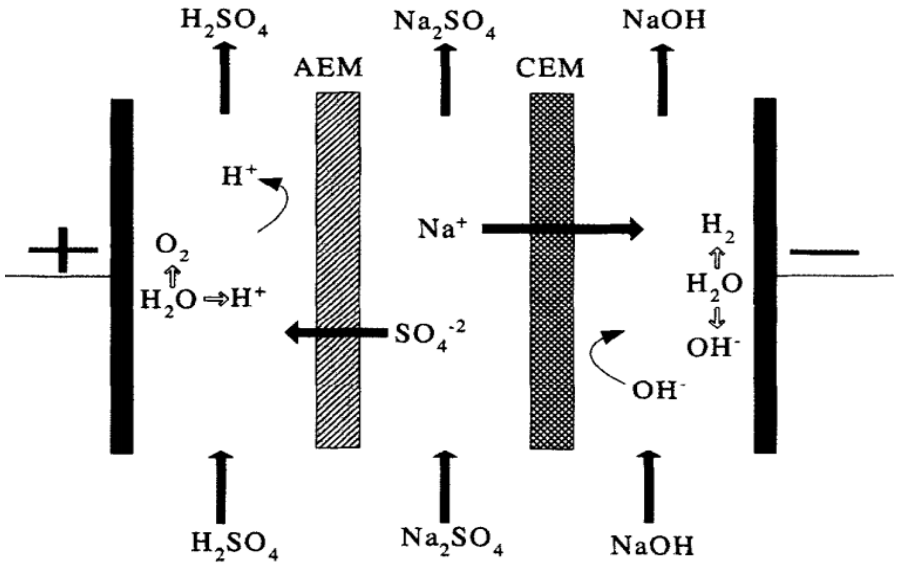

Figure 2. 1 A three compartments electrochemical cell with Na_2SO_4 electrolytes [15]

Divided into three compartments, the reactions taking place in each compartment provide for the recovery of sodium hydroxide and sulfuric acid. The following reactions proceed in the Na_2SO_4 electrodialysis cell:

In anodic compartment: $$2H_2O \rightarrow 4H^+ + O_2 + 4e^- \quad (2.3)$$

In cathodic compartment: $$4H_2O + 4e^- \rightarrow 4OH^- + 2H_2 \quad (2.4)$$

Overall cell reaction: $$2Na_2SO_4 + 6H_2O \rightarrow 4NaOH + 2H_2SO_4 + 2H_2 + O_2 \quad (2.5)$$

Therefore, in the anodic compartment, water is oxidized to form hydrogen ions and oxygen and in the cathodic compartment, water is reduced to form hydroxide ions and hydrogen. As sodium sulfate brine solution is introduced into the middle compartment, the overall cell reaction occurs and generates sodium hydroxide and sulfuric acid. The concentration of Na_2SO_4

in the middle compartment is reduced in the effluent after the treatment. This can be further expanded by stacking of these membranes to minimize the capital cost.

2.1.3 Effect of Impurities

In the operation of electrodialysis, other reactions can also take place in the cell due to the presence of impurities in the introduced brine solution. These impurities could block the transfer sites on the membranes, decreasing the overall flux of ions and reducing the cell efficiency. Therefore, the effect of impurities on the cell has been well studied by many researchers. Chen et al. [11] investigated the effects of co-existing cations (K^+, Na^+, Ca^{2+}, and Mg^{2+}) on the treatment of lithium brine by the electrodialysis process. This study concluded that the competitive migration between lithium ions and other co-existing ions results in lower recovery of lithium with the influence in the order of $K^+ > Na^+ > Ca^{2+} > Mg^{2+}$. The impact is further exacerbated with higher concentration of these interfering ions. In a similar fashion, Severin and Hayes [16] investigated the effect of divalent cations (Ca^{2+}, Mg^{2+}, and Ba^{2+}) and iron on the ED processing of flowback water from shale gas hydraulic fracturing. Apparent blockage of the cation transfer sites by the divalent cations caused the hindrance of total ion flux. Iron was also observed to precipitate and block the membrane.

Most notably, as undesirable ions pass through the membrane interface, it can cause contamination of products, corrosion of the anode and cathode, ultimately reducing the current efficiency and permanently damaging the cathode or anode. In particular, the presence of fluoride in electrochemical cell solutions can cause significant damage as it readily reacts with the cathode or anode metal alloy. Buarzaiga [17] studied different kinds of failure mechanisms of aluminum cathodes in zinc electrowinning, where the presence of halides in the electrolytes cause corrosion on the commercial grade Al-Ti cathode. In particular, fluoride ions even at low

concentration of 15 mg/L, can cause the pitting corrosion on these cathodes, which reduces the lifetime of the cathode and the zinc production rate due to difficulty of separating the deposited zinc from the corroded cathode plates. The formation of aluminum and fluoride complexes as fluoride attacks the alumina layer on the cathode sheet is shown by the following reaction.

$$Al_2O_3 + (2n)\ HF + (6 - 2n)\ H^+ \rightarrow 2AlF_{n(3-n)^+} + 3H_2O \quad (2.6)$$

A direct reaction between fluoride and aluminum cathode sheet is expressed in Equation (2.7).

$$Al + nHF + (3 - n)\ H^+ \rightarrow AlF_{n(3-n)^+} + 1.5\text{-}H_2 \quad (2.7)$$

Likewise, fluoride can react with the cathode or anode sheet with various types of metal alloys. Titanium-based oxide passivation films can be dissolved by HF and form soluble titanium-fluoride complexes [18]. Many researchers found that the corrosion rate for titanium especially accelerates when the concentration of fluoride exceeds a certain value, as little as the fluoride concentration of 11 mg/L [19, 20]. Therefore, the presence of fluoride in industrial processing solutions can be significantly detrimental due to the interactions between the fluoride ion and the plant materials. In any operation of an electrochemical cell, the control of impurities, specifically with the focus on fluoride in this work, is imperative to maintain the quality of the electrodialysis cells.

2.2 Fluoride Background

2.2.1 Source

The presence of fluoride at elevated concentration in both groundwater and industrial solutions imposes significant threats to human health and subsequent industrial processes. Fluoride can easily absorb through the skin and bloodstream causing fluorosis and many other systemic diseases. Accordingly, after 3 minutes of exposure to 5% HF, epidermal alternation

can be detected, and the dermal damage can be severely escalated at shorter exposure time with higher HF concentration [21]. Fluoride can be released to the environment or industrial plants in a number of various ways. Of all the possible factors, geological and anthropogenic sources have the greatest contribution to the undesirable increase in the fluoride concentration in solution.

The occurrence of fluoride in groundwater is primarily attributed to the weathering and dissolution of various fluoride containing minerals in the hard rocks, such as fluorspar (CaF_2), fluorapatite ($Ca_{10}(PO_4)_6F_2$), and cryolite (Na_3AlF_6). Out of 416 fluoride bearing minerals, other minerals that have high percentage of fluoride as a constituent are sellaite (MgF_2), villianmite (NaF), and topaz ($Al_2SiO_4(F, OH)_2$) [22]. The discovery and attention to fluoride began in the early 20_{th} century, when dental researchers studied the high prevalence of "Colorado Brown Stain" on the teeth of residents of Colorado Springs, USA, in which it is now called dental fluorosis [23]. Evidently, fluoride was largely present in groundwater of various areas in geographical belt that locates in East Africa and Mediterranean region; but the most indicative evidence of the presence of fluoride in the groundwater is through the incidence of fluorosis, predominantly reported in two heavily populated countries, India and China [24].

Unlike the natural occurrence of fluoride in groundwater, anthropogenic factors, such as manufacturing and mining activities can also concentrate and release fluoride to the environment. For instance, the use of hydrofluoric acid (HF) as an etchant for glass and in the semiconductor industry, fluorspar as a fluxing agent in open-hearth steelmaking process, and fluoropolymer production such as Teflon result in the requirement of fluoride removal system before releasing waste solutions to the environment.

2.2.2 Characteristics

Fluorine is in the halogen group with an atomic number of 9 and molecular weight of 18.998 g/mol. Hydrofluoric acid (HF) has a relatively high pKa of 3.2. As a solute and being a weak acid, fluoride ions presented in solution are converted into the form of HF under the acidic condition, specifically at pH 3.2 [25]. It is one of the most reactive and by far the most electronegative of all the elements. Occurring as both organic and inorganic compound, fluoride is the 13th most abundant element in the earth's crust [26]. Fluoride forms a variety of compounds with its oxidation state of -1. This great reactivity of fluoride can be related to its small dissociation energy of HF and forming of bonds with great strength, as indicated in **Table 2.1**.

Table 2. 1 Halogen bond energies (KJ/mol) [27]

X	XX	HX	BX_3	AlX_3	CX_4
F	*159*	*574*	*645*	*582*	*456*
Cl	243	428	444	427	327
Br	193	363	368	360	272
I	151	294	272	285	239

The tendency for fluoride to form strong fluoride complexes serves as a basis for the fluoride removal process in this study. As seen in **Table 2.2**, it is apparent that aluminum and zirconium can both readily form strong complexes with fluoride.

Table 2. 2 Stability constant for Al-F-H_2O and Zr-F-H_2O system at 25 °C [28]

Reactions	logK (I = 0)
$H^+ + F^- = HF$	3.17
$Al^{3+} + F^- = AlF^{2+}$	7
$Al^{3+} + 2F^- = AlF^{2+}$	12.6
$Al^{3+} + 3F^- = AlF_{3(aq)}$	16.7
$Al^{3+} + 4F^- = AlF_4^-$	19.1
$Al^{3+} + 5F^- = AlF_5^{2-}$	19.4*
$Al^{3+} + 6F^- = AlF_6^{3-}$	19.8*
$Zr^{4+} + F^- = ZrF^{3+}$	9.8
$Zr^{4+} + 2F^- = ZrF_2^{2+}$	17.2
$Zr^{4+} + 3F^- = ZrF^{3+}$	23.7
$Zr^{4+} + 4F^- = ZrF_{4(aq)}$	29.5
$Zr^{4+} + 5F^- = ZrF_5^-$	23.5
$Zr^{4+} + 6F^- = ZrF_6^{2-}$	28.3

*I, Ionic strength = 0.5

2.2.3 Eh-pH diagrams

In order to understand the aqueous chemistry of the fluoride ion, HSC 6.0 software was utilized to produce Eh-pH diagrams. **Fig. 2.2 (a)** illustrates the Eh-pH diagrams of the F-H_2O system with the conditions of 25 mg/L (1.3×10^{-3} M) of fluoride. Most of the experiments in this thesis were conducted with the initial fluoride concentration of 25 mg/L, which is low enough to test out the effectiveness of the removal process for the residual fluoride in solution. In terms of the Eh-pH diagram with the addition of 1.69 M Na^+, this represents the Na_2SO_4 brine concentration of 12 wt.%, which is a typical concentration of Na_2SO_4 brine solutions. Based on the HF/F^- boundary presented in Fig. 2.2 (a), F^- is the predominant species at pH above 3.17, while at acidic condition under pH 3.17, HF is the main species in solution. With the addition of 1 M Na^+ on F-H_2O Eh – pH diagram, Na^+ species dominates with no sign of F^- species if only 25 mg/L F^- is presented. Therefore, **Fig. 2.2 (b)** shows the effect of sodium ions in the presence of 1.3×10^{-3} M fluoride, where NaF predominantly forms throughout the extensive range of pH.

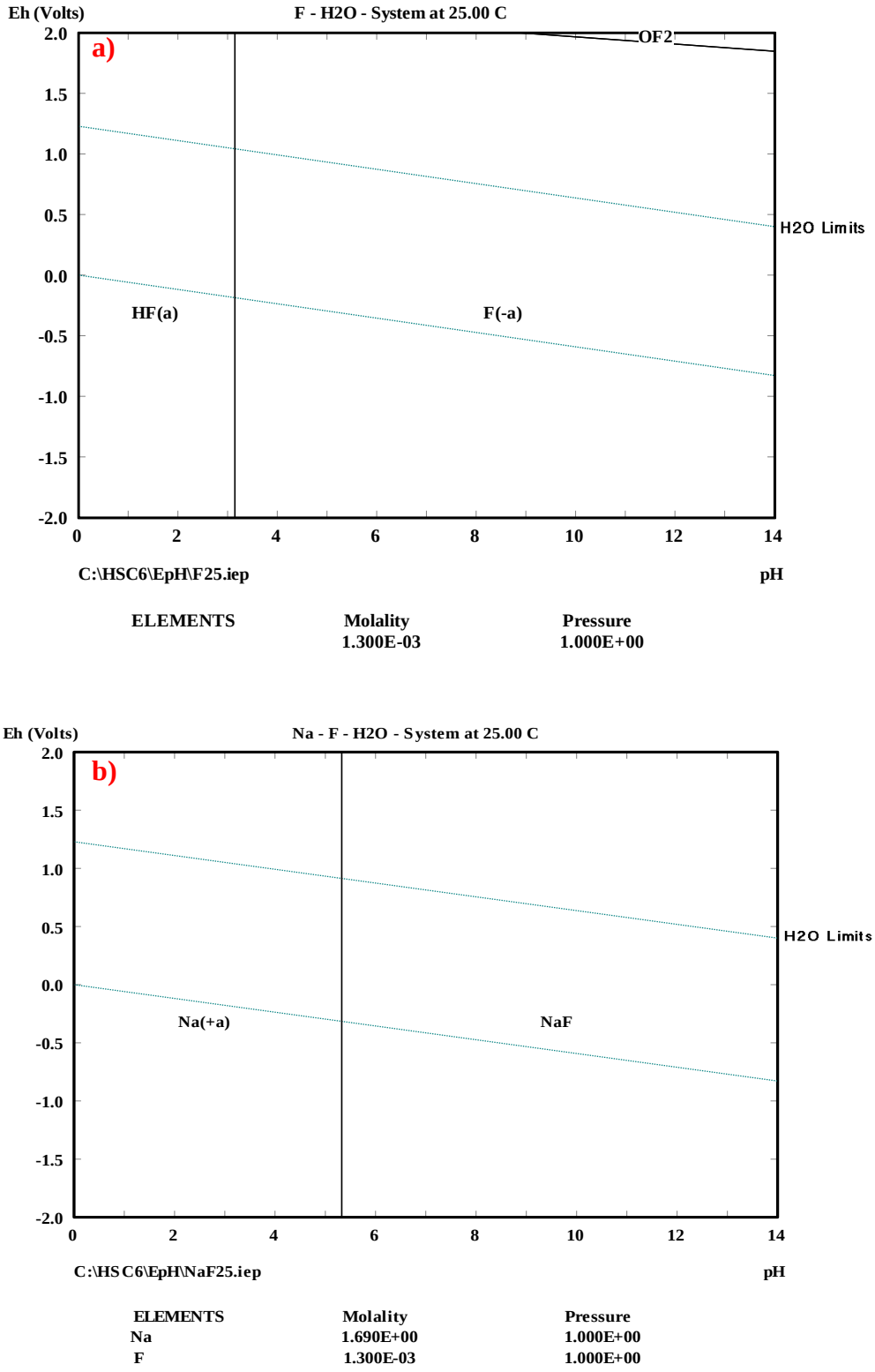

Figure 2. 2 Eh-pH diagram for F – H_2O system at 25.0 C, 1 atm, a) [F] = 1.3*10^{-3} M (25 mg/L), b) [F] = 1.3*10^{-3} M and [Na] = 1.69 M by HSC 6.0 software

In this thesis, a basis for a fluoride removal system is loading of fluoride onto an aluminum-loaded ion exchange resin, therefore, the Eh-pH diagram in terms of aluminum needs to be studied. **Fig. 2.3** is the Eh-pH diagram for aluminum in water. Aluminum shows an amphoteric behavior where it is in the form of Al^{3+} under the acidic condition and $Al(OH)_4^-$ under the sufficiently alkaline condition. In the presence of complexing ligand, fluoride, aluminum forms various types of Al-F species, as shown in **Fig. 2.4**. As HSC 6.0 software provided does not have all the aluminum fluoride complexes, thermodynamic data was manually added based on the stability constants provided in Table 2.2. It is seen that the addition of 25 mg/L F^- produces AlF^{2+}, AlF_2^+, and AlF_3 that predominantly form at pH < 5. A further increase in the concentration of fluoride to 1 M leads to the formation of Al-F anionic species, such as AlF_4^-, AlF_5^{2-}, and AlF_6^{3-}. The presence of fluoride in aluminum solution allows the existence of soluble species at wider range of pH.

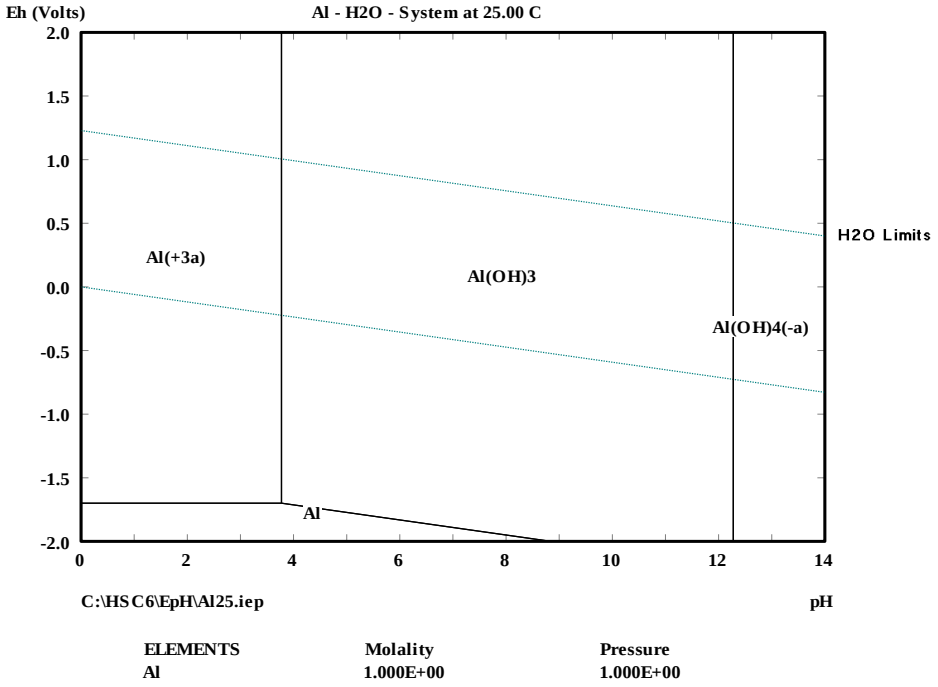

Figure 2. 3 Eh-pH diagram for Al – H_2O system at 25.0 C, 1 atm, [Al] = 1 M by HSC 6.0 software

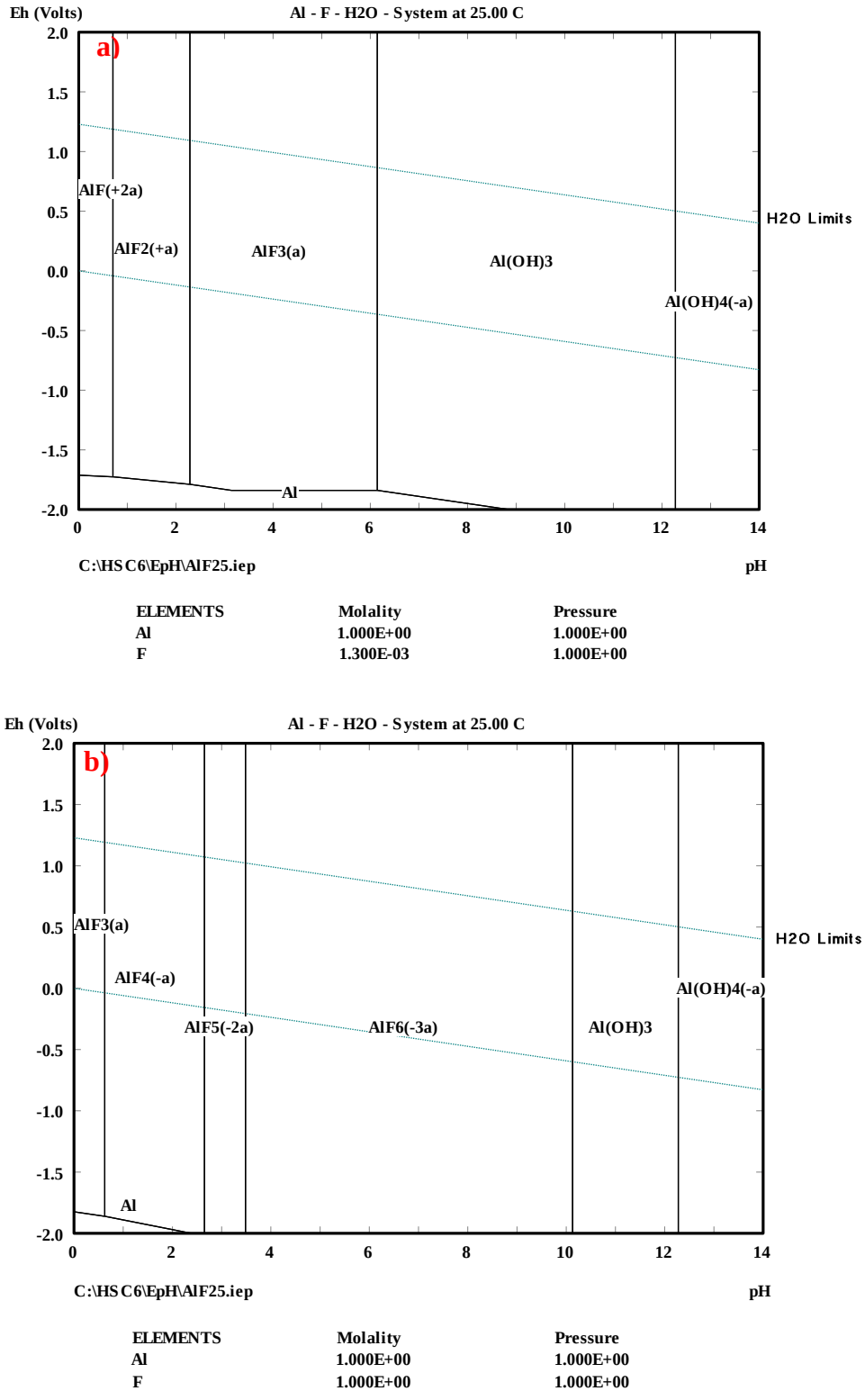

Figure 2. 4 Eh-pH diagram for Al – F – H_2O system at 25.0 C, 1 atm, [Al] = 1 M a) [F] = $1.3*10^{-3}$ M (25 mg/L), b) [F] = 1 M by HSC 6.0 software

Removal of fluoride was also investigated with zirconium-loaded ion exchange resin in this work. The Eh-pH diagram for the zirconium-water system is illustrated in **Fig. 2.5**. It is observed that the uncomplexed zirconium (Zr^{4+}) can only exist in very acidic solution under pH 1. As the pH increases, the zirconium ions start to get hydrolyzed in solution. Although the Eh-pH diagram created with the software indicates the formation of ZrO_2, it is generally zirconium hydroxide species that dominate in the steps of hydrolysis, as the complexing ability of Zr^{4+} with OH^- is much stronger than any other complexing ligand.

In the presence of fluoride in solution, zirconium fluoride complex dominates in the acidic pH region. All the Zr-F species, seen in Table 2.2 were manually added to construct Zr-F-H_2O Eh-pH diagram. As shown in **Fig. 2.6**, ZrF^{3+} dominates in acidic solution with the presence of 25 mg/L F^-. Gan et al. [29] also confirmed that the addition of F^- in Zr-H_2O system produces ZrF^{3+} as a dominant species in the acidic pH region. Further increase in fluoride concentration results in the formation of anionic Zr-F species, ZrF_6^{2-} as the dominant species.

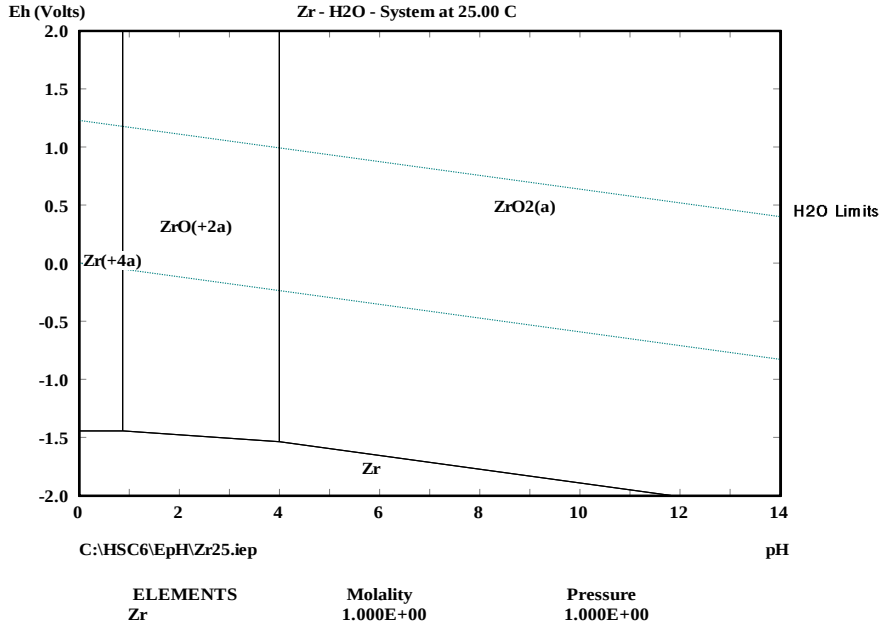

Figure 2. 5 Eh-pH diagram for a) Zr – H_2O system at 25.0 C, 1 atm, [Zr] = 1 M by HSC 6.0 software

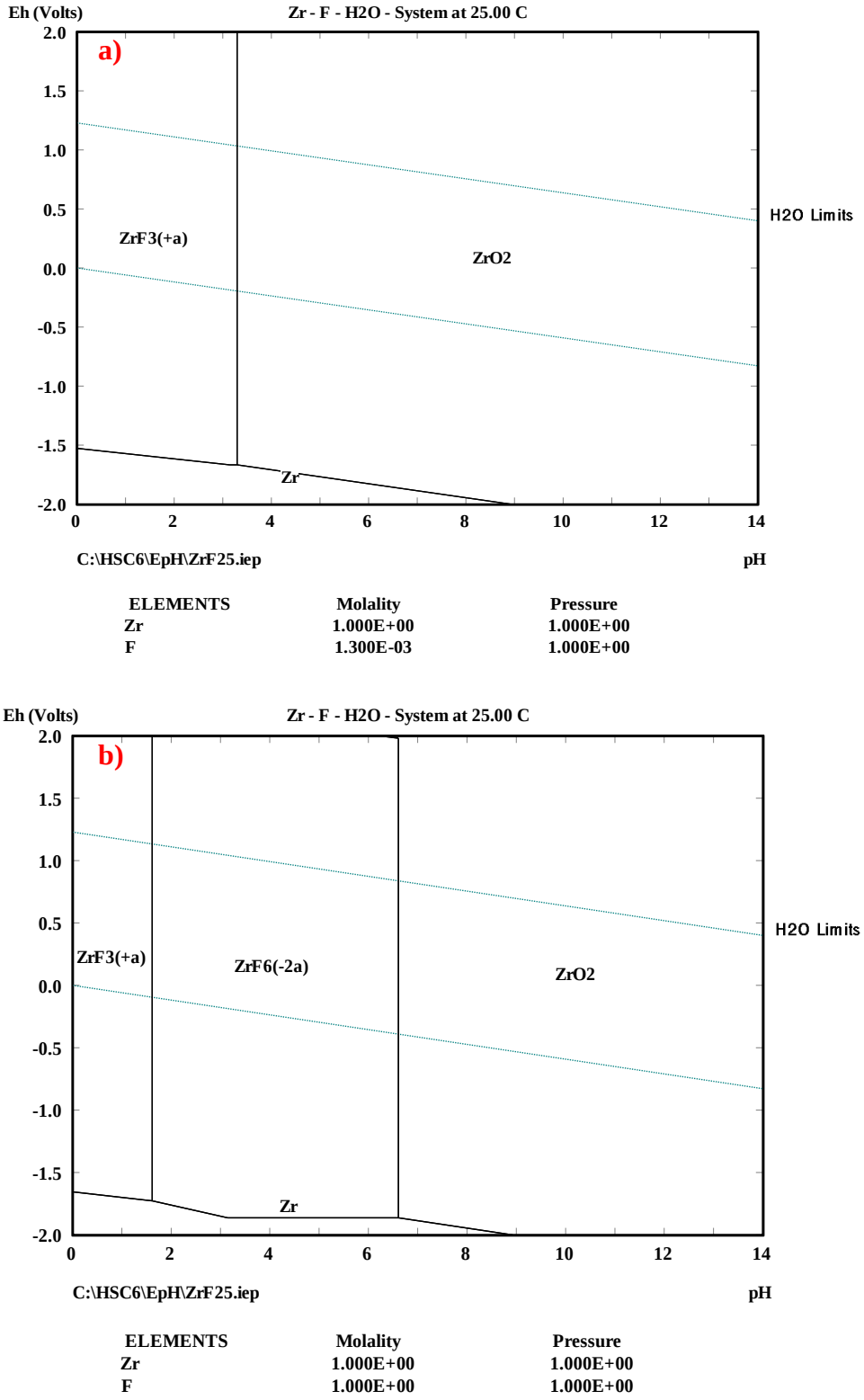

Figure 2. 6 Eh-pH diagram for Zr – F – H_2O system at 25.0 C, 1 atm, [Zr] = 1 M a) [F] = 1.3*10^{-3} M (25 mg/L), b) [F] = 1 M by HSC 6.0 software

2.3 Fluoride Removal Technologies

2.3.1 Overview

In the past few decades, a number of different fluoride removal technologies have been researched and employed. Of all the different options, adsorbents and coagulation methods have been most conventionally and effectively used in the treatment of wastewater, due to their ease of operation and profound fluoride loading capacities. This section discusses a number of prospective technologies that can be utilized for selective fluoride removal from aqueous solution.

Table 2. 3 Fluoride removal technologies and their advantages and limitations [30, 31]

Technology	Advantages	Restrictions
Adsorbents (Alumina)	• Ease of operation • Inexpensive	• Significant reduction in loading capacity after regeneration • Prone to fouling with high TDS solution
CaF_2 precipitation and Coagulation	• Ease of operation • Conventionally utilized technique • Economical choice	• Secondary contamination • Requires high chemical dosages • Residual fluoride contents in effluents
Ion Exchange	• Remove up to 90-95% fluoride • Relatively low cost	• Depending on the type of resin, interfering ions can significantly degrade the loading capacity • Potential high chemical and water use
Solvent Extraction	• Easy to perform extraction and stripping operation • Simple control and monitoring of process • Recyclability of extractant	• Difficult to attain low fluoride concentration • Possible entrainment of solvents, resulting in poor effluent quality
Membrane	• Can remove more than 90% fluoride, regardless of the initial fluoride concentration • Remove other impurities simultaneously	• Expensive process with slow output • Limited to pre-filtered solution

2.3.2 Activated Alumina Adsorbents

Adsorbents are considered a simple and economical choice over other techniques. Although conventional adsorbents, such as activated alumina, activated carbon, and rare earth oxides can be used for defluoridation, most of these adsorbents have not only relatively low loading capacity, but also the lower limit of fluoride reduction of approximately 2 mg/L [32]. These adsorbents are therefore not desirable options for applications that require process solutions with much lower fluoride concentrations. Other types of adsorbents were then sought after, where modified activated alumina has been shown to enhance the performance of adsorbents in reducing residual fluoride level and increasing fluoride loading capacity. An extensive range of research has been investigated recently on modified activated alumina to selectively adsorb fluoride from aqueous solution [33, 34, 35]

Generally, activated alumina containing aluminum oxide (Al_2O_3) provides a sorption surface for fluoride as aqueous solution passes through. The interaction of fluoride ions with aluminum hydroxide ($Al(OH)_3$) and aluminum oxide (Al_2O_3) creates Al-F complexes.

The formation of aluminum-fluoride complexation serves as a mechanism for fluoride removal by activated alumina. However, the predominant issues affecting the performance of activated alumina are pH and competing ions. Ghorai and Pant [32] illustrated the effect of pH in the range of 4 to 10, where the highest fluoride removal percentage was achieved at approximately pH 7. This phenomenon has universally been demonstrated by several other researchers [36, 35]. Among all the other factors, solution pH is the most important factor that controls the fluoride loading capacity of activated alumina. The presence of competing ions in solution has a significant influence on the ability of activated alumina to adsorb fluoride from solution. Tang et al. [37] studied the effect of bicarbonate (HCO_3^-), sulfate (SO_4^{2-}), chloride

(Cl-), and hydrogen phosphate (HPO_4^{2-}) on the fluoride sorption by activated alumina, in which all of the major anions negatively impacted the fluoride loading capacity in the following order: $HPO_4^{2-} > HCO_3^{-} > SO_4^{2-} > Cl^-$. This study also showed that the presence of co-existing ions such as those of arsenic and selenium can decrease fluoride loading capacity as both arsenic and selenium ions have some affinity for activated alumina. However, even if the fluoride sorption process is conducted with the optimum pH range and absence of competing ions, the fluoride loading capacity derived from a conventional activated alumina is not high enough. This drives researchers to investigate other element-modified activated alumina.

Modifications of alumina surface have been previously demonstrated with elements such as manganese, lanthanum, magnesium, iron, and calcium [30]. Cheng et al. [33] conducted a comparative analysis with activated alumina and lanthanum doped alumina, where the maximum fluoride loading capacities by the Langmuir model were reported to be 2.74 and 6.70 mg/g at pH 7, respectively. Likewise, Tripathy et al. [35] prepared aluminum impregnated activated alumina for the removal of fluoride from drinking water, which also exhibited an improvement in fluoride loading capacity.

Despite the plethora of research on modified activated alumina, there are still a number of limitations that prevent it from being an effective solution to fluoride removal. For instance, the affinity between fluoride adsorbing cations and activated alumina is not sufficiently strong enough to hold themselves tightly during regeneration cycles, which results in stripping of fluoride along with the impregnated elements. This then requires an additional preparation step for the next fluoride removal process.

2.3.3 CaF_2 precipitation and coagulation

Instead of adsorption by adsorbents, prompt defluoridation can be alternatively performed by the addition of coagulants. Although coagulation is based on a similar principal to that of adsorbents, the notable difference is that coagulation generally describes a chemical process that agglomerates suspended matter, directly or indirectly reacting with fluoride. The most traditional way of removing fluoride from wastewater in industrial settings is by precipitation of insoluble calcium fluoride by lime addition. As seen in **Table 2.4**, CaF_2 is the least soluble among the alkaline earth metal fluorides. Consequently, the ease of removing fluoride by converting into CaF_2 precipitates makes it the most widely used method. This fluoride removal method was reported soon after the discovery of the cause of fluorosis [38].

Table 2. 4 Solubility of alkaline earth metal fluorides in 25 ºC [39]

Compound	Solubility (g/L of water)
MgF_2	0.13
CaF_2	0.016
SrF_2	0.21
BaF_2	1.61

Initially, lime ($Ca(OH)_2$) is added to fluoride containing solution, and CaF_2 forms, as described in Equation (2.8). pH, affecting the degree of fluoride precipitation, is adjusted to the desired value of 10.5 or 12.5 [40]. CaF_2 having low solubility, can then be easily separated by the sedimentation method.

$$Ca(OH)_2 + 2HF \rightarrow CaF_2 + 2H_2O \quad (2.8)$$

Fig. 2.7 illustrates a conventional treatment flow of a fluoride removal system from wastewater by using lime as a treatment agent. After the sedimentation method, recovered sludge is processed through a dehydrator and is disposed of as an industrial waste.

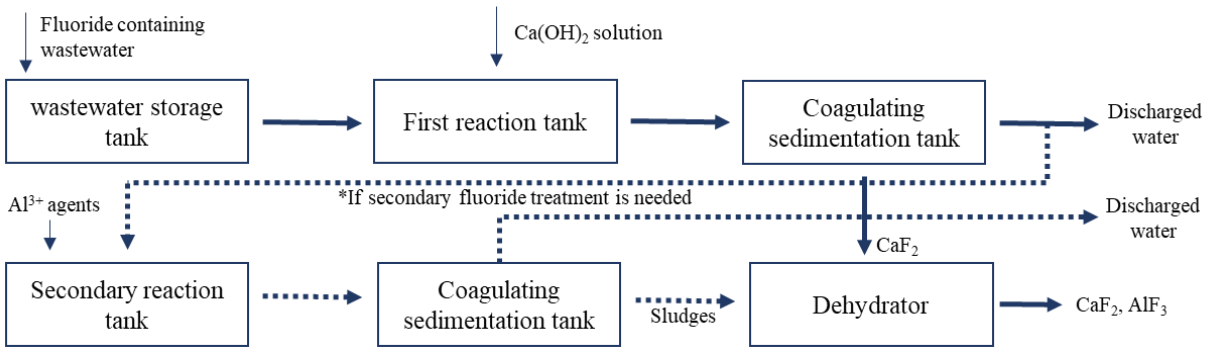

Figure 2. 7 Conventional wastewater treatment flow for fluoride removal [41]

As seen in Fig. 2.7, a conventional fluoride treatment system for wastewater, however, requires additional processing to further decrease the fluoride concentration in solution. This is due to the theoretical solubility of CaF_2 which leaves 8 mg/L F^- at stochiometric concentration of calcium [1]. Even if fluoride concentration of 8 mg/L F^- were to be achieved, it requires excessive amounts of $Ca(OH)_2$ that produces large amounts of waste sludges.

Therefore, alternatives to lime addition method were sought after. Many researchers used aluminum salts for efficient removal of fluoride by adjusting solution pH and delivering insoluble aluminum hydroxide ($Al(OH)_3$) that adsorbs fluoride. Due to aluminum's amphoteric behavior, a favorable reaction occurs at pH in the range of 5 – 7.5. E. Kowalchuk [42] conducted jar tests and obtained final fluoride concentration of close to 2 mg/L with the addition of 50 mg/L Al dosage at pH 6.5. The use of aluminum salts, however, left a noticeable amount of aluminum in the treated solution. In an effort to minimize this undesirable remnant, Gan et al. [29] evaluated $ZrCl_4$ as a coagulant and compared the overall performance with $Al_2(SO_4)_3$ coagulants. The author concluded that zirconium exhibited a better coagulation performance and lower residual metal concentration after recovery of Zr-F agglomerates. The pH range of precipitation for $Al(OH)_3$ is much narrower than for $Zr(OH)_4$ which requires a tight operating pH condition to prevent the formation of soluble species in solution. Meanwhile,

$Zr(OH)_4$ and $Zr(OH)_{3+}$ being the main mononuclear hydrolysates of Zr, fluoride ions were electrostatically attracted to the positively charged hydrolysates of Zr agglomerates. Nevertheless, the coagulation method poses a drawback where the release of undesirable metals in treated solution, even with zirconium salts, still persists.

2.3.4 Solvent Extraction

Solvent extraction (SX) is also a promising method that has undergone investigation for fluoride removal, due to its relatively low cost, high productivity, and recyclability of the fluoride extracting phase [43]. One of the unique advantages of SX method is its superior loading capacity, as compared to any other fluoride removal technologies. Therefore, this method is extensively studied by industries that tend to show high concentration of fluoride in their aqueous solution. In general, the component of organic extractants, organic to aqueous ratio, pH, temperature, and reaction time determines how effectively fluoride can be extracted from aqueous solution.

One of the commercial extractants, Alamine 336, provides ion exchange reactions with a host of anions, as seen in the equations:

$$NR_{3org} + HA_{aq} \leftrightarrow NR_3H_+A_{-org} \quad (2.9)$$

$$NR_3H_+A_{-org} + F^- \leftrightarrow NR_3H_+F_{-org} + A_{-aq} \quad (2.10)$$

Where Equation 2.9 represents an initial protonation of the amine organic phase, and Equation 2.10 follows for the exchange of anions between loaded anions and fluoride ions in aqueous solution. This process was investigated in a pilot plant scale by Kuhn et al. [44], where organic phase extracted halides and sulfate from zinc sulfate aqueous solution with Alamine 336. With the addition of tributyl phosphate (TBP) as a phase modifier, this SX process is intended to enhance fluoride extraction. In terms of the reactions, sulfuric acid reacts first with the organic

phase, as described in Equation 2.09, and halides including fluoride are extracted by exchange with sulfate. Along with this reaction, direct extraction of hydrogen fluoride can also occur by the unprotonated amine. In this study, the maximum halide extractions were 78% fluoride and 90% chloride [44]. More recently, Li et al. [45] significantly improved the extraction efficiency from the previous system involving Alamine 336 and TBP by adding boric acid to a solution containing fluoride. Tetrafluoroborate (BF_4^-) is formed, and this anion complex combines more strongly than fluoride itself with the organic extractant. The following reactions occur in this SX process [45]:

$$H_3BO_3 + 4HF \leftrightarrow H^+ + BF_4^- + 3H_2O \quad (2.11)$$

$$\overline{[\mathbf{NR_3H^+}]\mathbf{HSO_4^-}} + BF_4^- \leftrightarrow \overline{[\mathbf{NR_3H^+}]\mathbf{BF_4}} + H^+ + SO_4^{2-} \quad (2.12)$$

Where the bar denotes the organic phase. An extraction efficiency in the range of 85 – 98% was achieved. A solution of 1 M NaOH was then employed to effectively strip the loaded organic phase, where the remarkable recyclability of the SX process was confirmed.

In spite of its effectiveness in removing fluoride, this may not be an appropriate option for removal of fluoride to a residual trace concentration, especially for applications that require highly purified solution compositions. In addition, the entrainment of solvent phase in the aqueous solution after the SX process can detrimentally affect the performance in the subsequent processing step.

2.3.5 Membranes

Membrane technology can also be applied to minimize the concentration of fluoride in solution through a selectively permeable membrane. Of all membrane-based technologies, reverse osmosis (RO) and nano-filtration (NF) are the latest innovations for defluoridation of solution. In particular, reverse osmosis, by applying pressure through the membrane, was

confirmed to reject fluoride up to 98% from fluoride containing electronics industrial effluents [46]. Dolar et al. [47] investigated a reverse osmosis and nano-filtration membrane in the treatment of wastewater from the fertilizer industry, where reverse osmosis exhibited much higher retention of fluoride. Likewise, Bejaoui et al. [48] confirmed the effectiveness of RO and NF membrane technology in the treatment of fluoride containing metal packaging industrial effluent in Morocco, and further studied the effect of feed pressure, concentration, ionic strength, and pH on the percentage of fluoride removal. In terms of the effect of increased ionic strength, the percentage of fluoride removal significantly declines due to the formation of Na^+ layer on the surface of the membranes that hinders the repulsion of fluoride ions from the negatively charged membranes. Therefore, in this regard, RO or NF membrane technology may not be a feasible option for the treatment of highly concentrated Na_2SO_4 brine solution, where the ionic strength of the solution is much higher than the conditions tested in these past studies.

2.4 Ion Exchange

2.4.1 Principle

Ion Exchange (IX) resins consist of a polymer matrix with a functional group, essentially permanently bound within its polymer matrix. The most common polymer matrix is based on polystyrene with the addition of divinyl benzene (DVB) as a cross-linking agent. The degree of cross-linking in resins significantly affects the porosity and swelling properties of the resin. For instance, lower degree of cross-linking results in more swelling upon hydration, while higher degree of cross-linking results in finer pore size, reducing the available sorption sites.

The desired functional group then can be attached after matrix formation. Each type of functional group has a different order of selectivity and provides adsorption sites for

counterions. The chemical process is therefore best described by ions exchanged between aqueous solution and a solid ion exchanger, as shown below:

Cation-exchange resin: $$\overline{RA^+} + B^+ \leftrightarrow \overline{RB^+} + A^+ \quad (2.13)$$

Anion-exchange resin: $$\overline{\mathbf{RA^-}} + \mathbf{B^-} \leftrightarrow \overline{\mathbf{RA^-}} + \mathbf{A^-} \quad (2.14)$$

Where R is the either cation or anion exchange resin depending on the type of ions it exchanges with. A and B are counter ions. The bar indicates the phase of the solid ion exchanging resin. Once the ion exchange resin is introduced into aqueous solution, counterions typically continue to load on the functional group in accordance to their relative selectivity until equilibrium is reached. This also implies that if the resin has a greater selectivity for the newly introduced counterions than ions already in place, these ions in solution can displace the existing ions.

In general, the performance of a resin is determined by its exchange capacity, also called loading capacity or adsorption capacity, and the selectivity of the resin. The exchange capacity implies the amount of counter ions loaded per specified weight or volume of the resin. The amount of counter ions can be described in both gram and mole basis per unit mass or volume of adsorbent; but traditionally denoted in milli-equivalent basis. In order to attain higher loading capacity, the general rules below apply [49]:

1. Little or no cross-linking
2. Flexible cross-linking rather than rigid
3. Maximum number of active functional groups on the polymer matrix
4. High metal to ligand affinity (e.g. fast kinetics)
5. Strong metal-ligand bonds - slow rate of bond breaking
6. Low coordination number of metal

Selectivity refers to the preference of the resin for one specific ionic species over another. It is mainly governed by the nature of the polymer matrix and functional group attached. A number of rules also follow for the selectivity of standard ion exchange resin [49]:

1. Selectivity increases with the charge on the ion (e.g. Th(IV) » La(III) » Ca(II) » Na(I))
2. Selectivity increases with decreasing ionic radius
3. Selectivity increases with increasing polarizing power

In summary, ions with higher charge and smaller radius results in higher polarizing power and greater selectivity. Other effective interactions between ions and the processing environment can affect the selectivity as well [49].

2.4.2 Resin Manufacturers

This section briefly illustrates the commercially available resins, where the global market for ion exchange resin is projected to reach $2 billion by 2023, an increase of 25% from 2017 [50]. The most popular brands are shown in **Table 2.5**.

Table 2. 5 Ion exchange resin manufacturers and their brands

S.N.	Manufacturer	Brand
1	Lanxess	LEWATIT
2	Purolite	PUROLITE
3	Mitsubishi Chemical Holdings	DIAION
4	The Dow Chemical Company	DOWEX
5	Ion Exchange India Pvt. Ltd	INDION
6	Rohm and Haas Company	AMBERLITE
7	United Water Softeners	ZEROLIT
8	Samyang Corp.	TRILITE
9	Thermax Ltd.	TULSION
10	Resintech Inc.	RESINTECH

2.4.3 Applications

Ion exchange resin technology has been incorporated in a wide variety of industries in need of the following purposes: substitution, separation, and removal [51]. Substitution refers to the recovery of valuable ions such as gold and copper by the resin. Separation of different ions in the order of affinity for the resin from aqueous solution can serve as one of the functions. Lastly, ion exchange resin can be effectively utilized to remove deleterious or undesirable ions from aqueous solution in various applications. With all these categories with different purposes, ion exchange resin has been actively used in the following applications:

1. Water production and softening
2. Recovery of precious metals, rare earth metals, and transition metals
3. Separation of uranium, lithium, and boron in radioactive applications
4. Purification of sugar in food industry
5. Production of organic acids in biotechnological applications
6. Ion chromatography chemical analysis
7. Removal of heavy metals, colours, nitrate and ammonia in wastewater treatment

2.4.4 Resin Type

Ion exchange (IX) resins can be manufactured in five different ways: strong acid cation resin, weak acid cation resin, strong base anion resin, weak base anion resin, and lastly chelating resin. In this section, each type of the resin is discussed in the context of past studies on fluoride removal process.

2.4.4.1 Strong acid cation resin

Strong acid cation resins, the most widely used, have anionic functional groups such as sulphonate (SO_{3}^{-}), which is extensively used for lowering hardness in water softening

applications. Paudyal et al. [52] studied removal of fluoride by using spent cation exchange resin with sulphonic acid functional group, where spent cation resin was pulverized and mixed with an inorganic coagulating agent and zirconium oxychloride octahydrate in a batch-wise test. Zirconium providing preferential adsorption sites for fluoride. This study effectively demonstrated the adsorption of fluoride onto the newly synthesized resin and recyclability of the resin. The effect of interfering ions such as chloride, nitrate, and sulfate were studied, where chloride and nitrate displayed negligible influence on the fluoride adsorption, whereas sulfate ions exhibited a minor interference. Despite its notable loading capacity and recyclability, the resin synthesis step may limit the process applicability in a commercial scale. Instead of zirconium, Ku et al. [53] pre-loaded aluminum onto freshly manufactured Amberlite IR-120, strong acid cation resin with sulphonic acid functional group. This researcher concluded that it provides a good fluoride removal result when pH is less than 7.0. This Al pre-loaded strong acid cation resin however results in the release of aluminum ions into the treated solution during the fluoride removal process.

2.4.4.2 Weak acid cation resin

Weak acid cation resins, typically having carboxylic acid functional group ($RCOO^-$) can also be used for similar application as strong acid cation resin, but in only at specific range of pH, which allows simpler regeneration of the resin.

2.4.4.3 Anion resin

Strong base anion resin, commonly containing quaternary ammonia group, can be used for removal of nitrate, sulfate, and perchlorate over the entire pH range, while weak base anion resin, most having tertiary amino group, can only effectively work at a certain range of pH. Strong base anion resin was investigated by Samadi et al. [54], in which the isotherm study

reported the fluoride loading capacity of 13.7 g/kg resin. However, a significant adverse effect was also seen when other interfering ions were presented, which inhibits the selective fluoride removal process.

2.4.4.4 Chelating resin

Lastly, chelating resins have similar resin bead form and polymer matrix as other types of resin, but contain chelating agents as a functional group that may show higher selectivity toward certain ions in the sorption process. Viswanathan et al. [55] investigated INDION FR10, chelating resin with sulphonic acid functional group. The loading capacity was then compared with the resin in hydrogen, sodium, and aluminum form. In general, all the forms of resin showed fluoride uptake, where the loading mechanisms for hydrogen, sodium, and aluminum from resin were hydrogen bonding, electrostatic adsorption by sodium, and electrostatic adsorption with complexation between aluminum and fluoride, respectively. The author confirmed that the aluminum form of the resin exhibited the highest loading capacity. Similarly, Millar et al. [56] used Lanxess TP 208, a chelating resin with iminodiacetate functionality, to adsorb fluoride by pre-loading the resin with aluminum. Batch tests with the initial fluoride concentration of 10 mg/L and solution pH at 6.11, fluoride loading capacity of 1.3 g/kg resin was achieved. With the increase in initial fluoride concentration to 100 mg/L, fluoride loading capacity of 12.4 g/kg resin, ten-fold increase was attained. Generic structural models for aluminum loaded iminodiacetate chelating resin were also proposed as seen in **Fig. 2.8**.

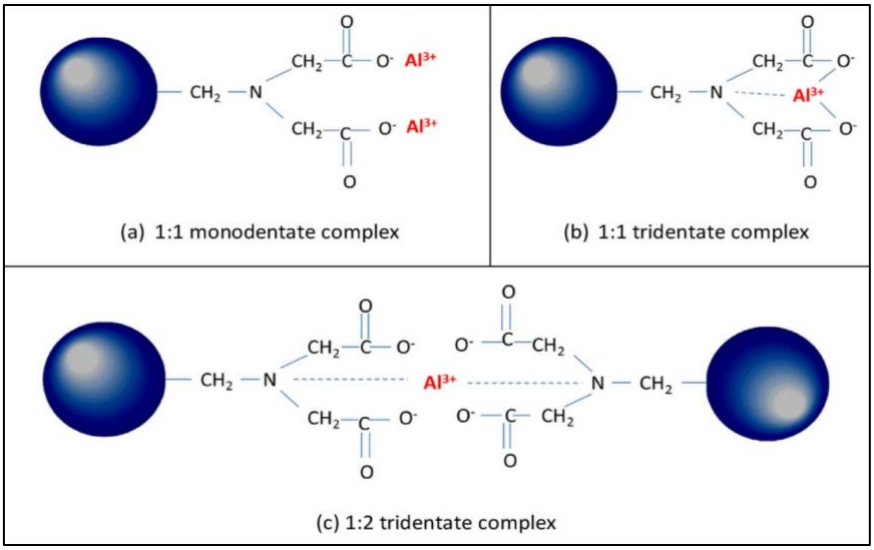

Figure 2. 8 Generic structural models of Al loaded chelating resin with iminodiacetate functional group [56]

2.4.5 LEWATIT Monoplus TP 260 resin

LANXESS LEWATIT Monoplus TP 260 resin was selected for study. It is a weak acid cation chelating resin with a functional group of amino-methyl-phosphonic acid (AMPA) with a matrix of polystyrene. The potential of this AMPA functional group for fluoride removal from solution was initially tested out by Popat et al. [57]. Aluminum chloride pre-loaded AMPA chelating resin was shown to be superior to strong acid resin in aluminum form for fluoride removal from drinking water. LEWATIT Monoplus TP 260, being commercially available, is therefore expected to exhibit great selectivity towards fluoride ions. In addition, Monoplus TP 260 resin has much more uniform bead size than just a regular TP 260 resin, resulting in higher loading capacity and stability. **Table 2.6** illustrates Monoplus TP 260 resin properties provided by the manufacturer.

Table 2. 6 Lanxess' LEWATIT Monoplus TP 260 product information [58]

Resin	*LEWATIT Monoplus TP 260*
Ionic form as shipped	Na^+
Functional group	Amino-methyl-phosphonic acid (AMPA)
Theoretical total capacity (min. eg./L)	2.4
Mean bead size (mm)	0.63 (+/- 0.05)
Bulk density (g/L)	720
Water retention (wt.%)	58-62
Volume Change (Na+ → H+), (vol.%)	-35

2.4.6 Isotherms

The evaluation on the effectiveness of the resin is mainly discussed with its maximum loading capacity. The amount of metal ion adsorbed by resins is obtained from Equation (2.15).

$$q_t = \frac{V}{m}(C_o - C_t) \tag{2.15}$$

Where q_t (g/kg resin) is the loading capacity, V is the solution volume (L), m is the mass of resin (g), C_o and C_t (mg/L) are the target ion concentration at time = 0 and t, respectively. In general, for column studies, m is expressed in volume of resin (L), as the bed volume (BV) is introduced.

Equilibrium isotherm studies offer not only an estimation of resin loading capacities, but also invaluable information on the phenomenon governing the adsorption of a substance from an aqueous media into a solid phase, resin in this case, at a constant temperature and solution normality. A variety of equilibrium isotherms models have been established, and the underlying thermodynamic assumptions from each model provide an insight into an adsorption mechanism.

Two most fundamental expressions have been predominantly used to fit the data: the Langmuir and Freundlich models.

The Langmuir isotherm model has a number of underlying assumptions. This expression assumes that adsorption can only take place on finite localized sites, and consequently generates a monolayer adsorption. Its derivation implies a homogenous adsorption, meaning that each site holds constant enthalpies and sorption activation energy. It also assumes that no interaction between adsorbed molecules takes place [59]. The Langmuir expression is written in Equation (2.16).

$$q_e = \frac{K_L q_m C_e}{1 + K_L C_e} \tag{2.16}$$

Where K_L (L/mg) represents the Langmuir constant related to q_e, equilibrium adsorption capacity. q_m is the maximum adsorption capacity in a monolayer form.

The Freundlich isotherm, not restricted to a monolayer formation, can be applied to multilayer adsorptions. This empirical model is based on the adsorption process occurring on heterogenous surfaces. The Freundlich isotherm expression, as shown in Equation (2.17) describes the exponential distribution of active sites and their energies [60].

$$q_e = K_F C_e^{\frac{1}{n}} \tag{2.17}$$

Where K_F is the Freundlich coefficient (mg/g (L/mg)$^{1/n}$) and 1/n is adsorption intensity. Higher adsorption intensity indicates more favorability towards ion adsorption.

2.4.7 Kinetics

Kinetic study with resins is often conducted as well to determine the contact time required for the equilibrium isotherm and predict the sorption mechanism. Lagergren created a pseudo first-order rate expression, as illustrated in Equation (2.18), which has been the most widely used to describe the adsorption uptake of ions of interest [61].

$$q_t = q_e(1 - \exp(-k_1 t)) \quad (2.18)$$

Where k_1 (min^{-1}) is the pseudo first-order adsorption rate constant. q_t and q_e ($g \cdot kg^{-1}$) are adsorption capacities at time t and equilibrium. Film diffusion is considered a rate limiting step for pseudo first order kinetics [62].

The pseudo second-order expression is given by Equation (2.19). Unlike pseudo first-order reaction, second-order infers that chemical interaction between the adsorbate and sorption sites is considered a rate limiting step. The following non-linearized version of pseudo second-order reaction expression was derived by Azizian [63].

$$q_t = \frac{k_2 q_e^2 t}{1 + k_2 q_e t} \quad (2.19)$$

Where k_2 ($g \cdot mg^{-1} \cdot min^{-1}$) represents the pseudo second-order adsorption rate constant. Derivation procedures for pseudo first-order and second-order adsorption rate expressions are explained in **Appendix A.**

2.4.8 Error Analysis

Linear regression analysis has been the most applicable method for analysis and interpretation of experimental data. The model fitting of ion exchange isotherms has been therefore commonly conducted with its linearized version in various isotherm studies. The goodness of fit in these linearized models is primarily estimated by the correlation coefficient (R^2) where a value of 1 signifies a perfect match between the experimental data and theoretical model. However, the recently published research on ion exchange isotherms has utilized non-linear methods, often called non-linear least squares (NLLS) to fit the models, most of which indicated its effectiveness over linearization of models. One particular example is the use of isotherm equations to predict the behavior of sodium ion exchange with strong acid cation resin, where linear least square

(LLS) method illustrated an inherent discrepancy in calculated adsorption capacities [64]. The author then concluded that both kinetics and isotherm models best fitted the data with the use of non-linear least square (NLLS) approach.

In comparison to linear regression, non-linear regression employs the minimization of error distribution between the experimental data and the selected isotherm model. Among a variety of NLLS approaches, Ayawei et al. [60] discussed five prime error functions (Sum Square of Errors (ERRSQ); Hybrid Fractional Error Function (HYBRID); Average Relative Error (ARE); Marquardt's Percent Standard Deviation (MPSD); Sum of Absolute Errors (EABS)) to derive the optimum fit of experimental data. Lastly, as a consequence of using different error functions, it is likely to generate different sets of equilibrium isotherm parameters. Normalization and comparison between the error functions is therefore conducted using "Sum of the Normalized Errors (SNE)" procedure. **Table 2.7** depicts of five different error functions that can be implemented with the use of Solver add-in in Excel. The terms n and p indicate the number of data points and parameters in model expression, respectively.

Table 2. 7 Non-linear least square (NLLS) error function for model fitting process [60]

Error Function	Equation
Sum Square of Errors (ERRSQ or SSE)	$\sum_{i=1}^{n}\left(q_{e,,\,calc.}-q_{e,\,meas.}\right)^2$
Hybrid Fractional Error Function (HYBRID)	$\frac{100}{n-p}\sum_{i=1}^{n}\left\lvert\frac{\left(q_{e,\,meas.}-q_{e,\,calc.}\right)^2}{q_{e,\,meas.}}\right\rvert$
Average Relative Error (ARE)	$\frac{100}{n}\sum_{i=1}^{n}\left\lvert\frac{q_{e,\,meas.}-q_{e,\,calc.}}{q_{e,\,meas.}}\right\rvert$
Marquardt's Percent Standard Deviation (MPSD)	$\sqrt{\frac{1}{n-p}\sum_{i=1}^{n}\frac{\left(q_{e,\,meas.}-q_{e,\,calc.}\right)^2}{q_{e,\,meas.}}}$
Sum of Absolute Errors (EABS)	$\sum_{i=1}^{p}\left\lvert q_{e,,\,calc.}-q_{e,\,meas.}\right\rvert$

2.5 Summary and Objectives

This chapter started with the overview of the electrodialysis process and how the impurities, such as fluoride can adversely impact the electrodes in the cell. With the review of fluoride characteristics and chemistry, a number of different approaches in solving the issue associated with the presence of fluoride in brine solutions was assessed. Out of all the options, ion exchange resin technology, specifically fluoride complexing metals pre-loaded chelating resin is selected to be focused on, as it provides effective fluoride adsorption sites with relatively lower metal leakage and can attain very low fluoride concentration in effluents.

LANXESS' LEWATIT Monoplus TP 260 resin is investigated in this thesis to treat Na_2SO_4 brine solution containing low concentration of fluoride in the range of 20 – 30 mg/L. Liu [65] studied the same resin type in removing fluoride from zinc sulfate electrolyte. The author evaluated the applicability of this resin technology in high zinc sulfate background concentration through a column study. The process sequence used is as illustrated in **Fig. 2.9**.

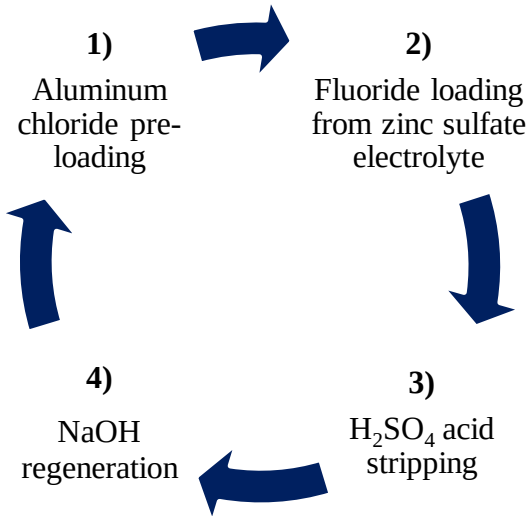

Figure 2. 9 Process flow for fluoride removal from zinc sulfate electrolyte

However, there remains some issues around fundamental understanding of the overall experimental methodologies, fluoride loading capacity, and the effect of operating parameters

on the adsorption process. Another case study conducted by Oke et al. [66] on fluoride removal with Al pre-loaded Monoplus TP 260 resin from chloride containing wastewater confirmed its scalability to a pilot plant level. Nevertheless, this was performed with an industrial wastewater, in which total dissolved solids (TDS) containing half NaCl and half Na_2SO_4 (wt. basis) was only tested up to 10 g/L. Therefore, an extensive gap in the understanding on the fluoride removal process by Monoplus TP 260 with strong Na_2SO_4 brine background remains to be investigated.

The objective of this work is to create a basis for the selective fluoride removal process with a metal-loaded chelating resin in Na_2SO_4 brine. This will be approached by answering three main questions.

1. **Quantify fluoride loading capacity of metal pre-loaded Monoplus TP 260 resin**

   Fluoride can be selectively adsorbed onto the resin by the available sorption sites. In general, fluoride complexing metals are pre-loaded on the resin before the fluoride removal process begins. Two literature sources described above utilized aluminum pre-loading step to provide a fluoride sorption sites. In this thesis, not only aluminum pre-loaded resin is to be investigated but zirconium pre-loaded resin will be studied as well. By conducting a batch study, this will effectively quantify the fluoride loading capacities of two different types of fluoride complexing metal pre-loaded Monoplus TP 260 resin.

2. **Assess the factors affecting for fluoride adsorption from sodium sulfate solutions**

   Although there are a number of literature sources identifying the effects of other parameters such as pH and temperature on fluoride loading capacity, no work has been reported with regards to Monoplus TP 260. Furthermore, the effect of high Na_2SO_4

concentration is yet to be explored. This will be therefore addressed by conducting tests with the variations of Na_2SO_4 concentration, pH, and temperature.

3. **Conduct column loading trials and explore regeneration strategies**

   Column loading trials are performed to ensure the scalability of the process. Aside from the fluoride loading capacities obtained from the batch isotherm studies, verifications on metal pre-loaded TP 260 resin are still needed in regards to the effluent fluoride concentration after the treatment and the degree of metal leakage during the loading cycles. Most notably, the regeneration strategies are to be explored for the pre-treated resins. The novelty in the fluoride removal process is to be found through an effective regeneration protocol which ensures the recyclability of the resin.

Chapter 3: Experimental Methods

3.1 Preparations

All the experiments in this study were conducted with synthetic aqueous solutions prepared with salts containing various metal elements and fluoride. This section summarizes the chemicals, ion exchange resin and apparatus used in the study.

3.1.1 Materials

The following materials were used, unless stated otherwise.

- Aluminum Standard for IC, 1000 mg/L in 2% nitric acid, Sigma Aldrich, Lot# BCBP3906V
- Aluminum sulfate octadecahydrate, ACS, Sigma Aldrich, (Lot# N/A)
- Buffer Reference Standard, pH 10.00 at 25 °C, VWR Chemicals, Lot# 4904C80
- Buffer Reference Standard, pH 4.00 at 25 °C, VWR Chemicals, Lot# 4904F14
- Buffer Reference Standard, pH 7.00 at 25 °C, VWR Chemicals, Lot# 4904E63
- Calcium Standard for IC, 1000 mg/L in 2% nitric acid, Sigma Aldrich, Lot# BCBR3915V
- Calcium sulfate anhydrous, 99% pure, ACROS Organics, (Lot# N/A)
- Fluoride Standard, 100 ppm, Ricca Chemical, Cat# ACCU0825500
- Fluoride Standard, 1000 ppm, Ricca Chemical, Product # 3173-16
- Hydrochloric acid, 36.5 – 38% ACS, VWR Chemicals, Lot# 2019040433
- Magnesium Standard for IC, 1000 mg/L in 2% nitric acid, Sigma Aldrich, Lot# BCBV4090
- Magnesium sulfate heptahydrate, Certified ACS, Fisher Chemical, Lot# 153479
- Nitric acid 68 – 70%, ACS, VWR Chemicals, Lot# 319263
- Sodium fluoride, Certified ACS, Fisher Chemical, Lot# 960066

- Sodium hydroxide 1.0 N, VWR Chemicals
- Sodium sulfate anhydrous, certified ACS, Fisher Chemical, Lot# 188777
- Sulfuric acid 95 – 98 w/w%, Certified ACS Plus, VWR Chemical, Lot# 2019061176
- Optimum Result A Fill solution (For F-ISE), Cole Parmer, Product# 900061
- Total Ionic Strength Adjustment Buffer II (TISAB II) with CDTA, Ricca Chemical, Product# 940909
- Total Ionic Strength Adjustment Buffer IV (TISAB IV) with tartrate, Ricca Chemical, Product# 8673-1
- Zirconium Standard for IC, 1000 mg/L in 2% nitric acid, Sigma Aldrich, Lot# BCBV2795
- Zirconium sulfate tetrahydrate, 98+% metal basis, Fisher Chemical, Lot# U19F058

3.1.2 Apparatus

The following equipment were used in the experiments.

- Fluoride Ion Selective Electrode (F-ISE), Thermo Scientific Orion, Cat# 9609BNWP
- Inductively Coupled Plasma Optical Emission Spectrometer (ICP-OES)
- pH and Eh meter
- pH probe
- Temperature controlled Water bath
- Water bath shaker, Thermo Scientific SWB 25

3.1.3 Resin Preparation

Prior to onset of any experiment, Lanxess' LEWATIT Monoplus TP 260 resins were pre-treated. With the resin in sodium form as freshly manufactured and shipped, deionized (DI)

water was used to wash the resins for several times to remove impurities. The resin was then immersed in DI water to keep it hydrated.

For batch isotherm studies, all the resins were dried at room temperature (21 – 23°C) for at least two days to a constant mass. In general, dried resins may lead to bead breakage when rehydrated due to the re-swelling of resins, and therefore, it is recommended to keep the resins hydrated. However, the use of resin in wet form resulted in high degree of error due to the difficulty in accurately determining the water content of the resin. In addition, the preliminary loading trial indicated that the use of dry resins did not produce a noticeable difference in loading behavior as compared to the hydrated resins. If the resin performance is to be compared with other published data, the resin preparation step should be checked as some studies used wet resins. In order to convert the units of wet resins (L) into dry resins (g), the bulk density (g wet resin/L resin) and water retention (wt.%) should be taken into account. In the measurement of resin mass, an analytical balance able to report to 0.0001 g (0.1 mg) was used.

For the experiments to measure the loading capacity for ions such as calcium, magnesium, aluminum, and zirconium, the resin was used as supplied in sodium form. As for fluoride loading capacity of Al pre-loaded resin, the resins were first pre-treated with a solution of aluminum (123.49 g/L of $Al_2(SO_4)_3 \cdot 18H_2O$) prior to use. A volume of 20 mL of wet resin was loaded in a column and a solution of aluminum sulfate was pumped at a rate of 5 BV/hr for 2.5 hours at 30 °C. Zr pre-loaded resin was prepared in the same way with a solution of zirconium (116.88 g/L of $Zr(SO_4)_2 \cdot 18H_2O$) at the same operating conditions**.** The resins were then removed from the column, rinsed with DI water, and dried at room temperature (21 – 23°C) for at least two days. Therefore, three sets of resins were prepared: Na^+ resin for Ca, Mg, Al, and Zr isotherm studies, Al^{3+} resin and Zr^{4+} resin for F^- isotherm studies.

For the column study, resin was used in wet form, as the loading capacity was calculated based on the resin volume, instead of resin mass. Prior to putting resin into a column, wet resins in sodium form were first placed in a 40 mL graduated cylinder and tapped to pack the resins. A sample of 20 mL of resin was placed in the columns for all the column tests. DI water was added into the columns to ensure that the resins were fully immersed in water with an extra 3 mL of water on top of the packed resin.

3.2 Procedures for Fluoride Removal with Ion Exchange Resin

3.2.1 Batch Isotherm Tests

Batch isotherm tests were performed to estimate the maximum loading capacity of the resin. With regard to the methodology on the equilibrium isotherm studies, two types of approaches have been widely used; “constant concentration” or “constant mass”. Unlike “constant mass” bottle-point method where the same amount of resin is added into bottles with varying solution concentration, “constant concentration” utilizes the varying amount of resin with the same solution concentration. In order to compare these two approaches, a number of research studies were carried out. Millar et al. [67] postulated that an experiment with a single mass of resin and varying exchanging ion concentration in solution can often result in insufficient and misleading estimation of resin adsorption capacity and sorption mechanism. Whereas, “constant concentration” approach not only satisfies an accurate definition of the term “equilibrium isotherm”, the system having a constant temperature and solution normality, but also delivers a suitably accurate representation of adsorption capacity. Study of the equilibrium isotherms in this work were therefore conducted with the samples with varying amount of resin (0.03 g – 1.02 g dry resin) and fixed exchanging ion concentration. pH of the solutions was initially adjusted, and no further pH control was made during the loading process. Each sample bottle

contained 80 mL of solution. At least 15 samples having the same ion concentration with different resin dosage were prepared to construct an isotherm curve. As for isotherm curves, loading capacity (g/kg resin) was plotted against the equilibrium concentration (mg/L) from which a suitable isotherm model can be used to predict the maximum loading capacity.

In order to identify the baseline loading capacity of Monoplus TP 260 resin, Ca^{2+} and Mg^{2+} equilibrium isotherms were first constructed with the variation on the concentration of Na_2SO_4 brine solution. This was repeated with Al^{3+}, Zr^{4+} and Na^{+} forms of resin to confirm whether these elements can be pre-loaded onto resin for the fluoride removal system. The pH of Al^{3+} and Zr^{4+} samples were adjusted to 2.5 and 1.5, respectively, to avoid precipitation by hydrolysis. At pH > 1.5, Zr^{4+} will hydrolyze to form zirconium hydroxide. The following **Table 3.1** outlines the isotherm curves generated in the baseline study. Fluoride equilibrium isotherms were also constructed with either Al^{3+} or Zr^{4+} pre-loaded resin. The effect of Na_2SO_4 brine concentration, pH, and temperature were studied, as seen in the conditions described in **Table 3.2**. Based on the preliminary kinetic tests, equilibrium was determined to be reached within 24 hours for all different species. Therefore, all the sample bottles were shaken in the water bath for 24 hours at 100 rpm. After 24 hours of shaking, 5 mL of sample solutions were extracted by pipette and prepared for ICP-OES analysis and F^- analysis by F-ISE. The data points were then fitted with the isotherm models by applying all the non-linear least square error functions, as described in Section 2.4.8. The maximum loading capacity is then reported with the values having the lowest Sum of the Normalized Error (SNE). The procedure for non-linear least square (NLLS) error analysis is described in **Appendix C**.

3.2.2 Stripping Tests

A stripping test was conducted on loaded resins to determine how much of the loaded metal ions can be recovered back into solution from the resins. In order to confirm the resin was fully stripped, 3 cycles of stripping were carried out with 1.8 M HCl solution. Prior to the stripping test, the loaded resins were washed with DI water to remove any residual ions on the resin surface. The resins were used in a hydrated form.

Each loaded resin was put into 80 mL of stripping solution. These sample bottles were placed in a shaking water bath with mixing of 24 hours at 100 rpm at 30 ºC. After the first stripping of resins, the resins were separated from the solutions and washed with DI water prior to the next stripping cycle. Stripping solutions were collected at each stage of stripping for ICP-OES analysis.

Table 3. 1 Isotherm studies list for the baseline study

Test No.	Elements	Resin form	Brine Na_2SO_4	Initial ion conc.	pH	Temperature
			(wt.%)	(mg/L)	-	(◦C)
1.01	Ca	Na	**0**	150	7	30
1.02	Ca	Na	**12**	150	7	30
1.03	Ca	Na	**24**	150	7	30
1.04	Mg	Na	**0**	150	7	30
1.05	Mg	Na	**12**	150	7	30
1.06	Mg	Na	**24**	150	7	30
1.07	Al	Na	**0**	150	2.5	30
1.08	Al	Na	**6**	150	2.5	30
1.09	Al	Na	**12**	150	2.5	30
1.10	Al	Na	**24**	150	2.5	30
1.11	Zr	Na	**0**	150	1.5	30
1.12	Zr	Na	**6**	150	1.5	30
1.13	Zr	Na	**12**	150	1.5	30
1.14	Zr	Na	**24**	150	1.5	30

Table 3. 2 Fluoride isotherm studies list

Test No.	Element	Resin form	Brine Na_2SO_4	Initial ion conc.	pH	Temperature
			(wt.%)	(mg/L)	-	(◦C)
2.01	F	Al	**6**	25	7	30
2.02	F	Al	**12**	25	7	30
2.03	F	Al	**24**	25	7	30
2.04	F	Al	12	25	**3**	30
2.05	F	Al	12	25	**5**	30
2.06	F	Al	12	25	**9**	30
2.07	F	Al	12	25	**11**	30
2.08	F	Al	12	25	7	**45**
2.09	F	Al	12	25	7	**60**
2.10	F	Zr	**6**	25	7	30
2.11	F	Zr	**12**	25	7	30
2.12	F	Zr	**24**	25	7	30
2.13	F	Zr	12	25	**3**	30
2.14	F	Zr	12	25	**5**	30
2.15	F	Zr	12	25	**9**	30
2.16	F	Zr	12	25	**11**	30
2.17	F	Zr	12	25	7	**45**
2.18	F	Zr	12	25	7	**60**

3.2.3 Column Tests

After the column resin preparation step, 20 mL of Na^+ form resins were packed in a 50 mL class A PYREX burette. Each bed volume (BV) of solution is therefore 20 mL. A water jacket was installed around the burette to maintain the temperature with the thermostatic water bath. Solutions were pumped with a Masterflex Peristaltic tubing pump and 14# L/S High-Performance Precision Pumping tubing, provided by Cole-Parmer. The column ion exchange experiments were performed with the apparatus shown in **Figure 3.1**.

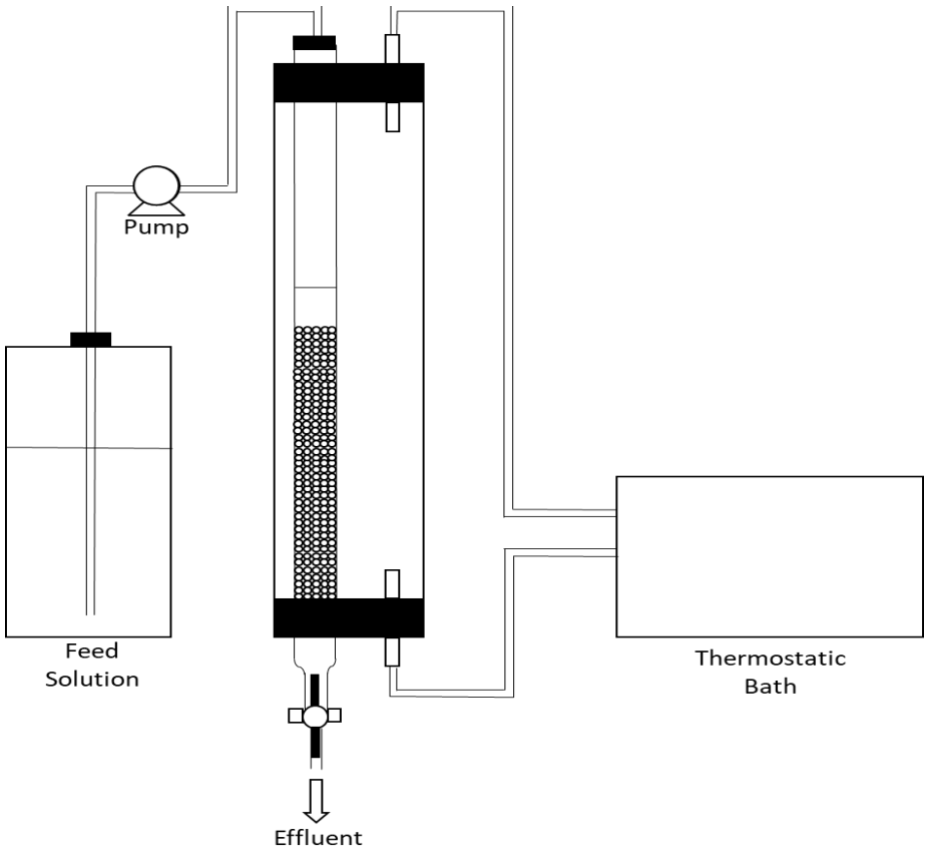

Figure 3. 1 Column ion exchange apparatus

In the initial pre-loading step, solution of 10 g/L Al (123.49 g/L of $Al_2(SO_4)_3 \cdot 18H_2O$) was fed into the column at 5 BV/hr and 30 ºC for approximately 2.5 hours. The concentrations of Al^{3+} in the initial and final solutions were analyzed with ICP-OES to determine the amount of Al^{3+} pre-loaded onto the resins. Zr^{4+} pre-loaded resins were prepared using a solution of 30 g/L Zr^{4+} (116.88 g/L of $Zr(SO_4)_2 \cdot 4H_2O$). pH in both pre-loading solutions was not adjusted. The column beds were flushed with DI water for at least 2 hours to rinse out any remaining metal pre-loading solution in columns. Both Al^{3+} and Zr^{4+} pre-loaded resins were studied throughout different regeneration and processing routes.

Pre-loading metals regeneration

1. The initial brine solution containing 12 wt.% Na_2SO_4 and 25 mg/L fluoride at pH 7 was prepared. With either Al^{3+} or Zr^{4+} pre-loaded resin in the column, this brine solution was pumped into the column at a flow rate of 5 BV/hr (100 mL/hr) at 30 ºC. The fluoride concentration in effluent was collected and analyzed with F-ISE every few hours until it reached a concentration of 25 mg/L F. The effluent samples for metal element analysis with ICP-OES were collected accordingly.
2. As the fluoride concentration in effluent reaches the equilibrium concentration, the fully exhausted resins were regenerated by pumping aluminum sulfate solution (123.49 g/L of $Al_2(SO_4)_3 \cdot 18H_2O$) for Al^{3+} resin and zirconium sulfate solution (116.88 g/L of $Zr(SO_4)_2 \cdot 18H_2O$) for Zr^{4+} resin at the same operating conditions as the initial metal pre-loading step.

After step 2, fluoride loading processes with the brine solutions were continued as per step 1. This was repeated for 3 loading cycles.

Acid or Base regeneration

1. The initial brine solution containing 12 wt.% Na_2SO_4 and 25 mg/L fluoride at pH 7 was prepared. With either Al^{3+} or Zr^{4+} pre-loaded resin in the column, this brine solution was pumped into the column at a flow rate of 5 BV/hr (100 mL/hr) at 30 ºC. The fluoride concentration in the effluent was analyzed with F-ISE every few hours until it reached the inlet concentration of 25 mg/L F. The effluent samples for metal element analysis with ICP-OES were collected accordingly.
2. As the fluoride concentration in effluent reaches the equilibrium concentration, the fully exhausted resins were regenerated by pumping 0.1 M H_2SO_4 solution for Al^{3+} resin and 1.0 M H_2SO_4 solution for Zr^{4+} resin at 5 BV/hr for 10 hours in a 30 ºC column jacket. After step 2, fluoride loading processes with the brine solution were continued as per step 1. This was repeated for 3 loading cycles. As for the base regeneration route, the fluoride loading process with Zr^{4+} resin was repeated with 1 M NaOH regeneration solution.

Al-F co-loading

A solution of 50 mg/L of Al (0.617 g/L of $Al_2(SO_4)_3 \cdot 18H_2O$) was added into brine solution containing 12 wt.% Na_2SO_4 and 25 mg/L fluoride. The solution pH was not adjusted and remained in pH of 4.3. This brine solution was then pumped into the column having 20 mL of resin in Na^+ form at a rate of 5 BV/hr in a 30 ºC column jacket. The effluent was collected every few hours for aluminum and fluoride analysis.

3.3 Analysis Procedures

3.3.1 Fluoride Ion Selective Electrode (F-ISE)

Fluoride concentration in brine solution with various conditions was determined by using a fluoride-ISE (Thermo Scientific Orion Fluoride ISE 9609 BNWP with a built-in reference

element) and pH-Eh meter. As F-ISE only measures free fluoride, total ionic strength adjustment buffer IV (TISAB IV) was added to stabilize ionic strength and pH of the solution. TISAB IV, having the composition of tartaric acid and tris (hydroxymethyl) methylamine, can also inhibit the interference of fluoride complexing ions such as aluminum and iron on the measurement of fluoride ions in solution.

Throughout the study, standard addition method was used. 3 mL of the aqueous samples were first diluted with the equal volume of TISAB IV and DI water in a 20 mL beaker, making up 9 mL in total. As a general guideline, solution mixed with TISAB IV should have pH adjusted to between 8 – 8.5. For the aqueous samples having extremely high or low pH, pH should be adjusted in advance to minimize the presence of HF and/or HF_2^-, which cannot be measured by F-ISE. The F-ISE was then immersed in the prepared sample under stirring of 200 rpm at constant room temperature (298 K). The initial potential reading was then recorded once the potential reading stabilized, which takes a few minutes. A known addition of standard fluoride solution was added to the sample, and the new potential was recorded. The amount of standard solution added should be approximately 1 vol% of the original solution to minimize the change in the ionic strength of the sample. In addition, the moles of added analyte should be approximately 50 -200% of the original analyte in solution being analysed. The change in potential was used to back-calculate how much free fluoride was present in the original solution based on the obtained Nernst equations, as shown below.

$$E = E° - \frac{2.3038RT}{nF} \log [F^-] \quad (3.1)$$

Where E is the cell potential (V), E° is the standard F-ISE potential, R is the gas constant (8.314 J/K/mol), T is the absolute temperature (298 K), n is the number of electrons transferred in the cell reaction, F is the Faraday constant (96,485 C/mol), and $[F^-]$ is the molarity of free fluoride.

Throughout a series of merasurements, unless stated otherwise, the cell potential is the only variable with respect to the change of fluoride concentration in solution. A detailed calculation example is summarized in **Appendix B**.

3.3.2 Inductively Coupled Plasma Optical Emission Spectrometer (ICP-OES)

Other elements such as calcium, magnesium, aluminum, and zirconium were all analyzed with ICP-OES. The aqueous sample solutions were diluted with 2% nitric acid (HNO_3) and sent for ICP-OES analysis at the UBC Earth and Ocean science department. The average of intensities from three different wavelengths for each element was used to report the concentration. The wavelengths set for the analysis are in **Table 3.3**.

Table 3. 3 ICP-OES Wavelengths for the elements

Elements	Wavelength (nm)		
	1	**2**	**3**
Calcium	315.89	317.94	396.85
Magnesium	279.55	280.27	285.21
Aluminum	236.71	237.31	394.4
Zirconium	327.31	343.82	349.62

Chapter 4: Batch Fluoride Removal with Pre-loaded resins

4.1 Batch kinetics trial

Prior to conducting any batch isotherm study, a kinetics trial was first conducted to determine the minimum contact time required for the resin to reach equilibrium concentration in solution. Calcium and magnesium loading onto Na^+ form resins were tested. Conditions and results of the experiments are outlined in **Table 4.1**. In this kinetic study, with the initial metal ions concentration of 150 mg/L, the effect of Na_2SO_4 concentration was analyzed with respect to contact time. Pseudo first and second-order models were fitted to the experimental data. For the sake of brevity, non-linear least square (NLLS) model fitting procedure was conducted only with sum square of errors (SSE) function, where lower SSE signifies a better model fit to the experimental data.

Table 4. 1 Experimental conditions and Non-linear least square (NLLS) kinetic model data for ion exchange of metals on TP 260 resin (303 K; pH 7; 80 mL of solution)

Metal	Sample #	Conditions		Experimental (at t = 1800 min)	Pseudo first-order expression			Pseudo second-order expression		
		Resin dosage (g)	Na_2SO_4 (wt.%)	q_e (g/kg)	q_e (g/kg)	k_1 (min^{-1})	SSE	q_e (g/kg)	$k_2 * 10^3$ ($g \cdot mg^{-1} \cdot min^{-1}$)	SSE
Mg^{2+}	1	0.2	0	44.6	44.3	0.023	16.8	46.4	0.84	14.0
	2	0.2	12	28.2	28.1	0.016	18.8	29.9	0.83	7.0
	3	0.2	24	22.5	22.3	0.014	13.0	23.8	0.89	3.4
Ca^{2+}	1	0.2	0	54.7	54.7	0.052	0.0	55.8	2.54	0.8
	2	0.2	12	39.5	38.1	0.015	30.2	40.7	0.55	2.6
	3	0.2	24	32.7	31.6	0.013	43.8	33.9	0.57	9.0

In comparison of SSE function, Pseudo second-order expression exhibits lower SSE than the first-order expression for both Ca^{2+} and Mg^{2+} kinetic results. This indicates that chemical interaction between the adsorbate and sorption sites is considered the rate limiting step. By

visual observation from **Fig. 4.1**, it is obvious that the adsorption takes place rapidly in the first 70 minutes, attributed to excess exchange sites of Monoplus TP 260 chelating resins available in the beginning. Between 70 to 450 minutes, the rate of adsorption started to decline as exchanging sites were progressively being filled up. After approximately 500 minutes, the rate of adsorption significantly decreased as indicated by horizontal plateau lines.

With the rise in Na_2SO_4 concentration, the rate constant decreases, especially for Ca^{2+}, implying a longer contact time required to reach the equilibrium concentration. However, it is observed that a contact time of 10 hours is sufficient even with the addition of Na_2SO_4. Kinetic trials for the fluoride sorption, as seen in **Fig. 4.2**, also indicated that 24 hours of contact time is sufficient to reach the equilibrium concentration, and thus, 24 hours of mixing was used throughout all the batch isotherm studies.

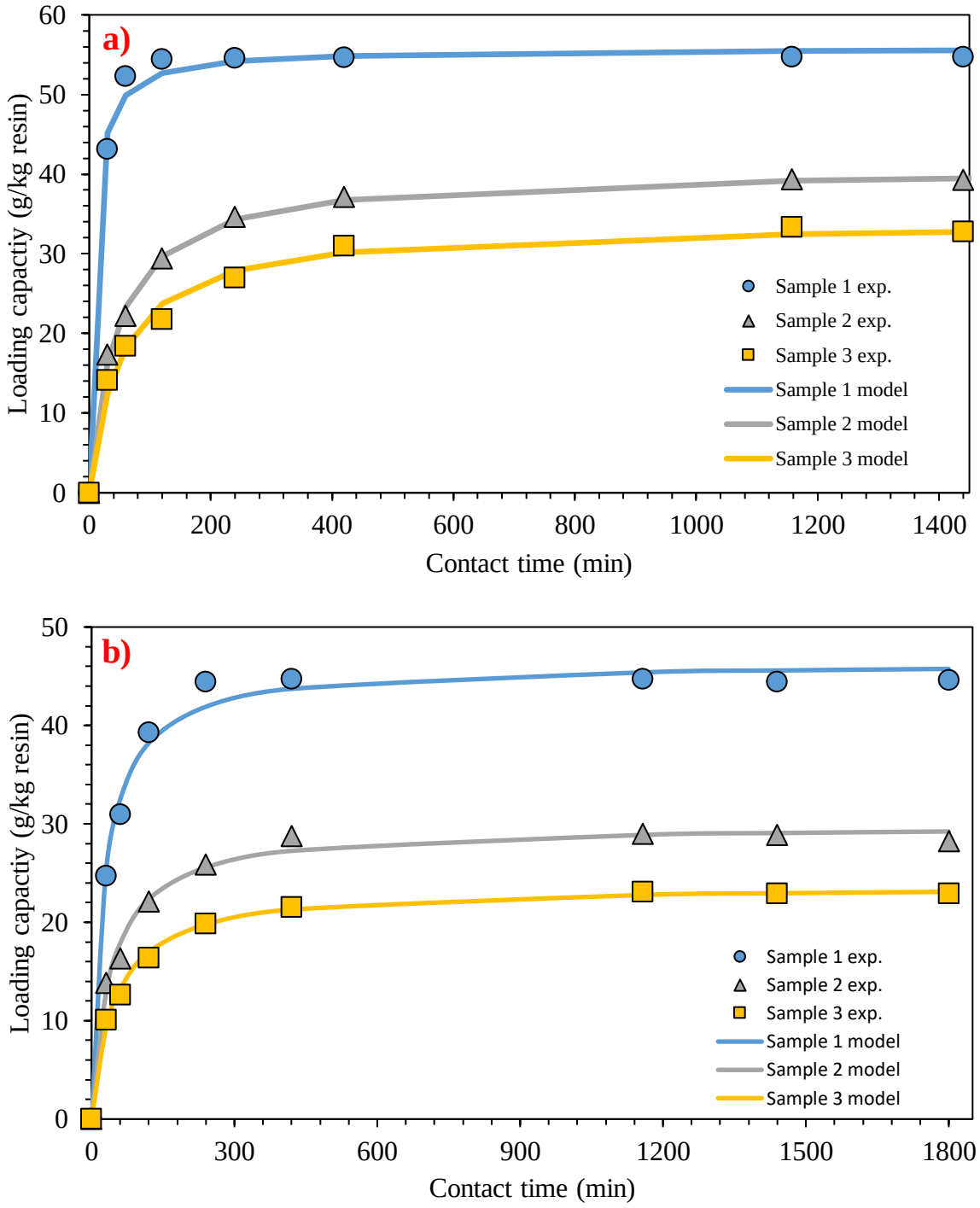

Figure 4. 1 Removal of a) Ca^{2+} or b) Mg^{2+} with respect to contact time (303 K; pH 7). Round markers and lines indicate the experimental values and Non-linear least square (NLLS) fitted pseudo second-order model, respectively.

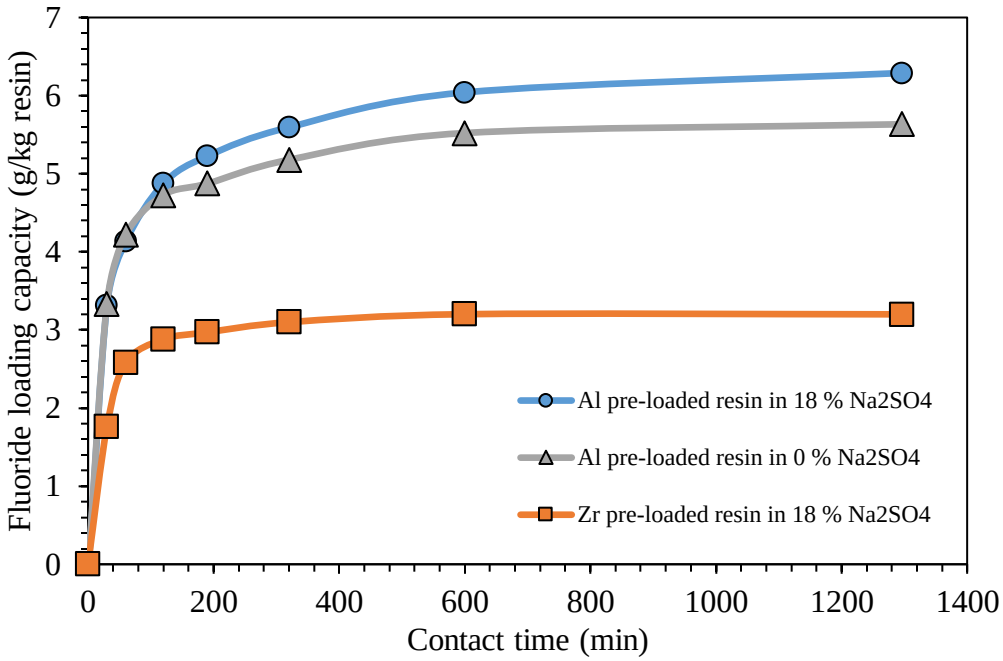

Figure 4. 2 Removal of fluoride with respect to contact time (303 K; pH 7)

4.2 Batch isotherm study on the resin in sodium form

In the analysis of equilibrium isotherms, all five non-linear least square (NLLS) error functions were used. All the NLLS model fit analysis are tabulated in **Appendix D**. All the calculated model parameters from the isotherm studies are attached under the NLLS fitting analysis.

4.2.1 Calcium and Magnesium

Ion exchange (IX) technology is commonly used to deal with hardness removal, mainly implying calcium and magnesium removal. Therefore, the establishment of Ca^{2+} and Mg^{2+} equilibrium isotherms would provide a baseline for the evaluation of the resin performance in the loading process with other elements. **Fig. 4.3** illustrates the equilibrium isotherm profiles for Ca^{2+} and Mg^{2+} loading on Lewatit Monoplus TP 260 resin from a set of Na_2SO_4 solutions, where the Langmuir model lines were plotted along with the experimental values.

The adsorption of both Ca^{2+} and Mg^{2+} were strongly favorable as the Ca^{2+} and Mg^{2+} loading rapidly increases at low equilibrium concentration, C_e, especially for the process with 0 wt.% Na_2SO_4. The maximum Langmuir Ca^{2+} loading capacities estimated were 1.34, 1.10, and 0.82 mol Ca^{2+}/kg resin with the Na_2SO_4 brine concentration of 0, 12, 24 wt.%, respectively. The maximum Langmuir Mg^{2+} loading capacities estimated were 1.49, 1.10, and 0.97 mol Mg^{2+}/kg resin with the Na_2SO_4 brine concentration of 0, 12, 24 wt.%, respectively. In comparison with Ca^{2+} equilibrium isotherms, Mg^{2+} exhibited slightly higher loading capacities with TP 260 AMPA resin. This can be confirmed by the stability constants of Ca^{2+} and Mg^{2+} with this amino methyl phosphonic acid (AMPA) functional group provided by R. M. Smith et al. [68]. The stability constants are 3.84 and 4.25 for Ca^{2+} and Mg^{2+}, respectively, at 25°C and the ionic strength of 0.5.

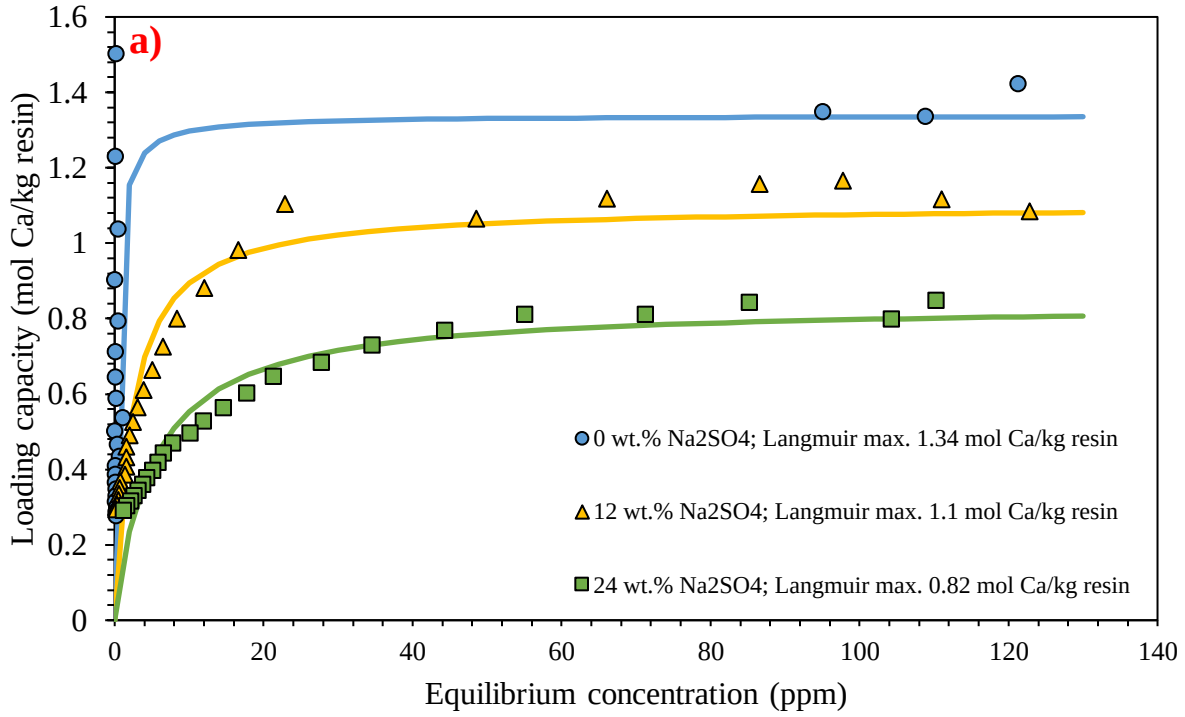

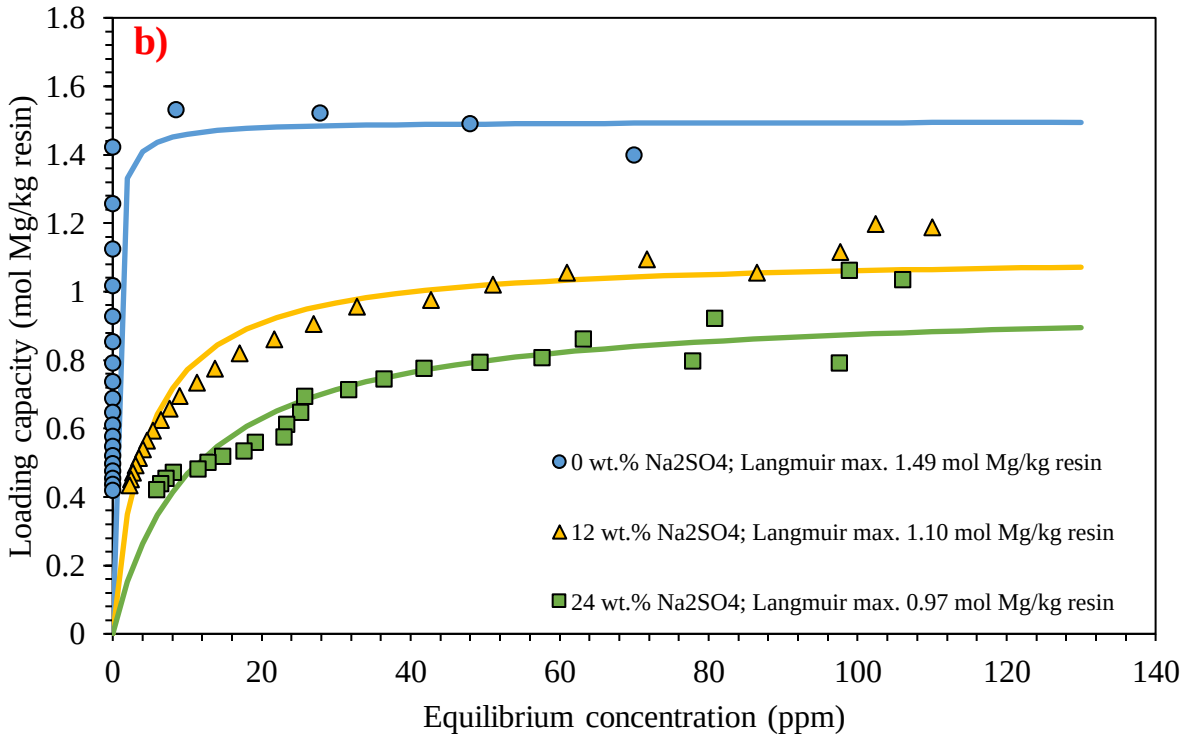

Figure 4. 3 Equilibrium isotherms of a) Ca^{2+} b) Mg^{2+} with Monoplus TP 260 AMPA chelating resin in 0, 12, and 24 wt.% Na_2SO_4 solution (303 K; Initial conc. ~150 ppm Ca^{2+} or Mg^{2+}; pH 7); • Experimental data, — Langmuir isotherm best fit

The isotherm results obtained were compared with the Langmuir loading capacities obtained by Zhang et al. [69] to assess the efficacy of the methodology used in this thesis. This author used Amberlite IRC 747, Lewatit TP 208, and Lewatit TP 260 to obtain Ca^{2+} and Mg^{2+} loading capacities in saline solution. The maximum Langmuir Ca^{2+} and Mg^{2+} loading capacities of TP 260 reported were 1.88 and 2.33 mol/(kg dry resin), respectively at 298 K and the salinity of 35 g/L with the 2:1 mass ratio of NaCl and Na_2SO_4. These loading capacities are noticeably higher than the data attained in this thesis. However, it is speculated that the Langmuir isotherm model parameters may have been overestimated, as the experimental data reported in various figures in this publication are substantially less than the maximum loading capacities predicted by the Langmuir parameters. The experimental Ca^{2+} and Mg^{2+} loading capacities attained at pH 7, 298K, and the salinity of 35 g/L were estimated to be 1.40 and 1.44 mol/(kg dry resin), respectively. This isotherm data is similar to the loading capacities obtained in this thesis, confirming that the methodology devised is reliable.

The discrepancy in loading capacities from model prediction may be due to the use of linear least square (LLS) fitting method for the Langmuir equations; whereas non-linear least square (NLLS) fitting method was used for the isotherms in this thesis. According to Millar et al. [64], depending on the type of isotherms and linearized version of model equations, the fit of the equilibrium data can substantially over-estimate the resin capacity.

A similar observation from both Ca^{2+} and Mg^{2+} isotherm graphs was a reduction in loading capacities with the increasing amount of Na_2SO_4 in solution. The decrease in loading capacities in accordance with the increase in Na_2SO_4 concentration is suggested to be due to the competition between Ca^{2+} or Mg^{2+} and Na^{+} for the available binding sites on the resins. This was further verified in the later part of this chapter, where fluoride sorption onto either Al^{3+} or

Zr^{4+} pre-loaded resins was not interfered with by the presence of Na^{+}, as the binding sites were no longer for the cation exchange. This indicates that the reduction in Ca^{2+} and Mg^{2+} loading capacities with the resins in sodium form is solely due to the interfering ions, Na^{+}.

Millar et al. [70] observed the phenomena of sodium desorption from Na^{+} form weak acid cation resin during the calcium loading process, and exhibited a stoichiometric ratio of sodium desorption to calcium loaded. This is indicative of the resin's ability to readily absorb Ca^{2+} or Mg^{2+}. However, as the amount of Na^{+} in solution increases, Ca^{2+} or Mg^{2+} loading capacity gradually decreases, as seen in **Figure 4.4**. The linear dashed trendlines imply that 0.308 eq./(kg Na-resin) is maintained with loaded Na^{+} for every 1 M of Na^{+} addition in solution containing Ca^{2+} or Mg^{2+}.

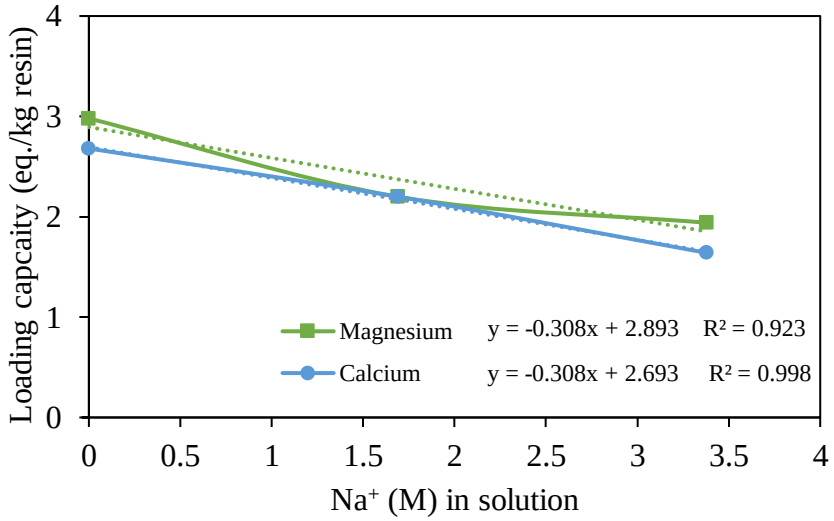

Figure 4. 4 Ca^{2+} and Mg^{2+} loading capacity with respect to Na^{+} addition in solution

4.2.2 Aluminum and Zirconium

Equilibrium isotherms were constructed with respect to aluminum and zirconium to confirm whether the pre-loading of these metal species onto the resin can be effectively carried out. **Fig. 4.5** illustrates the equilibrium isotherm profiles for Al^{3+} and Zr^{4+} loading on Lewatit Monoplus TP 260 resin from a set of Na_2SO_4 solutions, where the Langmuir model lines were plotted

along with the experimental values. The maximum Langmuir Al^{3+} loading capacities estimated were 1.21, 1.05, 0.99, and 0.98 mol Al^{3+}/kg resin with the Na_2SO_4 brine concentration of 3, 6, 12, and 24 wt.%, respectively. The decrease in loading capacities with the increase in Na_2SO_4 concentration follows what was observed in the Ca^{2+} and Mg^{2+} equilibrium isotherm profiles due to the competition with the Na^{+} for the sorption sites on the resin. The aluminum loading result having comparable loading capacities as the Ca^{2+} and Mg^{2+} loading process suggests that $Al(OH)^{2+}$ species is mainly loaded onto the resin.

The maximum Langmuir Zr^{4+} loading capacities estimated were 0.32, 0.26, 0.29, and 0.37 mol Zr^{4+}/kg resin with the Na_2SO_4 brine concentration of 0, 6, 12, and 24 wt.%, respectively. In comparison with Ca^{2+} and Mg^{2+} baseline loading process, Zr^{4+} loading capacities were significantly lower than the other loading capacities throughout all different concentration of Na_2SO_4. It is speculated that the use of low pH to avoid the formation of precipitates during the batch operation inevitably interferes with the loading of zirconium with the increased amounts of protons presented in solution. The presence of H^{+} competes with Zr^{4+} for the available sorption sites. Therefore, zirconium loading never reaches saturation of the ion exchange sites in this batch experiment. A number of data points at higher range of equilibrium concentration, especially at 24 wt.% Na_2SO_4, exhibit a drastic increase in loading capacities. Such ions uptake at the high equilibrium concentration range may be an indication of further zirconium loading onto the resins due to the high ratio of ions to the resin mass.

A further investigation can be done by repeating the zirconium loading process with the resins treated once with the zirconium solution to verify if additional zirconium loading takes place.

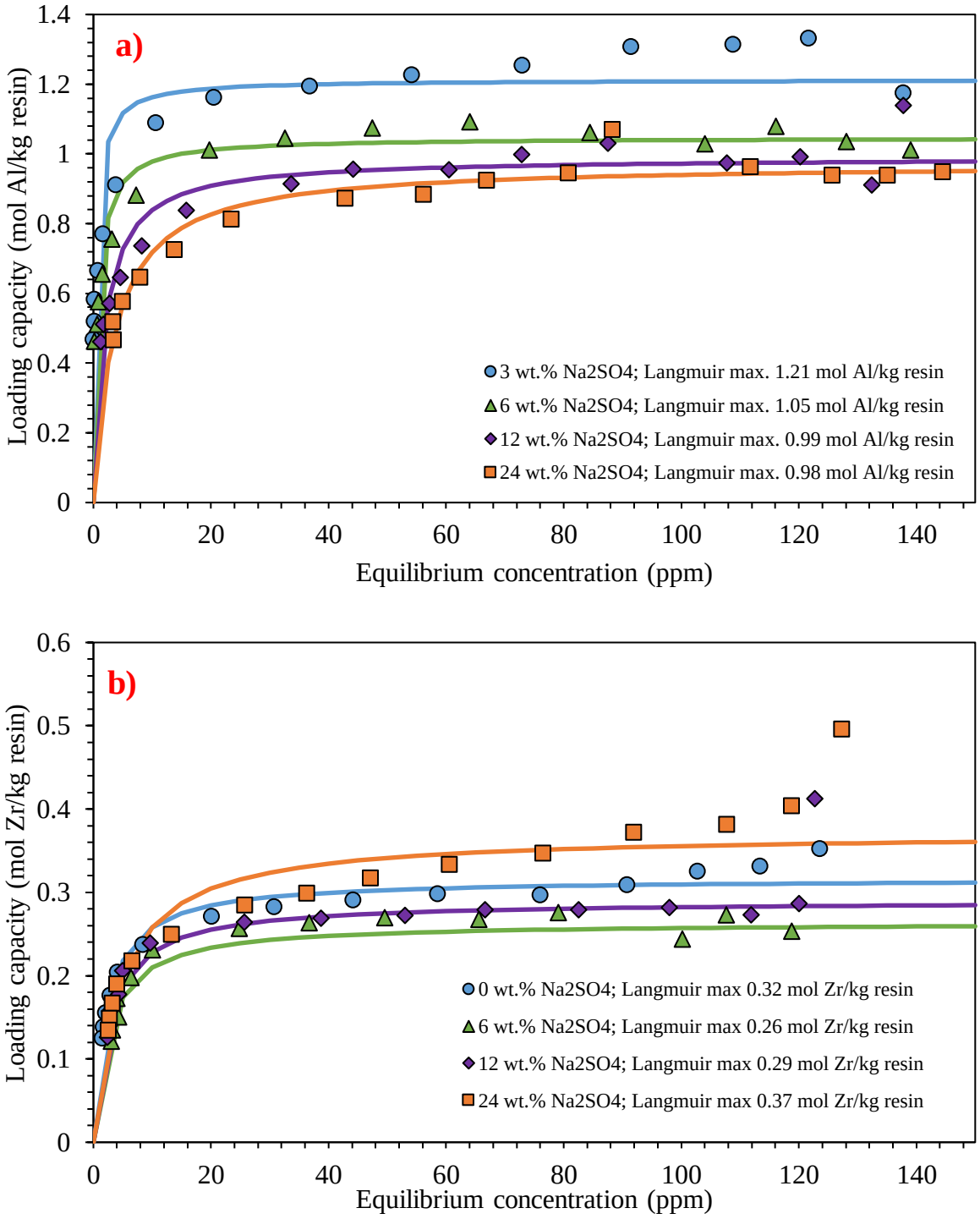

Figure 4. 5 Equilibrium isotherms of a) Al^{3+} b) Zr^{4+} with Monoplus TP 260 AMPA chelating resin in 0 - 24 wt.% Na_2SO_4 solution (303 K; Initial conc. ~150 ppm Al^{3+} or Zr^{4+}; pH 2.5 for Al^{3+} and pH 1.5 for Zr^{4+}); • Experimental data, — Langmuir isotherm best fit

4.2.3 Stripping tests

Stripping tests were conducted to ascertain if the metals loaded on the resins can be successfully recovered, or to what degree they remain permanently adsorbed. **Fig. 4.6** indicates that both Ca^{2+} and Mg^{2+} can be readily stripped from the resin into a 1.8 M HCl stripping solution in the first stripping cycle, most of which established >90% metal recovery. Al^{3+} recovered was in the range of 55 – 70 %, and Zr^{4+} recovered was less than 10 % even after 3 HCl stripping steps. According to Smith et al. [71], imino bis (methylene phosphonic acid) group, the functional group of Monoplus TP 260 resin, has the stability constants of $Al^{3+} \gg H^{+}$, $La^{3+} > Mg^{2+}, Ca^{2+}$. Though the stability constant of zirconium with this functional group is not provided, low zirconium recovery implies that methylene phosphonic acid functional group has higher stability constant with zirconium than any other cations in this stripping test.

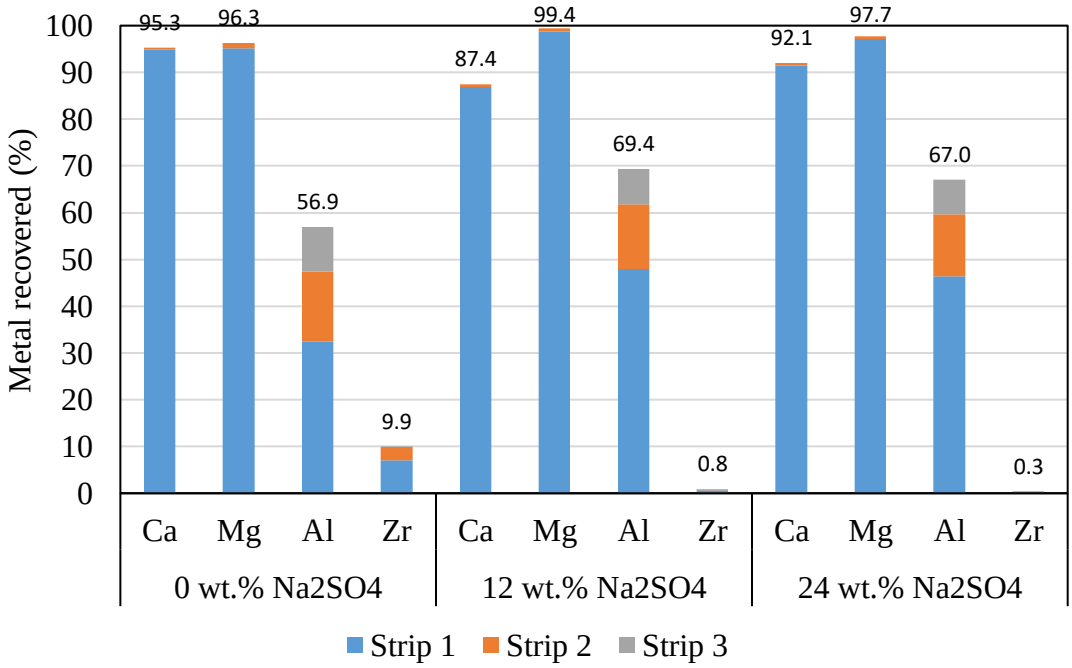

Figure 4. 6 Stripping analysis of Ca, Mg, Al, and Zr with 1.8 M HCl

4.3 Fluoride Batch isotherm study with Al-resin

4.3.1 Effect of Na_2SO_4

In the Al^{3+} pre-loading step, approximately 1.0 mol Al^{3+}/L resin was loaded. **Fig 4.7 a)** illustrates the equilibrium isotherms of F^- on Al^{3+} pre-loaded Monoplus TP 260 AMPA type resin with the variation of Na_2SO_4 brine concentration. To fit the data, the Dubinin-Radushkevich isotherm model was used, frequently applied in equilibrium adsorption studies having S-shaped isotherms. It should be noted that the maximum fluoride loading capacities obtained from the model projection are rather overestimated, and there is actually little difference in fluoride loading capacities between the samples with different concentration of Na_2SO_4. Nevertheless, based on the model projections, the increase in Na_2SO_4 concentration slightly increases the fluoride loading capacities, where the loading capacities of 1.29, 1.30, and 1.37 mol F^-/kg Al-resin were obtained in 6, 12, and 24 wt.% Na_2SO_4 solution, respectively. It is deduced that as the available sorption sites are no longer for cation exchange, the presence of high concentration of Na^+ does not create any adverse impact on fluoride adsorption on the resin. Likewise, the presence of SO_4^{2-} is observed to have no interfering effect on fluoride adsorption. In comparison with baseline Ca^{2+} and Mg^{2+} equilibrium isotherms, fluoride loading by Al-loaded resin has illustrated a promising result with its comparably high fluoride loading capacities at various Na_2SO_4 concentration range.

However, as seen in **Fig 4.7 b)**, even if Al^{3+} has relatively high stability constant with AMPA type resin, aluminum still leaks into the solution from the resin during the sorption process. Displacement of aluminum by sodium in solution and stripping of aluminum by complexation with fluoride in solution occurs simultaneously as fluoride is complexed by the Al-loaded resin. A general trend for all the Al^{3+} and Zr^{4+} leakage plots against the resin mass

has high stripping percentage in the low range of resin mass and low stripping percentage in the high range of resin mass employed. It is deduced that relatively high fluoride concentration to the resin mass rather pulls metal out from the resins to form a metal-fluoride complexes.

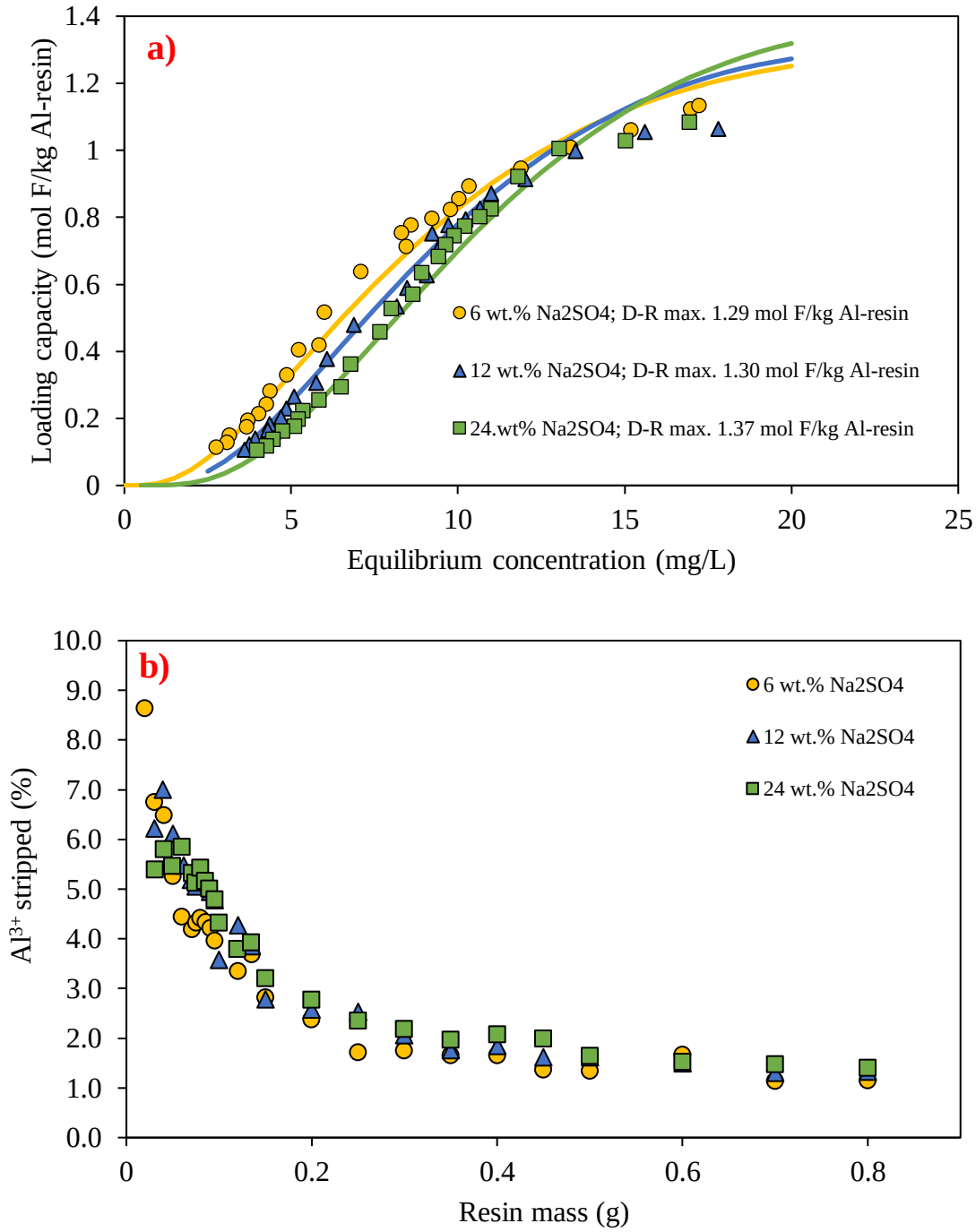

Figure 4. 7 a) Equilibrium isotherms of F^- on Al^{3+} pre-loaded Monoplus TP 260 resin in 0 - 24 wt.% Na_2SO_4 solution (303 K; Initial conc. ~25 ppm F^-; pH 7), b) Aluminum leakage (%) during the sorption process from the Al^{3+} loaded resins; • Experimental data, — Dubinin-Radushkevich isotherm best fit

4.3.2 Effects of pH and temperature

The effect of pH in the fluoride sorption process was investigated, where pH in the range of 3 to 11 were tested, as illustrated in **Fig. 4.8 a)**. Solution pH 7 showed the highest loading capacities, and pH 5 and 7 have comparably high fluoride loading capacities. However, as the solution pH further decreases or increases, the loading capacities starts to decline. At pH 11, it is postulated that the increased concentration of hydroxide in solution competes with fluoride for the available anionic sorption sites. Whereas, at pH 3, as seen in **Fig. 4.8 b)**, the substantial amount of aluminum stripping during the loading process rather reduces the aluminum sorption sites for fluoride, which eventually decreases the fluoride loading capacities to a great extent. This is indicated by the lowest loading capacities as compared to other isotherms results with different operating pH.

Temperature was also varied, as seen in **Fig. 4.9**, where temperature during the loading process was initially elevated to 318 K from 303 K. The Dubinin-Radushkevich isotherm model was used to fit the data. Although the model estimated that higher temperature results in lower maximum loading capacity, it did not accurately predict the higher equilibrium concentration range. By visual observation of the experimental data, no significant change in loading capacities was seen between these two different conditions.

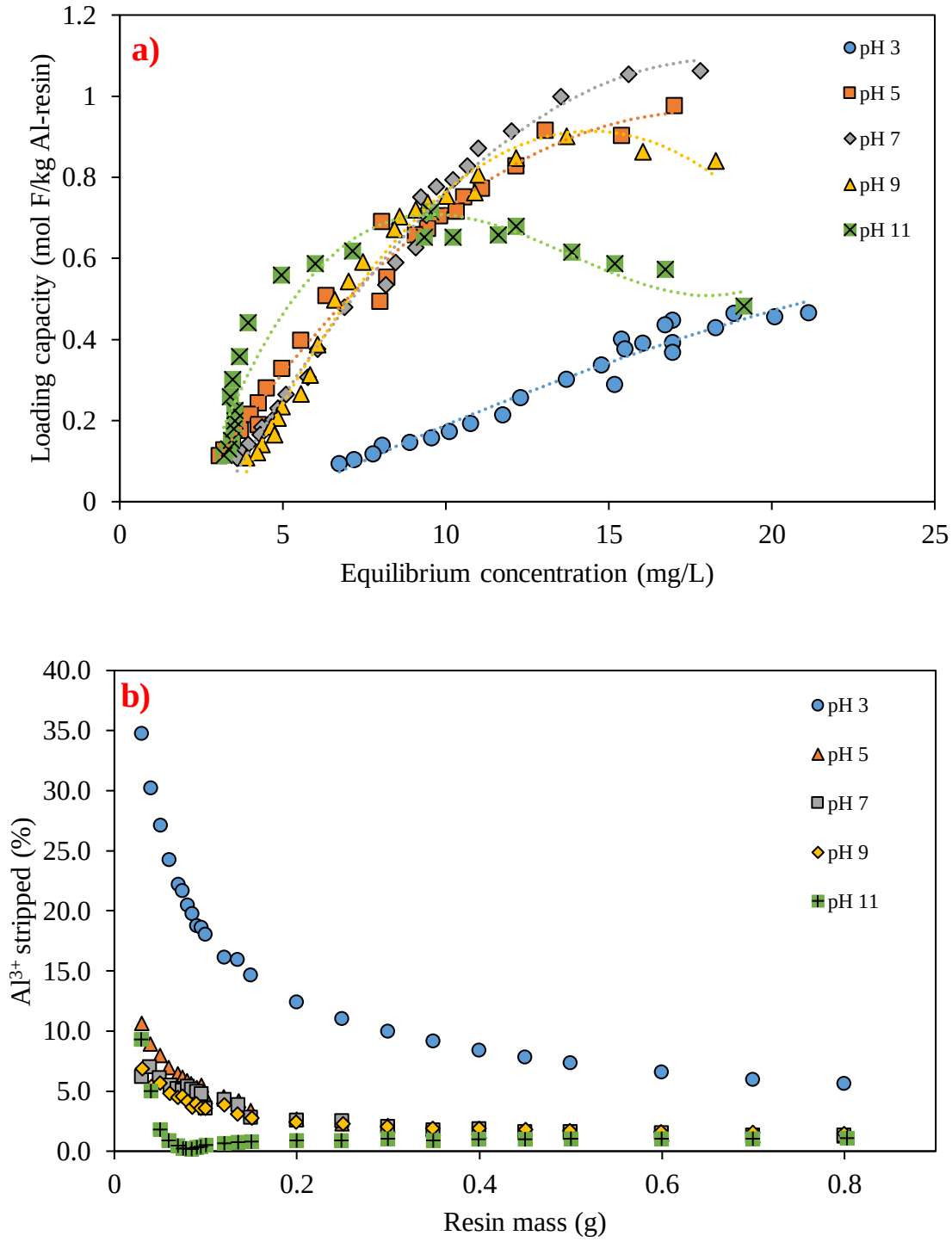

Figure 4. 8 a) Loading curves of F^- on Al^{3+} pre-loaded Monoplus TP 260 resin in solution pH of 3 - 11 (303 K; Initial conc. ~25 ppm F^-; 12 wt.% Na_2SO_4), b) Aluminum leakage (%) during the sorption process from the Al^{3+} loaded resins; • Experimental data

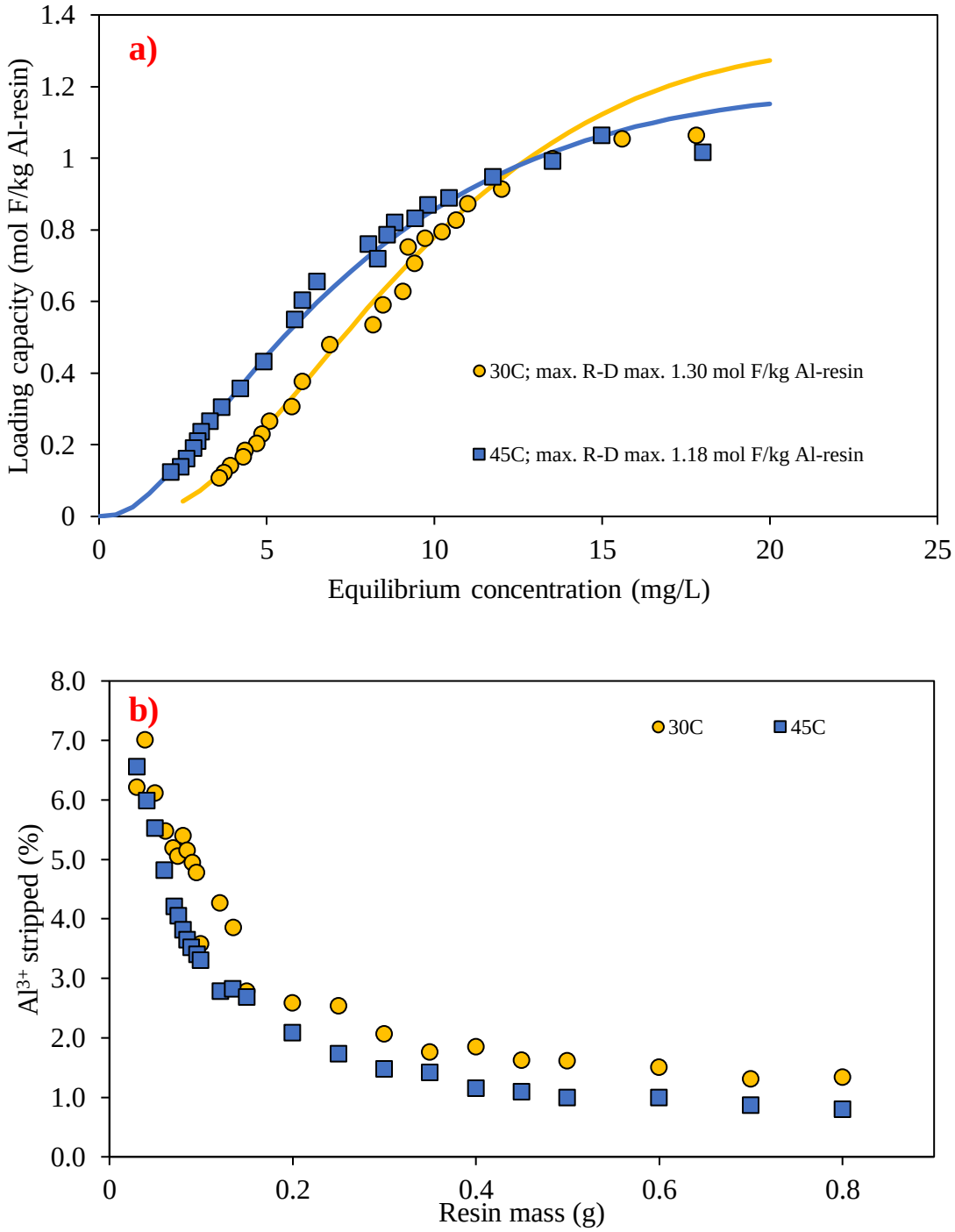

Figure 4. 9 a) Equilibrium isotherms of F^- on Al^{3+} pre-loaded Monoplus TP 260 resin in solution Temperature of 303 and 318 K (Initial conc. ~25 ppm F^-; 12 wt.% Na_2SO_4; pH 7), b) Aluminum leakage (%) during the sorption process from the Al^{3+} loaded resins; • Experimental data, — Dubinin-Radushkevich isotherm best fit

4.4 Fluoride Batch isotherm study with Zr-resin

4.4.1 Effect of Na_2SO_4

In the Zr^{4+} pre-loading step, approximately 0.35 mol Zr^{4+}/L resin was loaded. **Fig 4.10 a)** illustrates the equilibrium isotherms of F^- on Zr^{4+} pre-loaded Monoplus TP 260 AMPA type resin with the variation of Na_2SO_4 brine concentration. Although further comprehensive chemical analysis on the speciation of the Zr in the resin needs to be determined in the future, a number of possible loading reactions between the Zr pre-loaded resin and fluoride ions are shown below:

$$R_2ZrO + F^- + H_2O = R_2Zr(OH)F + OH^- \quad (4.1)$$

$$R_2ZrO + 2F^- + H_2O = R_2ZrF_2 + 2OH^- \quad (4.2)$$

Based on the Langmuir model projections, the increase in Na_2SO_4 concentration slightly increases the fluoride loading capacities, where the loading capacities of 0.68, 0.70, 0.72 mol F^-/kg Zr-resin were obtained in 6, 12, 24 wt.% Na_2SO_4 solution, respectively. However, the Langmuir model does not fit with the experimental data of 6 wt.% Na_2SO_4 solution at higher range of equilibrium concentration range. This phenomenon is still unclear, but the maximum loading capacity of 0.68 mol F^-/kg Zr-resin is slightly overestimated considering the visual observation of the data.

Similar to fluoride adsorption on the Al-resin, the presence of Na^+ and SO_4^{2-} does not affect the loading capacities. In comparison with Al pre-loaded resin, Zr pre-loaded resin was observed to have 46% less fluoride loading capacity at 12 wt.% Na_2SO_4. However, in consideration of the amount of zirconium pre-loaded on the resin as compared to the aluminum pre-loaded, fluoride loading capacities of Zr-resin are considerably higher on mol/mol Zr basis.

As seen in **Fig 4.10 b)**, zirconium leakage during loading process is substantially lower than aluminum leakage from Al-resin. All of samples had less than 1 mg/L of zirconium leakage, which is an indicative of its great stability with AMPA chelated resin. It is postulated that zirconium, having higher charge than aluminum, forms stronger bonds with the functional group of the resin.

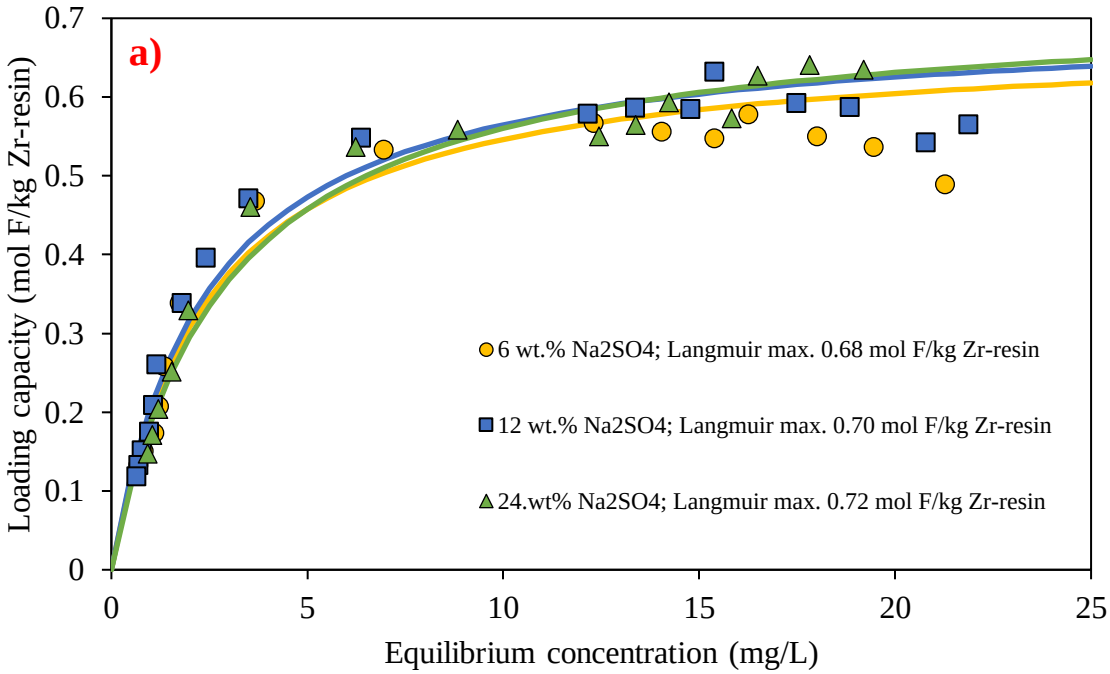

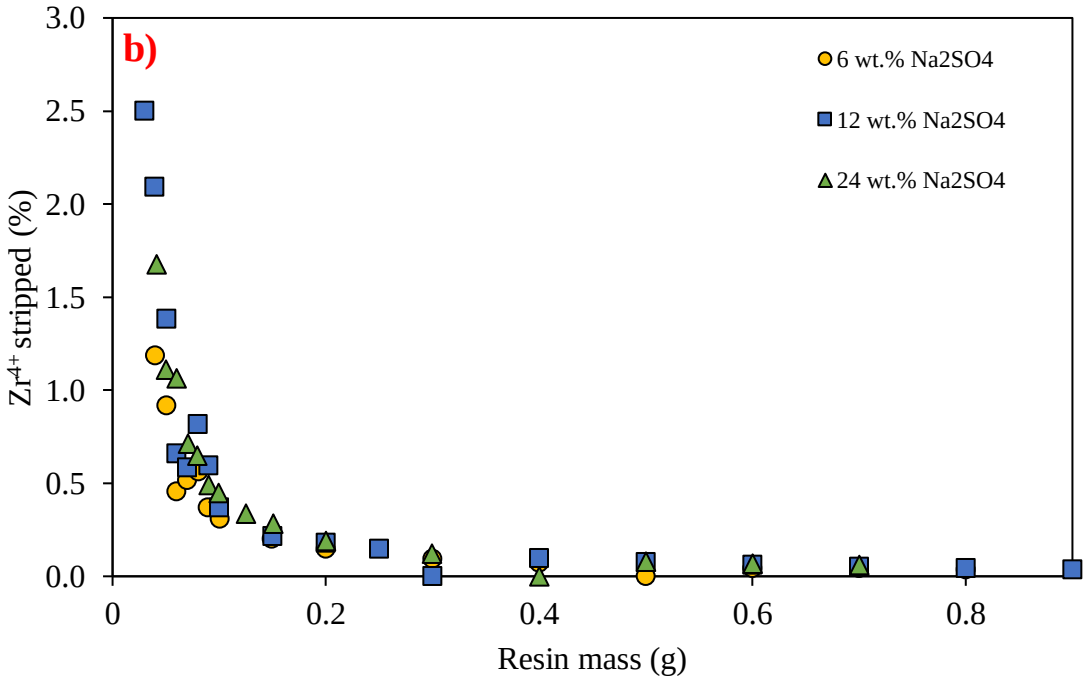

Figure 4. 10 a) Equilibrium isotherms of F^- on Zr^{4+} pre-loaded Monoplus TP 260 resin in 0 - 24 wt.% Na_2SO_4 solution (303 K; Initial conc. ~25 ppm F^-; pH 7), b) Zirconium leakage (%) during the sorption process from the Zr^{4+} loaded resins; • Experimental data, — Langmuir isotherm best fit

4.4.2 Effect of pH and temperature

The effect of pH in fluoride sorption process was investigated, where pH in the range of 3 to 11 were tested, as illustrated in **Fig. 4.11 a)**. pH in the range of 5 – 9 showed relatively high fluoride loading capacities. However, as the solution pH increases to 11, the loading capacities starts to decline, likely due to the increased concentration of hydroxide in solution that competes with fluoride for the anionic sorption sites. As for pH 3, unlike Al-resin, the fluoride loading capacity of Zr-resin was the highest. A spike of loading capacity in the high end of equilibrium concentration range was observed for pH 3. The Langmuir maximum loading capacities of 0.79, 0.67, 0.70, 0.62, and 0.40 mol F^-/kg Zr-resin were obtained with solution pH of 3, 5, 7, 9, and 11, respectively. However, the Langmuir model does not fit well to the loading isotherm at pH 11. More comprehensive chemical analysis is needed to have a concrete understanding on the batch isotherm studies in the future.

The notable difference as compared to Al-resin is the amount of zirconium leakage during the loading process at acidic condition of pH 3, as seen in **Fig. 4.11 b)**, where zirconium leakage was reported to be under 1 mg/L Zr^{4+} in solution. This is a clear indication that zirconium is much more strongly bonded with the functional group of the resin than the bonds between aluminum and resin.

Temperature was also changed in the range of 303 – 333 K, as seen in **Fig. 4.12**. According to the Langmuir isotherm model, the fluoride loading capacities of 0.70, 0.49, 0.33 mol F/kg Zr-resin were estimated at 303, 318, and 333 K, respectively. The decrease in loading capacity with the increase in temperature indicates that fluoride adsorption is an exothermic process.

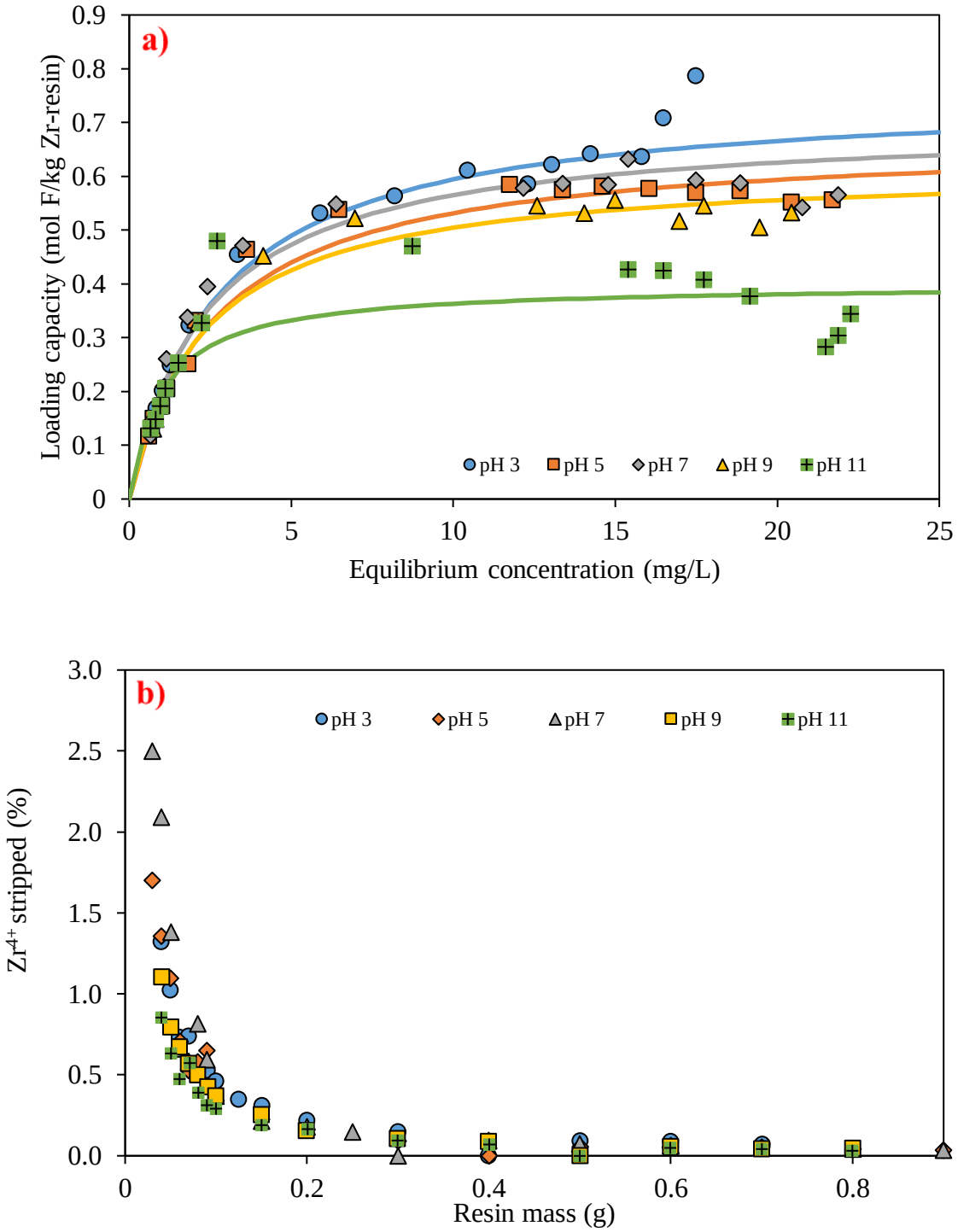

Figure 4. 11 a) Loading curves of F^- on Zr^{4+} pre-loaded Monoplus TP 260 resin in solution pH of 3 - 11 (303 K; Initial conc. ~25 ppm F^-; 12 wt.% Na_2SO_4), b) b) Zirconium leakage (%) during the sorption process from the Zr^{4+} loaded resins; • Experimental data, — Langmuir isotherm best fit

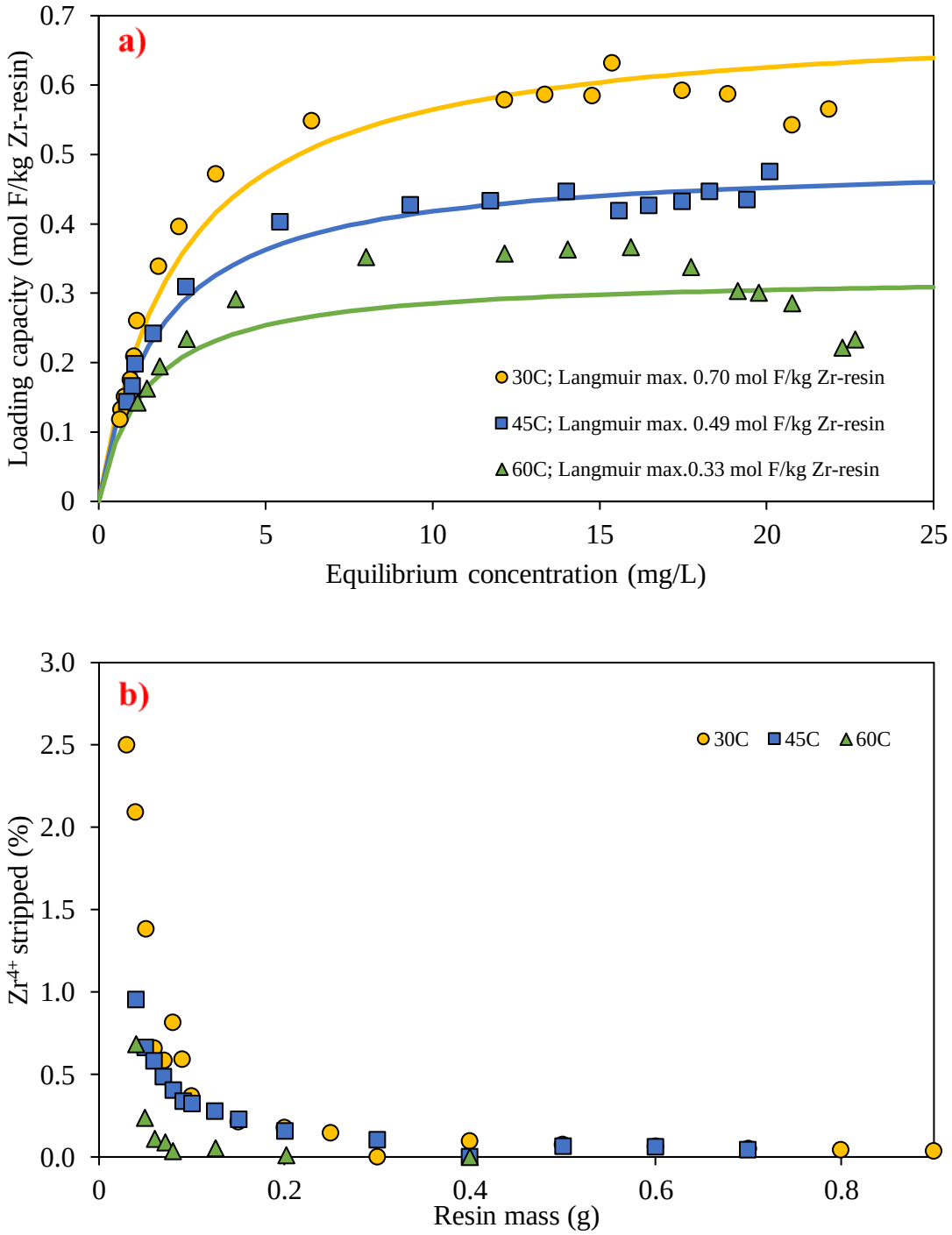

Figure 4. 12 a) Equilibrium isotherms of F^- on Zr^{4+} pre-loaded Monoplus TP 260 resin in solution Temperature of 303, 318, and 333 K (Initial conc. ~25 ppm F^-; 12 wt.% Na_2SO_4; pH 7), b) Zirconium leakage (%) during the sorption process from the Zr^{4+} loaded resins; • Experimental data, — Langmuir isotherm best fit

Chapter 5: Column Fluoride Removal with Pre-loaded Resins

5.1 Pre-loading Metal Regeneration Cycles

5.1.1 Aluminum pre-loaded resin

A column loading trial was first conducted with $Al_2(SO_4)_3$ pre-loaded Monoplus TP 260 resin with the initial fluoride concentration of 25 mg/L in a 12 wt.% Na_2SO_4 brine solution. After the resin was fully loaded with fluoride, it was regenerated with $Al_2(SO_4)_3$ pre-loading solution. Previously, the case study conducted by Oke et al. [66] provided a suggestion that the regeneration can be carried out with Al pre-loading solution, where it was postulated that fluoride on the resin would be removed to the eluent due to the shift of equilibrium. As for the Al-F regenerants, solution pH is adjusted to between 5 – 7. Al-F precipitates can be filtered out, and regenerants free of aluminum and fluoride can be safely disposed. Further investigation is however needed to find an effective regenerant removal step.

Fig. 5.1 illustrates three loading cycles with aluminum sulfate regeneration steps. It is a clear indication that the resin can be recycled by this regeneration method. Instead of conventional ion exchange resin regeneration method that incorporates multiple steps, 1) pre-loading of resin, 2) loading of F^-, 3) H_2SO_4 stripping, 4) NaOH regeneration, this pre-loading metal regeneration route can simplify the fluoride removal system.

Nevertheless, there was a reduction in loading capacity of 0.6 g F/L resin as the next cycle proceeds. Although, the fluoride concentration in effluent below 1 mg/L could be achieved in the first cycle, the minimum F^- concentration in the initial part of the loading process gradually increases as the next loading cycle proceeded.

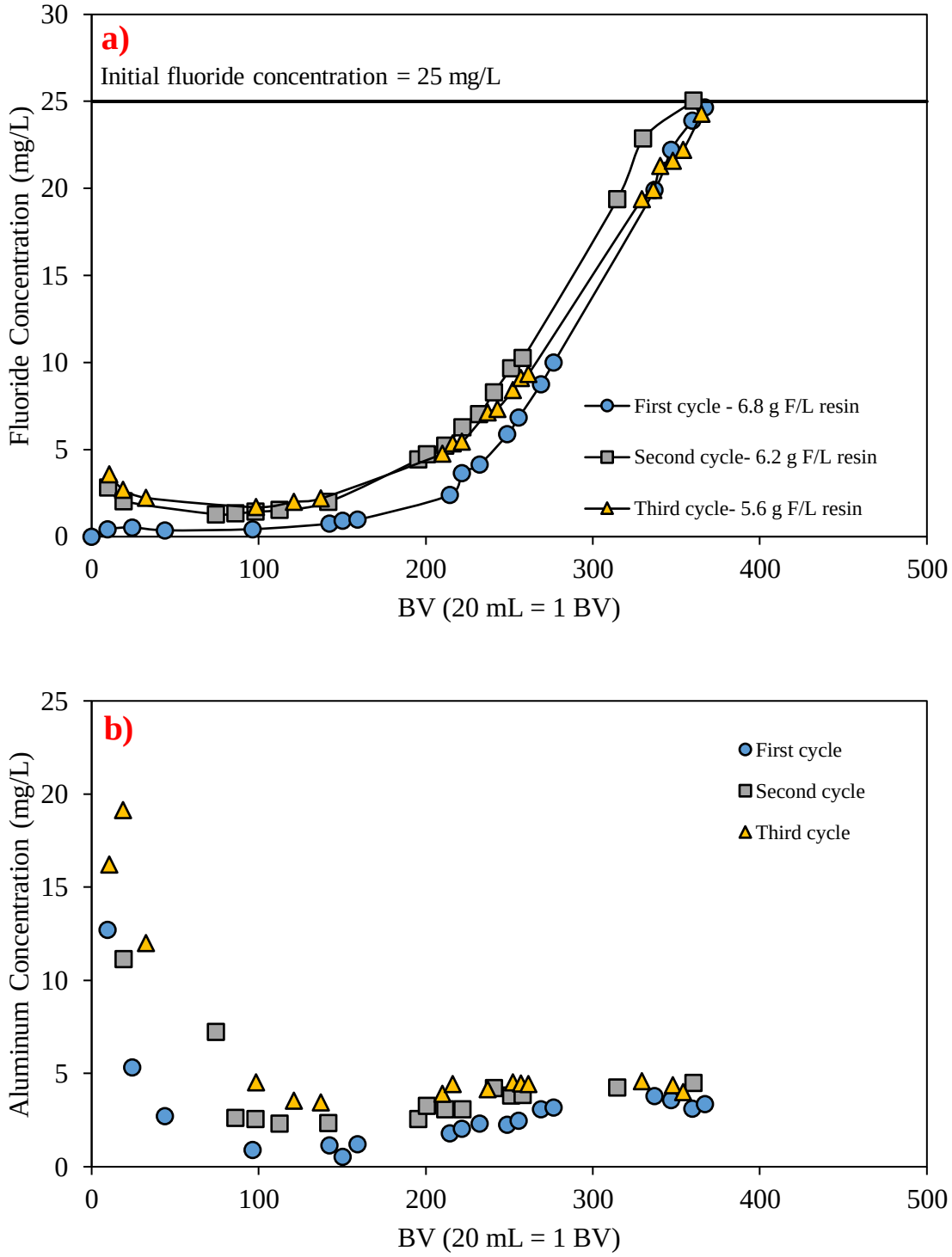

Figure 5. 1 a) Column breakthrough curves of F^- on Al^{3+} pre-loaded Monoplus TP 260 with $Al_2(SO_4)_3$ regeneration cycles (Initial conc. ~25 ppm F^-; 12 wt.% Na_2SO_4; 303 K; pH 7; 5 BV/hr), b) Aluminum leakage during the sorption process

5.1.2 Zirconium pre-loaded resin

Monoplus TP 260 resin with zirconium sulfate pre-loaded was also investigated with a cyclical column trial. After the exhaustion of the resin, it was regenerated with $Zr(SO_4)_2$ pre-loading step solution where fluoride on the resin is stripped off by high concentration of zirconium in solution. Hence, it is also expected the resin in zirconium form can be recycled as fluoride makes contact in the next loading cycle.

Fig. 5.2 shows the breakthrough curves of three loading cycles, where the loading capacities substantially increases as the next cycles proceed. At the end of the third cycle, fluoride loading capacity was comparable with the loading capacity of aluminum pre-loaded resin reported in the first cycle. Previously, Fig. 4.5 b) indicates that the resins cannot be fully saturated with Zr in the first pre-loading phase due to the use of very low pH. Therefore, the increase in loading capacity in the later loading cycles may be due to further adsorption of zirconium on the unexploited sites of the resins that provides additional fluoride adsorption sites.

In addition to its profound performance in terms of resin recyclability, it was once again proven that the use of zirconium has minimal metal leakage during the loading process, which makes it an attractive option. As observed in stripping analysis in Section 4.2.3, zirconium is the most tightly bound ion on the resin, resulting in zirconium leakage of less than 1 mg/L throughout the fluoride loading process. Along with this extremely low zirconium leakage, the most notable finding from the use of Zr pre-loaded resins that differentiate it from Al pre-loaded resins is its capability of reducing the effluent fluoride concentration below 0.5 mg/L in all three fluoride loading cycles.

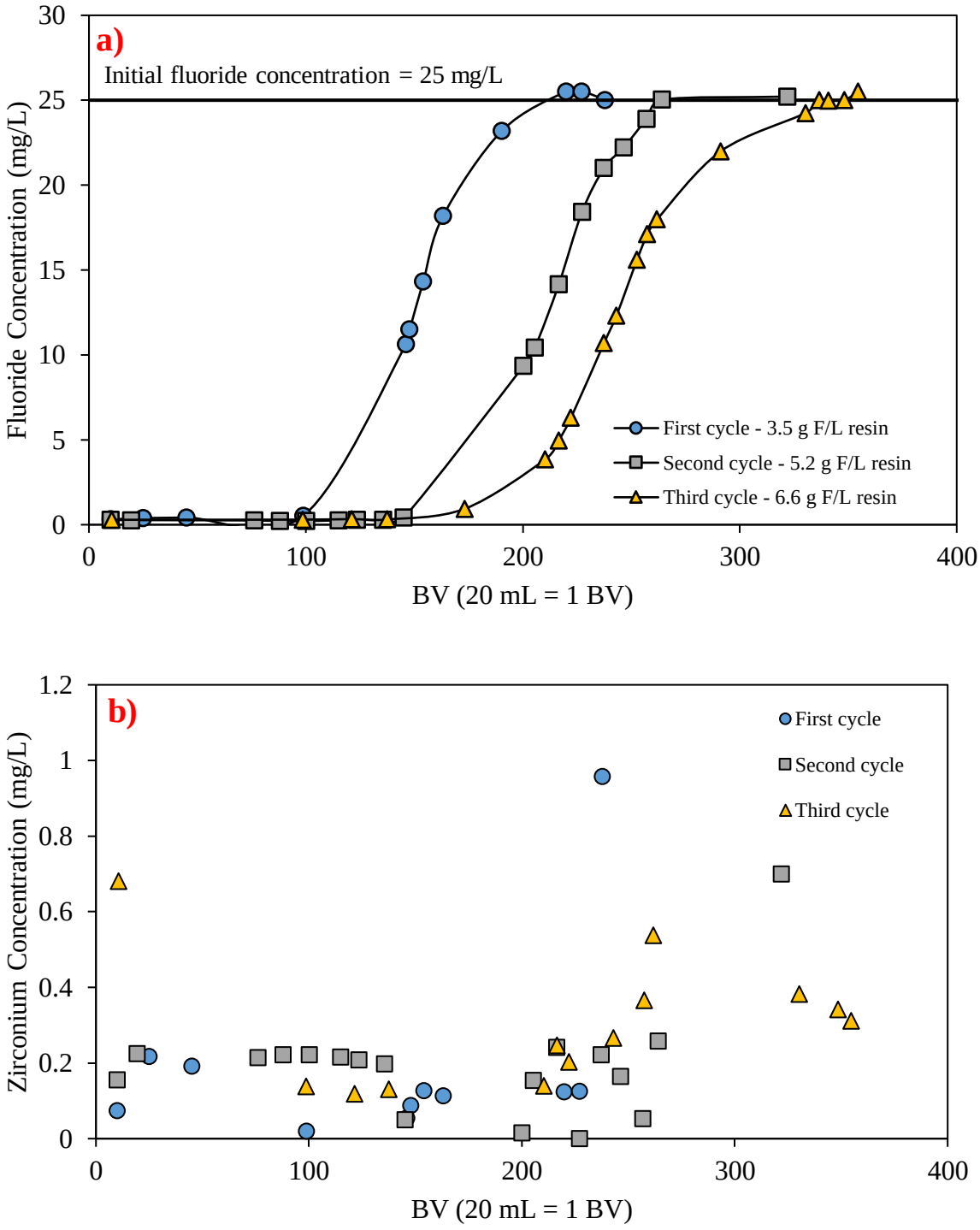

Figure 5. 2 a) Column breakthrough curves of F^- on Zr^{4+} pre-loaded Monoplus TP 260 with $Zr(SO_4)_2$ regeneration cycles (Initial conc. ~25 ppm F^-; 12 wt.% Na_2SO_4; 303 K; pH 7; 5 BV/hr), b) Zirconium leakage during the sorption process

5.2 Acid Regeneration Cycles

5.2.1 Aluminum pre-loaded resin

After the fluoride loading process with Al pre-loaded resin, the exhausted resins were regenerated with 0.1 M H_2SO_4 solution. No additional pre-loading step was conducted before the onset of second loading cycle. **Fig. 5.3** indicates the significant reduction in fluoride loading capacities as the next cycle follows. This implies that protons not only pull fluoride off from the resin, but also aluminum off from the resin, resulting in loss of sorption sites in the subsequent loading cycles. Approximately 56 % reduction in loading capacity was reported in comparison between first and second loading cycle. Therefore, this regeneration method is not an effective route for the fluoride removal system, unless Al is loaded again.

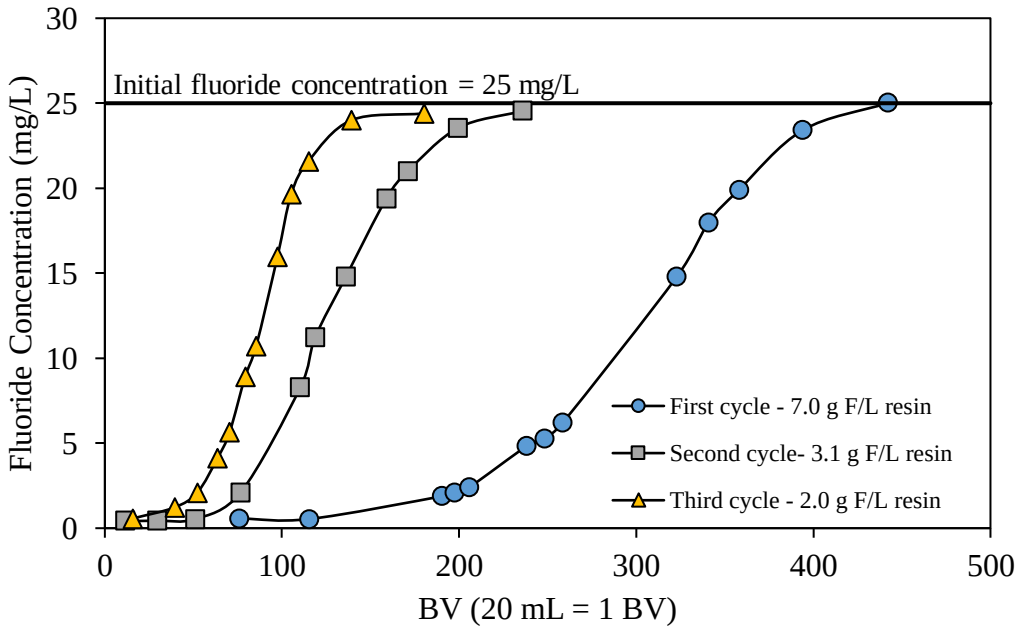

Figure 5. 3 a) Column breakthrough curves of F^- on Al^{3+} pre-loaded Monoplus TP 260 with 0.1 M H_2SO_4 regeneration cycles (Initial conc. ~25 ppm F^-; 12 wt.% Na_2SO_4; 303 K; pH 7; 5 BV/hr)

5.2.2 Zirconium pre-loaded resin

In this section, fluoride loaded zirconium pre-loaded resins were regenerated with 1.0 M H_2SO_4. This was also repeated with 1.0 M NaOH base. **Fig. 5.4** illustrates the column loading trials with acid and base regeneration cycles. In terms of H_2SO_4 acid regeneration routes, approximately 36% reduction of fluoride loading capacity in the second cycle was reported as compared to the loading capacity in the first cycle. This result indicates that a sole use of H_2SO_4 as a regeneration method is not optimal to fully regenerate the resins. Nevertheless, the reduction in loading capacity is not as significant as aluminum pre-loaded resins, which is indicative of the greater stability of the zirconium-resin complexes.

With the NaOH regeneration routes, a small fraction of fluoride was loaded in the second loading cycle. As previously investigated in the batch isotherm study, hydroxide species compete with fluoride for the zirconium sorption sites on the resins during the loading process. Likewise, this column trial result indicates that as high concentration of hydroxide exchanges with fluoride complexed with zirconium, these replaced hydroxide species are so tightly bound to the zirconium on the resins, resulting in difficulty in the loading of fluoride as the next cycle proceeds. Indeed, as illustrated in **Table 5.1**, although the formation constant of fluoride with zirconium is much higher than with sulfate, it is still substantially lower than with hydroxide ligand.

Table 5. 1 Cumulative formation constant for metal complexes [72]

Ligand with Zr	$\log\beta_1$	$\log\beta_2$	$\log\beta_3$	$\log\beta_4$
Fluoride	8.8	16.12	21.94	-
Sulfate	3.79	6.64	7.77	-
Hydroxide	14.3	28.3	41.9	55.3

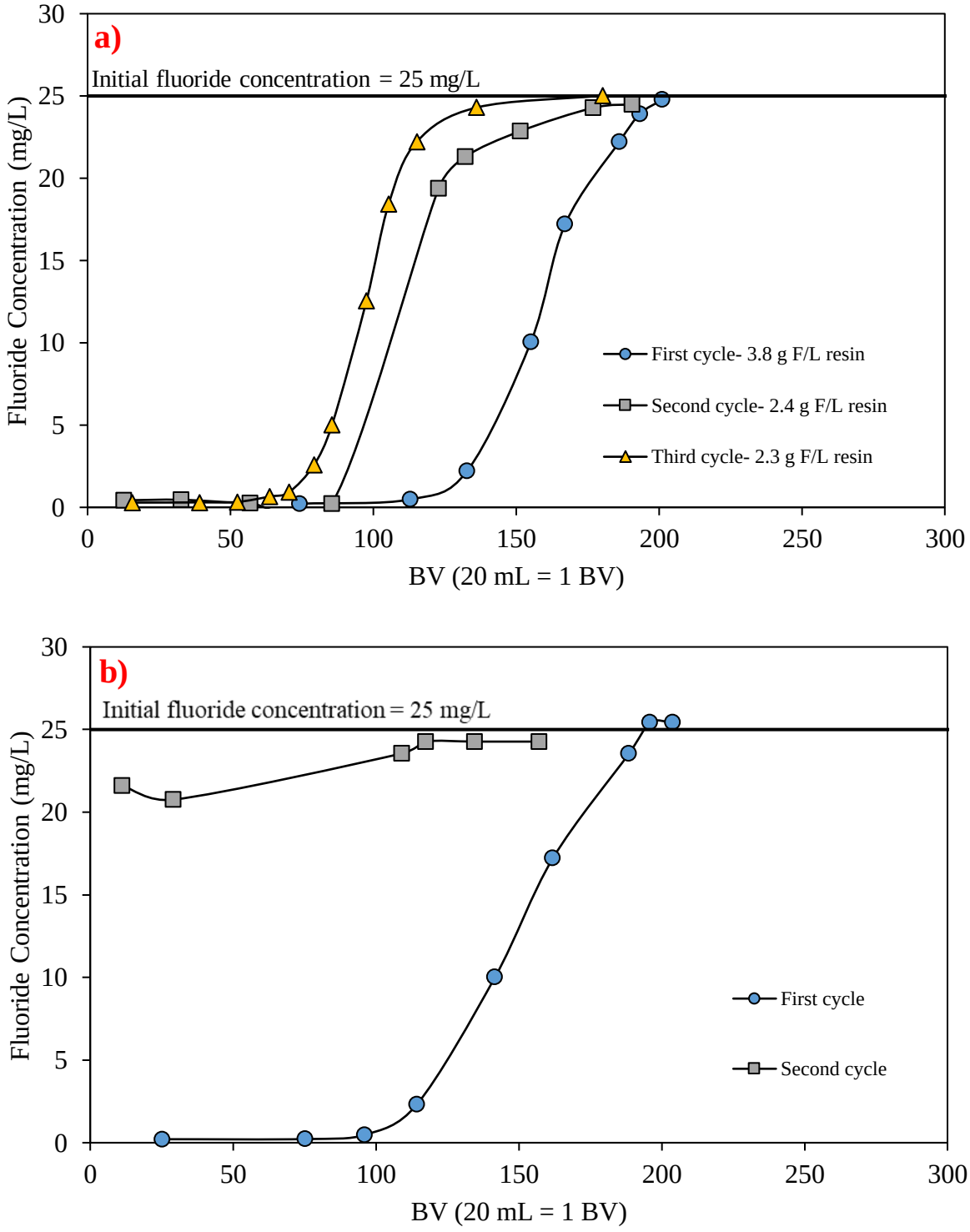

Figure 5. 4 Column breakthrough curves of F^- on Zr^{4+} pre-loaded Monoplus TP 260 with a) 1.0 M H_2SO_4 b) 1.0 M NaOH regeneration cycles (Initial conc. ~25 ppm F^-; 12 wt.% Na_2SO_4; 303 K; pH 7; 5 BV/hr)

5.3 Aluminum-Fluoride Co-loading Cycles

Instead of incorporating regeneration routes, aluminum was rather injected into the brine solution containing fluoride. The formation of aluminum and fluoride complexes in brine solution is expected to occur and co-load on the functional sites of sodium form Monoplus TP 260 resin. For the fractional amount of aluminum that does not form complexes with fluoride, it is expected to exchange with sodium on the resins and provide sorption sites for the incoming fluoride. Indeed, as seen in **Fig. 5.5**, for the first 200 BV, the fluoride concentration in effluent was reduced to approximately 15 mg/L from the initial concentration of 25 mg/L, and the aluminum was also loaded readily, below 1 mg/L. Although, further study utilizing different operating conditions is required to confirm the efficacy of this process, this provides a possibility of minimizing the regeneration cycles.

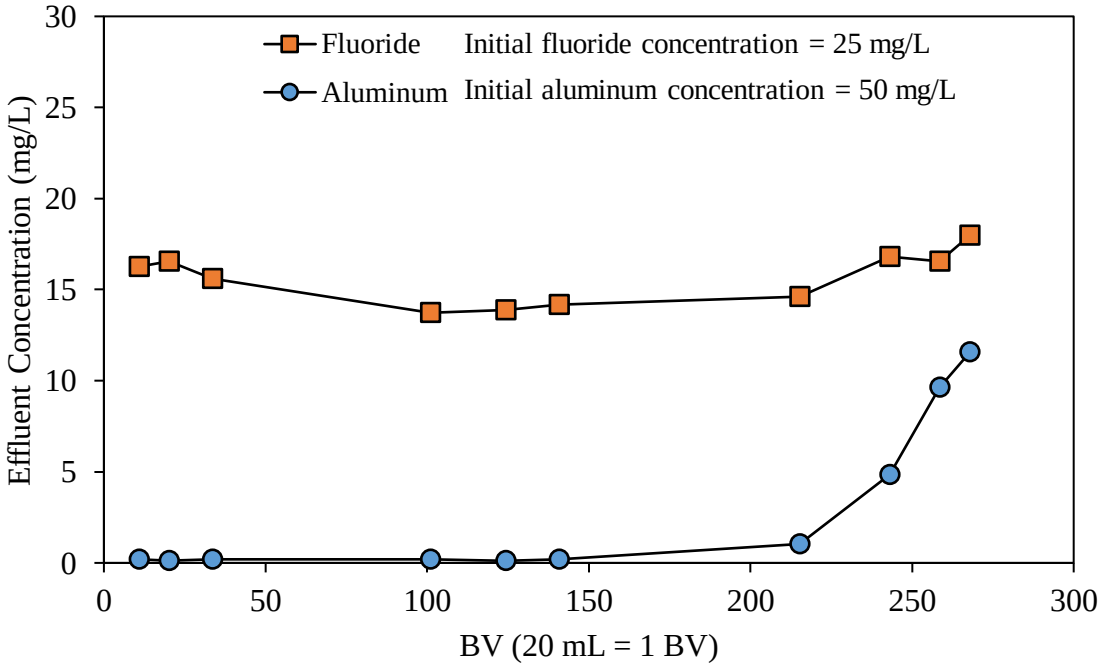

Figure 5. 5 Column loading of Al^{3+} and F^{-} on Na^{+} form Monoplus TP 260 (12 wt.% Na_2SO_4; 303 K; pH 5; 5 BV/hr)

Chapter 6: Conclusion and Future Work

6.1 Summary

The main purpose of this study was to investigate Lanxess' LEWATIT Monoplus TP 260 resin in selectively removing fluoride from brine solution, specifically concentrated sodium sulfate solution. In order to quantify and assess the performance of this AMPA group resin, a series of batch and column tests were conducted under various operating conditions; and different regeneration routes were explored to examine whether this resin can be reused for numerous cycles. The following is a review of the results.

- Problems with fluoride determination in the presence of high background concentration at various solution pH using an ion selective electrode can be overcome by the use of the standard addition method. The addition of Total Ionic Strength Adjusting Buffer (TISAB) in the samples is imperative to adjust the sample pH and ionic strength, stabilizing the potential reading. TISAB IV can specifically reduce the interference from other fluoride complexing elements such as aluminum and iron.
- Calcium and magnesium batch isotherm study provided baseline data for a direct comparison of the loading capacities for other ions. Approximately 1.1 mol/kg loading onto the Na-resin was attained for both calcium and magnesium from 12 wt.% Na_2SO_4 solution at initial pH 7.0. This data was then compared with Al^{3+} and Zr^{4+} loading capacities, where Al^{3+} loading capacity was comparable with the Ca^{2+} and Mg^{2+} loading capacity. Zirconium exhibited lower loading capacity, primarily attributed to the operating pH of 1.5 due to its solubility limit. This baseline data was comparable with Ca^{2+} and Mg^{2+} loading capacities of the same type of the resin reported by Zhang et al. [69].

- With the resin in either aluminum or zirconium pre-treated form, fluoride loading capacities in 12 wt.% Na_2SO_4 solution at pH 7 are 1.30 mol F/kg Al-resin and 0.70 mol F/kg Zr-resin. As loading is highly dependent on pH, an effective pH range for the fluoride sorption is 5 to 9 for Al-resin and 3 to 9 for Zr-resin. Increase in temperature results in the decrease in fluoride loading capacity.
- The column trials with $Al_2(SO_4)_3$ and $Zr(SO_4)_2$ regeneration steps results in fluoride loading capacities of 6.8 g F/L Al-resin and 3.5 g F/L Zr-resin in the first cycle, in which Al-resin exhibited much higher loading capacity. However, as the repeated tests proceed up to 3 cycles, fluoride loading capacity of Al-resin decreased by 9%; whereas fluoride loading capacity of Zr-resin actually increased by 44%. Metal leakage was also monitored where much higher leakage was seen from Al-resin than the Zr-resin throughout the test work. Unlike the Al-resin, the Zr-resin reduced the fluoride concentration below 0.5 mg/L throughout all three loading cycles. The superior stability of zirconium on TP 260 resin was previously confirmed with the stripping test.
- The H_2SO_4 acid regeneration route was investigated where a substantial decline in fluoride loading capacities was observed as the next cycle proceeded. The loading capacity of the Zr-resin, however, exhibited a reduction to a lesser degree. It is apparent that a certain degree of displacement of metal ion by H^+ displaces metal ions out from the resin, decreasing available fluoride sorption sites. Displacement of F- from the resin as HF did not appear to occur.

6.2 Conclusion

An ion exchange resin, especially pre-loaded with metal ions that complex fluoride has been shown to provide promising performance in providing fluoride sorption sites. In this study,

three questions were posed with regards to LANXESS Lewatit Monoplus TP 260 resin. Al and Zr pre-loaded resins were separately tested in which each proved to have its own value.

1. What is the fluoride loading capacity of TP 260 resin?

With 12 wt.% Na_2SO_4 solution at pH 7, 1.30 mol F/kg Al-resin and 0.70 mol F/kg Zr-resin were attained. LANXESS states that Monoplus TP 260 resin is specific for selectively removing transition heavy metal and alkaline earth metals, and thus, considering the resin capacity as indicated by Ca^{2+} and Mg^{2+} loading, fluoride loading capacity of Al-resin is concluded to be outstanding. Zr-resin also showed relatively high loading capacity considering the amount of Zr initially loaded onto the resin. However, the most notable advantage of utilizing Zr-resin is its minimal Zr leakage during the loading process, and its capability to reduce the fluoride concentration in effluent below 0.5 mg/L throughout all the loading cycles trialed in this thesis. In addition, although Zr-resin may have comparably low fluoride loading capacities in the first few cycles, it would eventually surpass the loading capacity of Al-resins with further loading of zirconium on the unexploited sites of the resins in the next regeneration cycles.

2. What are the factors affecting fluoride adsorption on TP 260 resin?

Batch isotherms were established with the change in Na_2SO_4 concentration, solution pH, and temperature. Unlike Ca^{2+} and Mg^{2+}, which display a significant reduction in loading capacity with the increase in Na_2SO_4 concentration, fluoride loading capacities of both Al and Zr pre-loaded resin were not adversely impacted by the increase in Na_2SO_4 concentration, and thus, excess of sodium and sulfate ions proved not to interfere with fluoride adsorption. Processes with ion exchange resins involved are generally influenced by solution pH, and Monoplus TP 260 resin was no exception. A significant reduction in the loading capacities were noticed if

operated outside of the recommended pH range, especially with Al pre-loaded resin. Increasing operating temperature was also another factor that decreases fluoride loading capacities.

3. What are the regeneration strategies?

As the resin in column reaches the exhaustion point, a regeneration step needs to be conducted. High concentrations of $Al_2(SO_4)_3$ and $Zr(SO_4)_2$ as regenerants shift the chemical equilibrium of the resin and effectively strip out fluoride from the resin, refreshing the sorption sites for the next loading cycle. Especially for the Zr-resin, the loading capacities were observed to rather improve with subsequent regeneration cycles. By the end of third loading cycle, fluoride loading capacity of Zr-resin surpassed the Al-resin performance for fluoride adsorption. However, this regeneration strategy results in significant chemical consumption. In an effort to minimize the cost, H_2SO_4 acid regeneration was attempted, but stripping of pre-loaded ions results in adverse impact on the next loading cycle, especially for Al-resin primarily due to lower stability of Al complexation with the resin compared than with Zr.

Upon reflection on the column trials, the establishment of a robust Zr-resin system may be possible if $Zr(SO_4)_2$ regeneration cycle is used until it finally reaches its maximum fluoride loading capacity and also utilize H_2SO_4 acid regeneration to minimize Zr reagent consumption.

6.3 Future Work

This work has made a number of findings in IX technology, but also raised a number of issues and questions. Suggested future work listed below could be performed to provide a better understanding of the process.

- As compared to TP 208 resin having iminodiacetate (IDA) functional group studied by Millar et al. [56], Monoplus TP 260 resin having AMPA functional group exhibited higher fluoride loading capacity. However, there is still no clear fundamental understanding in

differentiating the effect of these functional groups on fluoride adsorption. Further study on the resin structure and composition of all different forms of resin, Na-resin, H-resin, Al-resin, Zr-resin, Al-F-resin, and Zr-F-resin by using FTIR analysis may offer some insights on this chelating resin. This analysis would further aid the mass balance associated with the fluoride sorption and pre-loading metals.

- More comprehensive chemical analysis of the batch loading solutions should be required. Speciation of the Zr in the resin needs to be determined, which may be challenging research work. However, this analysis would offer an insight on the chemical reactions' stoichiometries during the loading and regeneration process.
- More cyclical column tests should be conducted to confirm the fluoride loading capacities after numerous regeneration cycles. For instance, the column tests with $Zr(SO_4)_2$ regeneration should be repeated until the resin is completely saturated with zirconium and no further improvement in fluoride loading capacity is observed. In terms of acid regeneration, different acid concentration can be attempted to selectively remove fluoride from the resin while minimizing metal leakage. As for base regeneration, a short acid pre-treatment step should be added after NaOH regeneration step to decrease the amount of hydroxide species on the pre-loaded resin.
- Aluminum and fluoride co-loading process may be beneficial for the application where fluoride spike in short duration is detected in the electrochemical cell feed solution as it does not require pre-treating the resin with aluminum sulfate solution. However, this future direction requires an extensive study as there is no clear comprehension on the effect of Al/F ratio, pH, and the impact of other interfering ions.

- All the tests in this study were conducted with lab grade chemicals with minimal impurities compared to what may exist in the industrial brine solutions. Further verification is required with the actual industrial brine solutions and should be compared with the results in this work.

Bibliography

[1] C. J. Huang, J.C. Liu, "Precipitate flotation of fluoride-containing wastewater from a semiconductor manufacturer," *Water Research* , vol. 33, no. 16, pp. 3403-3412, 1999.

[2] N. Tzanetakis, J. Varcoe, R. S. Slade, K. Scotta, "Salt splitting with radiation grafted PVDF membranes," *Desalination,* pp. 275-282, 2003.

[3] S. M. Davis, G. E. Gray, P. A. Kohl, "Candidate membranes for the electrochemical salt-splitting," *J Appl Electrochem,* p. 777–783., 2008.

[4] Bożenna P., Hanna J., Wojciech M., Mariusz N., Barbara C., Halina S., Paweł M., "Application of electro-electrodialysis for processing of sodium sulphate waste solutions containing organic compounds: Preliminary study," *Journal of Cleaner Production,* pp. 3741-3747, 2017.

[5] D. C. Buzzi, L. S. Viegas, M. A. S. Rodrigues, A. M. Bernardes, J. A. S. Tenórioa, "Water recovery from acid mine drainage by electrodialysis," *Minerals Engineering,* pp. 82-89, 2013.

[6] M. C. Martí-Calatayud, D. C. Buzzi, M. García-Gabaldón. E. Ortega, A. M. Bernardes, J. A. S. Tenório, V. Pérez-Herranz, "Sulfuric acid recovery from acid mine drainage by means of electrodialysis," *Desalination,* pp. 120-127, 2014.

[7] Schiff N., Grosgogeat B., Lissac M., Dalard F., "Influence of fluoride content and pH on the corrosion resistance of titanium and its alloys," *Biomaterials,* vol. 23, no. 9, pp. 1995-2002, 2002.

[8] D. C. Buzzi, L. S. Viegas, M. A. S. Rodrigues, A. M. Bernardes, J. A. S. Tenório, "Water recovery from acid mine drainage by electrodialysis," *Minerals Engineering,* vol. 40, pp. 82-89, 2013.

[9] Y. Zheng, Z. Li, X. Wang, X. Gao, C. Gao, "The treatment of cyanide from gold mine effluent by a novel," *Electrochimica Acta,* vol. 169, pp. 150-158, 2015.

[10] X. Y. Nie, S. Y. Sun, X. Song and J. G. Yu, "Further investigation into lithium recovery from salt lake brines with different feed characteristics by electrodialysis," *Journal of Membrane Science,* vol. 530, pp. 185-191, 2017.

[11] Q. B. Chen, Z. Y. Ji, J. Liu, Y. Y. Zhao, S. Z. Wang and J. S. Yuan, "Development of recovering lithium from brines by selective-electrodialysis: Effect of coexisting cations on the migration of lithium," *Journal of Membrane Science,* vol. 548, pp. 408-420, 2018.

[12] Y. Song and Z. Zhao, "Recovery of lithium from spent lithium-ion batteries using precipitation and electrodialysis techniques," *Separation and Purification Technology,* vol. 206, pp. 335-342, 2018.

[13] B. Pisarska, H. Jaroszek, W. Mikołajczak, M. Nowak, B. Cichy, H. Stopa and P. Markowicz, "Application of electro-electrodialysis for processing of sodium sulphate waste solutions containing organic compounds: Preliminary study," *Journal of Cleaner Production,* vol. 142, no. 4, pp. 3741-3747, 2017.

[14] M. A. Masigol, A. Moheb, A. M. Zeinabad, "An experimental investigation into batch electrodialysis process for removal of sodium sulfate from magnesium stearate aqueous slurry," *Desalination,* vol. 300, pp. 12-18, 2012.

[15] N. Tzanetakis, W. M. Taama, K. Scott, "Salt splitting in a three-compartment membrane electrolysis cell," *Filtration & Separation,* vol. 39, no. 3, pp. 30-38, 2002.

[16] B. F. Severin, T. D. Hayes, "Electrodialysis of concentrated brines: Effects of multivalent cations," *Separation and Purification Technology,* vol. 218, pp. 227-241, 2019.

[17] M. Buarzaiga, "An investigation f the failure mechanisms of aluminum cathodes in zinc electrowinning cells," *The University of British Columbia* , p. [PhD dissertation], 1999.

[18] M. J. Mandry, G. Rosenblatt, "Effect of fluoride ion on anodic behavior of titanium in sulfuric-acid," *Journal of The Electrochemical Society,* vol. 119, pp. 29-32, 1972.

[19] M. Nakagawa, S. Matsuya, K. Udoh, "Effects of fluoride and dissolved oxygen concentrations on the corrosion behavior of pure titanium, and titanium alloys," *Dental Materials Journal,* vol. 21, pp. 83-92, 2002.

[20] Y. Fovet, J.Y. Gal, F. Toumelin-Chemla, "Influence of pH and fluoride concentration on titanium passivating layer: stability of titanium dioxide," *Talanta,* vol. 53, pp. 1053-1063, 2001.

[21] E. B. Valjakova, V. K. Stevkovska, S.Georgieva, K. Ivanovski, C. B. Misevska, A. Mijoska, A. Grozdanov, "Hydrofluoric Acid: Burns and Systemic Toxicity, Protective Measures, Immediate and Hospital Medical Treatment," *Macedonian Journal of Medical Sciences,* vol. 6, no. 11, pp. 2257-2269, 2018.

[22] Brindha K., Elango L., "Fluoride in Groundwater: Causes, Implications and Mitigation Measures," *Applications and Environmental Management,* pp. 111-136, 2011.

[23] "National Institute of Dental and Craniofacial Research," July 2018. [Online]. Available: https://www.nidcr.nih.gov/health-info/fluoride/the-story-of-fluoridation. [Accessed 12 Feb. 2020].

[24] J. Fawell, K. Bailey, J. Chilton, E. Dahi, L. Fewtrell and Y. Magara , "WHO; Fluoride in Drinking-water," 2006. [Online]. Available: https://www.who.int/water_sanitation_health/publications/fluoride_drinking_water_full.pdf.

[25] R. A. Smith, Fluorine compounds, inorganic, hydrogen, New York: John Wiley & Sons, Inc., 2003.

[26] Weinstein L. H., Davison A., Fluoride in the Environment, CABI Publishing, 2003.

[27] N. N. Greenwood, Chemistry of the elements, Butterworth-Heinemann, 1997.

[28] R. M. Smith, A. E. Martell, Critical stability constant, vol. 4, New York: Springer, 1976.

[29] Y. Gan, X. Wang, L. Zhang, B. Wu, G. Zhang and S. Zhang, "Coagulation removal of fluoride by zirconium tetrachloride: Performance evaluation and mechanism analysis," *Chemosphere,* vol. 218, pp. 860-868, 2019.

[30] M. Mohapatra, S.Anand, B. K. Mishra, D. E.Giles and P. Singh, "Review of fluoride removal from drinking water," *Journal of Environmental Management,* vol. 91, no. 1, pp. 67-77, 2009.

[31] S. Sanghratna, T. A. Waghmare, "Fluoride Removal from Water by various techniques: Review," *International Journal of Innovative Science, Engineering and Technology,* vol. 2, no. 9, 2015.

[32] S. Ghorai, K.K. Pant, "Investigations on the column performance of fluoride adsorption by activated alumina in a fixed-bed," *Chemical Engineering Journal,* vol. 98, no. 1-2, pp. 165-173, 2004.

[33] J. Cheng, X. Meng, C. Jing and J. Hao, "La3+-modified activated alumina for fluoride removal from water," *Journal of Hazardous Materials,* vol. 278, pp. 343-349, 2014.

[34] M. M. Shihabudheen, S. Shukla, L. Philip, I. M. Nambi, "Enhanced fluoride removal from drinking water by magnesia-amended activated alumina granules," *Chemical Engineering Journal,* vol. 140, no. 1-3, pp. 183-192, 2008.

[35] S. S. Tripathy, J. Bersillon, K. Gopal, "Removal of fluoride from drinking water by adsorption onto alum-impregnated activated alumina," *Separation and Purification Technology,* vol. 50, no. 3, pp. 310-317, 2006.

[36] K. Young, C. Hweimei, "The Adsorption of Fluoride Ion from Aqueous Solution by Activated Alumina," *Water, Air and Soil Pollution,* vol. 133, no. 1-4, pp. 349-361, 2002.

[37] Y. Tang, X. Guan, T. Su, N. Gao and J. Wang, "Fluoride adsorption onto activated alumina: Modeling the effects," *Colloids and Surfaces A: Physicochemical and,* vol. 337, pp. 33-38, 2009.

[38] C. S. Boruff, "Removal of fluoride from drinking water," *Ind. Eng. Chem.* , vol. 26, no. 1, pp. 69-71, 1934.

[39] J. R. Rumble, CRC Handbook of Chemistry and Physics, Vol. 5, CRC Press, 1977.

[40] P. Melidis, "Fluoride Removal from Aluminium Finishing Wastewater by Hydroxyapatite," *Env. Proc.* , vol. 2, no. 1, pp. 205-213, 2015.

[41] H. Kurosaki, "Reduction of Fluorine-containing Industrial Waste Using Aluminum-Solubility Method," *Oki Technical Review,* vol. 63, 1998.

[42] E. E. Kowalchuk, "Selective fluoride removal by aluminum precipitation & membrane filtration, master of science, thesis," University of New Mexico, 2012.

[43] Y. Zuo, Q. Chen, C. Li, C. Kang and X. Lei, "Removal of Fluorine from Wet-Process Phosphoric Acid Using a Solvent Extraction Technique with Tributyl Phosphate and Silicon oil," *ACS Omega,* vol. 4, pp. 11593-11601, 2019.

[44] J. M. Kuhn., R. S. M. Cashman, J. R. Harlamovs, W. B. Michael, E. M. Buchalter, "Piloting of the Halogon process with Mixer-Settlers and Bateman Pulsed Columns," *Hydrometallurgy,* vol. 1, 2003.

[45] J. Li, H. Zhang, J. Zhang, Q. Xiao, X. Du and T. Qi, "Efficient Removal of Fluoride by Complexation Extraction: Mechanism and Thermodynamics," *Environ. Sci. Technol.* , vol. 53, no. 15, pp. 9102-9108, 2019.

[46] P. I. Ndiaye, P. Moulin, L. Dominguez, J. C. Millet and F. Charbita, "Removal of fluoride from electronic industrial effluentby RO membrane separation," *Desalination,* vol. 173, no. 1, pp. 25-32, 2005.

[47] D. Dolar, K. Košutić and B. Vučić, "RO/NF treatment of wastewater from fertilizer factory — removal of fluoride and phosphate," *Desalination,* vol. 265, no. 1-3, pp. 237-241, 2011.

[48] I. Bejaoui, A. Mnif and B. Hamrouni, "Performance of Reverse Osmosis and Nanofiltration in the Removal of Fluoride from Model Water and Metal Packaging Industrial Effluent," *Separation science and technology,* pp. 1135-1145, 2013.

[49] M. J. Hudson, "Coordination Chemistry of Selective Ion Exchange Resin," in *Ion Exchange Science and Technology* , NATO ASI Series, 1985.

[50] "Ion Exchange Resins Market," 2018. [Online]. Available: http://ezproxy.library.ubc.ca/login?url=https://search-proquest-com.ezproxy.library.ubc.ca/docview/2079812669?accountid=14656.

[51] P. Sahu and R. Jaiswani, "Ion Exchange Resins: An approach for the Development of advanced Materials with Industrial, Pharmaceutical and Clinical," *International journal of advanced research, ideas, and innovation in technology* , vol. 4, no. 1, 2018.

[52] H. Paudyal, K. Inoue, H. Kawakita, K. Ohto, H. Kamata and S. Alam, "Removal of fuoride by efectively using spent cation exchange," *The Journal of Material Cycles and Waste Management* , vol. 20, no. 2, pp. 975-984, 2018.

[53] Y. Ku, H. M. Chiou, W. Wang, "The removal of fluoride ion from aqueous solution by a cation synthetic resin," *Separation Science and Technology*, vol. 37, pp. 89-103, 2002.

[54] M.T. Samadi, M. Zarrabi, M.N. Sepehr, S.M. Ramhormozi, S. Azizian, A. Amrane, "Removal of fluoride ions by ion exchange resin: kinetic and equilibrium studies," *Environ. Eng. Manage. J.*, vol. 13, pp. 205-214, 2014.

[55] N. Viswanathan and S. Meenakshi, "Role of metal ion incorporation in ion exchange resin on the selectivity," *Journal of Hazardous Materials*, vol. 162, pp. 920-930, 2009.

[56] G. J. Millar, S. J. Couperthwaite, D. B. Wellner, D. C. Macfarlane and S. A. Dalzell, "Removal of fluoride ions from solution by chelating resin with iminodiacetate functionality," *Journal of Water Process Engineering*, vol. 20, pp. 113-122, 2017.

[57] K. M. Popat, P. S. Anan, B. D. Dasare, "Selective removal of fluoride ions from water by the aluminium form of the aminomethylphosphonic acid-type ion exchanger," *React. Polym.*, vol. 23, pp. 23-32, 1994.

[58] "Product Information Lewatit Monoplus TP 260," LANXESS, 2011. [Online]. Available: https://www.lenntech.com/Data-sheets/Lewatit-MonoPlus-TP-260-L.pdf. [Accessed 2019].

[59] Y. Foo and B. Hameed, "Insights into the modeling of adsorption isotherm systems," *Chemical Engineering Journal,* vol. 156, pp. 2-10, 2010.

[60] N. Ayawei, A. Ebelegi and D. Wankasi, "Modelling and Interpretation of Adsorption Isotherms," *Journal of Chemistry,* 2017.

[61] S. Y. Ho, G. Mckay, "Pseudo-second order model for sorption processes," *Process Biochemistry,* pp. 451-465, 1999.

[62] S. Y. Ho, "Citation review of Lagergren kinetic rate equation," *Scientometrics,* vol. 59, pp. 171-177, 2004.

[63] J. Lehto, R. Harjula, "Experimentation in ion exchange studies - the problem of getting reliable and comparable results," *Reactive and Functional Polymers,* vol. 27, no. 2, pp. 121-146, 1995.

[64] G. J. Millar, G. L. Miller, J. C. Sara, S. Papworth, "Factors influencing kinetic and equilibrium behavior of sodium ion exchange with strong acid cation resin," *Separation and Purification Technology,* vol. 163, no. 11, pp. 79-91, 2016.

[65] Y. Liu, "Fluoride removal from Zinc sulfate solution," *The University of British Columbia,* p. [Master's thesis], 2017.

[66] K. Oke, S. Neumann, A. Beryn, "Selective Fluoride Removal," *Water Today,* pp. 76-80, 2011.

[67] G. J. Millar, J. C. Sara, W. C. Leung , "An examination of isotherm generation: Impact of bottle-point method upon potassium ion exchange with strong acid cation resin.," *Separation and Purification Technology,* pp. 366-377, 2015.

[68] R. M. Smith, A. E. Martell, "Critical Stability constant, vol. 6," New York, Springer, 1989, pp. 291-298.

[69] X. Zhang, C. Ye, K. Pi, J. Huang, M. Xia, A. R. Gerson , "Sustainable treatment of desulfurization wastewater by ion exchange and biploar membrane electrodialysis hybrid technology," *Separation and Purification Technology,* vol. 211, pp. 330-339, 2019.

[70] G. J. Millar, S. Papworth, S. J. Couperthwaite, "Exploration of the fundamental equilibrium behavior of calcium exchange with weak acid cation resins," *Desalination,* vol. 351, pp. 27-36, 2014.

[71] E. A Martell, M. R. Smith, Critical stability constant, Boston, MA: Springer, 1982.

[72] J. A. Dean, Lange's Handbook of Chemistry, New York: McGraw-Hill, 1999.

[73] S. Y. Ho, F. J. Porter and G. Mckay, "Equilibrium Isotherm Studies for the Sorption of Divalent Metal Ions onto Peat: Copper, Nickel and Lead Single Component Systems," *Water Air and Soil Pollution,* vol. 141, no. 1-4, pp. 1-33, 2002.

[74] G. J. Millar, Sara J. C., L. A. Dawes, S. Thompson, J. Spencer, "Activated alumina for the removal of fluoride ions from high alkalinity groundwater: New insights from equilibrium and column studies with multicomponent solutions," *Separation and Purification Technology,* vol. 187, pp. 14-24, 2017.

[75] E. L. Grégorio C., "Advantages and disadvantages of techniques used for wasterwater treatment," *Environmental Chemistry Letters,* vol. 17, no. 1, pp. 145-155, 2019.

[76] J. Ramkumar, T. Mukherjee, "Principles of Ion Exchange Equilibria," in *Ion Exchange Technology,* Springer, 2012.

[77] J. Singh, P. Singh, A. Singh, "Fluoride ions vs removal technologies: A study," *Arabian Journal of Chemistry,* vol. 9, pp. 815-824, 2016.

[78] J. Cai, X. Zhao, Y. Zhang, Q. Zhang, B. Pan, "Enhanced fluoride removal by La-doped Li/Al layered double hydroxides," *Journal of Colloid and Interface Science,* vol. 509, pp. 353-359, 2018.

[79] M. M. Dubinin, "The potential theory of adsorption of gas and vapors for adsorbents with energetically nonuniform surface," *Chem. Rev.,* vol. 60, pp. 235-266, 1960.

[80] T. Xue, W. C. Cooper, R. Pascual, S. Saimoto, "Effect of fluoride ions on the corrosion of aluminium in sulphuric acid and zinc electrolyte," *Journal of Applied Electrochemistry,* vol. 21, pp. 238-246, 1991.

Appendices

Appendix A Derivations for kinetic models

In this thesis, pseudo first-order and second-order rate expressions were used to determine the reaction rate limiting step and fit the kinetic data. This section explains the derivation steps for these kinetic models. Lagergren first-order rate equation for the adsorption of an adsorbate from solution is expressed as follows:

$$\frac{dx}{dt} = k_1(X - x) \tag{6.1}$$

Where X and x (mg ·g^{-1}) are the loading capacities at equilibrium and time t, respectively. k_1 (min^{-1}) is the pseudo first-order reaction rate constant. By integrating Eq. 6.1 with the boundary conditions of t = 0 to t = t, Eq. 6.1 is expressed as follows:

$$\ln\left(\frac{X}{X-x}\right) = k_1 t \tag{6.2}$$

and

$$x = X(1 - \exp(-k_1 t)) \tag{6.3}$$

X and x can be expressed in a conventional form of loading capacities, q_e and q_t, respectively.

$$q_t = q_e(1 - \exp(-kt)) \tag{6.4}$$

The linearized form of Eq. 6.4 can be used to determine the rate constant, k, as seen Eq. 6.5

$$\log(q_e - q_t) = \log(q_m) - \frac{k_1 t}{2.303} \tag{6.5}$$

In the case of second-order mechanism, the rate of sorption is expressed as follows:

$$\frac{dx}{dt} = k_2(X - x)^2 \tag{6.6}$$

Where X and x (mg ·g^{-1}) are the loading capacities at equilibrium and time t, respectively. k_2 (g ·mg^{-1} ·min^{-1}) is the pseudo second-order reaction rate constant. By integrating Eq. 6.6 with the boundary conditions of t = 0 to t = t, Eq. 6.6 is expressed as follows:

$$\frac{1}{\mathrm{X}-\mathrm{x}} - \frac{1}{X} = k_2 t \tag{6.7}$$

In addition to the use of loading capacities in the form of q_e and q_t, this can be rearranged in this form:

$$\mathrm{q_t} = \frac{\mathrm{t}}{\frac{1}{\mathrm{k_2} q_e^2} + \frac{\mathrm{t}}{\mathrm{q_e}}} \tag{6.7}$$

Further rearrangement of Eq. 6.7 can be made:

$$\mathrm{q_t} = \frac{k_2 q_e^2 t}{1 + \mathrm{k_2} q_e t} \tag{6.8}$$

Appendix B Determination of fluoride example calculation

In this section, an example calculation of standard addition method is provided. An example calculation of standard addition method is provided. Previously, a test sample containing 5 mg/L of fluoride was measured with the potential of 55.6 and 38.0 mV in E_1 and E_2, respectively. E_1 represents the initial potential measured in the 25 mL of solution, diluted with 5 mL of 5 mg/L fluoride test sample, 5 mL of TISAB IV, and the rest 15 mL with DI water. E_2 represents the updated potential with the addition of 0.25 mL of 100 mg/L fluoride into the 25 mL of solution. As discussed in the description for the fluoride measurement in Experimental methods section, the amount of a known addition of standard solution is 1 vol% of the original solution to minimize the change in the ionic strength and overall condition of the solution. In addition, the moles of added analyte is 50 – 200% of the original analyte in solution being analyzed to have a sufficient degree of change in the potential reading. Two obtained Nernst equations are shown below. In the calculation, a Nernstian response is assumed with the measurement.

$$\mathrm{E} = \mathrm{E}^\circ - \left(\frac{2.303\mathrm{RT}}{\mathrm{nF}}\right)\log\left[\mathrm{F}^-\right]$$

$$\mathrm{E}_1 = 0.0556\ \mathrm{V} = \mathrm{E}^\circ - 0.05916\log\left(\frac{\mathrm{x\ mol\ F}^-}{0.025\ \mathrm{L}}\right)$$

$$\mathrm{E}_2 = 0.038\ \mathrm{V} = \mathrm{E}^\circ - 0.05916\log\left(\frac{\mathrm{x\ mol\ F}^- + 100 * 10^{-3}\frac{\mathrm{g}}{\mathrm{L}} * 0.00025\ \mathrm{L} * \frac{1\ \mathrm{mol\ of\ F}^-}{19\ \mathrm{g}}}{0.025\ \mathrm{L} + 0.00025\ \mathrm{L}}\right)$$

This allows to solve for x mole of F^- originally presented in the initial 25 mL sample solution by subtracting E_1 from E_2, where x is calculated to be $1.31*10^{-6}$ mole of F^-. It is then used to determine the concentration of fluoride presented in the initial 5 mL test sample, as shown below.

$$\text{Initial } [F^-] \text{ in test sample} = \frac{1.31 * 10^{-6} \text{ mole}}{0.005 \text{ L of test sample}} * \frac{19 \text{ g}}{1 \text{ mole of } F^-} * \frac{1000 \text{ mg}}{1 \text{ g}}$$

$$= 4.98 \frac{\text{mg}}{\text{L}} \text{ of } F^-$$

This calculation step is used throughout the standard addition method in this report. Results can be more accurate if the effects of several additions of standards are averaged.

Appendix C Procedure for non-linear least square (NLLS) error analysis

The procedure for NLLS error analysis is explained in details by Ho et al. [73]. The error functions employed in this study were outlined in **Section 2.4.8**. The normalization and combination of all the error functions were conducted to produce 'sum of the normalized error'. The calculation methods for this process are as follows:

1) Select one isotherm model and one error function to determine the isotherm parameters
2) By using excel Solver, minimize the error function and produce the isotherm parameters for that specific error function
3) Calculate all the other error functions by using the isotherm parameters obtained
4) Repeat the step 1-3 with each error functions and obtain 5 by 5 matrix of error functions values
5) Calculate the 'sum of the normalized errors' for each parameter set

Appendix D Error functions and isotherm parameters for the batch isotherms

Table A. 1 Non-linear least square (NLLS) analysis of Langmuir model for Ca^{2+} and Mg^{2+} equilibrium isotherm profiles in 0 , 12 and 24 wt.% Na_2SO_4 solution with Lewatit Monoplus TP 260 resin. Minimum error values are indicated with bold numbers. (303 K; Initial conc. ~150 ppm Ca^{2+} and Mg^{2+}; pH 7)

Calcium						Magnesium					
	SSE	HYBRID	ARE	MPSD	EABS		SSE	HYBRID	ARE	MPSD	EABS
	Langmuir - 0 wt.% Na_2SO_4						***Langmuir - 0 wt.% Na_2SO_4***				
SSE	**5376.9**	6534.8	7489.1		5734.7	SSE	6904.1	6904.1	6907.1	6904.5	6907.3
HYBRID	843.5	**669.6**	802.8		785.6	HYBRID	1320.1	**1320.1**	1320.4	1320.2	1320.5
ARE	50.3	39.1	**38.0**		43.4	ARE	67.1	67.1	**67.2**	67.1	67.2
MPSD						MPSD	0.8	0.8	0.8	**0.8**	0.8
EABS	301.6	302.9	290.0		**270.4**	EABS	334.0	334.1	334.9	334.2	**334.9**
SNE	3.7	3.4	3.7		**3.5**	SNE	**5.0**	5.0	5.0	5.0	5.0
q_m (g^1kg^{-1} resin)	42.1	29.2	53.9		**53.7**	q_m (g^1kg^{-1} resin)	**36.1**	36.0	36.4	36.1	36.4
K_L (L^1mg^{-1})	7.63	11.37	1.32		**3.13**	K_L (L^1mg^{-1})	**417.60**	923.70	3.99	29.16	3.80
	Langmuir - 12 wt.% Na_2SO_4						***Langmuir - 12 wt.% Na_2SO_4***				
SSE	**347.5**	377.8	358.9	607.8	363.0	SSE	**42.6**	45.1	54.8	52.8	44.2
HYBRID	80.5	**76.1**	88.0	88.7	90.0	HYBRID	9.4	**8.8**	9.6	9.4	9.2
ARE	15.0	15.9	**14.8**	16.7	14.8	ARE	5.9	5.5	**5.4**	5.5	5.6
MPSD	0.2	0.2	0.3	**0.2**	0.3	MPSD	0.1	0.1	0.1	**0.1**	0.1
EABS	78.8	91.1	74.5	110.4	**73.5**	EABS	27.9	27.3	28.4	28.7	**27.0**
SNE	**4.0**	4.1	4.1	4.8	4.2	SNE	4.7	**4.5**	4.8	4.7	4.6
q_m (g^1kg^{-1} resin)	**44.1**	42.2	44.5	38.3	45.0	q_m (g^1kg^{-1} resin)	27.5	**26.9**	26.1	23.8	27.0
K_L (L^1mg^{-1})	**0.43**	0.52	0.39	0.72	0.37	K_L (L^1mg^{-1})	0.21	**0.23**	0.25	0.32	0.22
	Langmuir - 24 wt.% Na_2SO_4						***Langmuir - 24 wt.% Na_2SO_4***				
SSE	**94.7**	102.9	95.2	141.0	105.0	SSE	**65.3**	68.3	70.8	78.3	68.5
HYBRID	24.9	**23.4**	25.6	25.8	30.9	HYBRID	15.9	**15.3**	16.1	16.0	16.5
ARE	8.2	8.5	**8.1**	9.0	8.5	ARE	7.6	7.3	**7.1**	7.3	7.2
MPSD	0.1	0.1	0.1	**0.1**	0.2	MPSD	0.1	0.1	0.1	**0.1**	0.1
EABS	38.1	43.1	37.5	50.4	**36.6**	EABS	31.4	31.1	30.2	32.1	**29.8**
SNE	**4.0**	4.1	4.0	4.6	4.4	SNE	4.8	**4.7**	4.7	4.8	4.8
q_m (g^1kg^{-1} resin)	**33.6**	42.2	33.6	30.5	34.4	q_m (g^1kg^{-1} resin)	24.6	**23.5**	23.6	22.5	24.2
K_L (L^1mg^{-1})	**0.19**	0.52	0.19	0.27	0.16	K_L (L^1mg^{-1})	0.08	**0.09**	0.09	0.11	0.08

Table A. 2 Non-linear least square (NLLS) analysis of Langmuir model for Al^{3+} and Zr^{4+} equilibrium isotherm profiles in 0 - 24 wt.% Na_2SO_4 solution with Lewatit Monoplus TP 260 resin. Minimum error values are indicated with bold numbers. (303 K; Initial conc. ~150 ppm Al^{3+} and Zr^{4+}; pH 2.5 for Al^{3+} and pH 1.5 for Zr^{4+})

Aluminum						Zirconium					
	SSE	HYBRID	ARE	MPSD	EABS		SSE	HYBRID	ARE	MPSD	EABS
	Langmuir - 3 wt.% Na_2SO_4						***Langmuir - 0 wt.% Na_2SO_4***				
SSE	**348.8**	354.8	353.9	371.7	361.9	SSE	25.5	25.9	32.4	26.6	32.4
HYBRID	179.4	**177.2**	178.1	178.8	190.8	HYBRID	7.0	**6.9**	8.2	7.0	8.2
ARE	19.5	19.4	**19.4**	19.9	19.0	ARE	4.2	3.7	**3.3**	3.5	3.3
MPSD	0.4	0.4	0.4	**0.4**	0.4	MPSD	0.1	0.0	0.1	**0.0**	0.1
EABS	52.8	54.2	53.6	58.0	**50.1**	EABS	15.4	14.3	13.3	13.9	**13.3**
SNE	**4.73**	4.75	4.74	4.89	4.79	SNE	4.64	4.41	4.65	**4.36**	4.65
q_m (g^1kg^{-1} resin)	**32.7**	32.0	32.8	31.2	32.8	q_m (g^1kg^{-1} resin)	29.3	29.1	28.2	**28.9**	28.2
K_L (L^1mg^{-1})	**2.330**	2.871	1.668	3.304	1.668	K_L (L^1mg^{-1})	0.415	0.431	0.460	**0.442**	0.460
	Langmuir - 6 wt.% Na_2SO_4						***Langmuir - 6 wt.% Na_2SO_4***				
SSE	**71.0**	73.5	71.5	86.8	71.5	SSE	**94.4**	96.9	114.4	106.6	115.5
HYBRID	37.5	**36.6**	38.6	38.5	38.6	HYBRID	44.1	**43.2**	54.2	44.5	57.2
ARE	7.7	8.9	**7.4**	10.7	7.4	ARE	10.3	10.5	**8.9**	11.1	9.7
MPSD	0.2	0.2	0.2	**0.2**	0.2	MPSD	0.2	0.2	0.2	**0.2**	0.2
EABS	20.8	24.6	19.7	31.6	**19.7**	EABS	27.5	29.0	23.4	32.1	**23.1**
SNE	4.15	4.35	4.14	4.93	**4.14**	SNE	**4.23**	4.27	4.41	4.52	4.59
q_m (g^1kg^{-1} resin)	28.1	27.7	28.2	26.9	**28.2**	q_m (g^1kg^{-1} resin)	**24.1**	23.6	25.7	23.0	25.6
K_L (L^1mg^{-1})	1.515	1.755	1.420	2.135	**1.420**	K_L (L^1mg^{-1})	**0.387**	0.385	0.285	0.391	0.373
	Langmuir - 12 wt.% Na_2SO_4						***Langmuir - 12 wt.% Na_2SO_4***				
SSE	**38.7**	39.7	39.9	42.6	40.0	SSE	**128.8**	130.2	145.7	132.7	145.7
HYBRID	13.4	**13.0**	13.9	13.4	13.9	HYBRID	29.2	**28.8**	31.4	29.0	31.4
ARE	6.0	5.8	**5.8**	5.9	5.8	ARE	6.7	6.0	**4.6**	5.5	4.6
MPSD	0.1	0.1	0.1	**0.1**	0.1	MPSD	0.1	0.1	0.1	**0.1**	0.1
EABS	18.6	18.5	18.0	19.3	**18.0**	EABS	26.0	23.6	18.6	21.9	**18.6**
SNE	4.80	**4.72**	4.83	4.85	4.85	SNE	4.81	4.59	**4.40**	4.48	4.40
q_m (g^1kg^{-1} resin)	27.0	**26.7**	26.7	26.4	26.8	q_m (g^1kg^{-1} resin)	27.9	27.5	**26.4**	27.2	26.4
K_L (L^1mg^{-1})	0.511	**0.554**	0.499	0.596	0.497	K_L (L^1mg^{-1})	0.337	0.349	**0.370**	0.352	0.370
	Langmuir - 24 wt.% Na_2SO_4						***Langmuir - 24 wt.% Na_2SO_4***				
SSE	**19.8**	20.0	21.1	20.5	20.9	SSE	**191.5**	199.2	260.9	215.4	224.4
HYBRID	6.4	**6.4**	6.7	6.4	6.5	HYBRID	43.6	**41.1**	49.3	42.3	43.5
ARE	3.6	3.5	**3.4**	3.5	3.5	ARE	9.7	8.3	**7.5**	7.8	7.6
MPSD	0.1	0.1	0.1	**0.1**	0.1	MPSD	0.1	0.1	0.1	**0.1**	0.1
EABS	11.8	11.4	11.0	11.4	**11.3**	EABS	39.0	36.7	36.7	36.0	**35.5**
SNE	4.88	**4.81**	4.87	4.83	4.84	SNE	4.62	4.29	4.64	**4.29**	4.33
q_m (g^1kg^{-1} resin)	26.4	**26.3**	26.0	26.1	26.0	q_m (g^1kg^{-1} resin)	36.1	34.8	32.3	**33.9**	33.5
K_L (L^1mg^{-1})	0.272	**0.282**	0.275	0.290	0.289	K_L (L^1mg^{-1})	0.179	0.208	0.259	**0.228**	0.225

Table A. 3 Non-linear least square (NLLS) analysis of D-R and Langmuir model for F^- equilibrium isotherm profiles in 6 - 24 wt.% Na_2SO_4 solution with Al^{3+} and Zr^{4+} pre-loaded Lewatit Monoplus TP 260 resin. Minimum error values are indicated with bold numbers. (303 K; Initial conc. ~25 ppm F^-; pH 7)

Fluoride on Al pre-loaded resin						Fluoride on Zr pre-loaded resin					
	SSE	HYBRID	ARE	MPSD	EABS		SSE	HYBRID	ARE	MPSD	EABS
	Dubinin-Radushkevich - 6 wt.% Na_2SO_4						*Langmuir - 6 wt.% Na_2SO_4*				
SSE	**12.0**	14.3	15.1	14.3	12.1	SSE	6.1	6.7	9.0	7.8	8.3
HYBRID	6.7	**5.0**	5.2	5.0	7.1	HYBRID	8.0	**7.0**	8.5	7.5	7.9
ARE	8.5	6.0	**5.8**	6.0	8.8	ARE	9.4	8.3	**7.1**	7.6	7.4
MPSD	0.3	0.2	0.2	**0.2**	0.3	MPSD	0.1	0.1	0.1	**0.1**	0.1
EABS	13.5	15.6	16.1	15.6	**13.4**	EABS	8.1	8.2	8.4	8.3	**8.2**
SNE	4.52	**4.15**	4.27	4.15	4.64	SNE	4.58	**4.22**	4.55	4.29	4.40
q_m (g^1kg^{-1} resin)	23.8	**24.5**	24.2	24.5	23.7	q_m (g^1kg^{-1} resin)	12.6	**12.9**	13.1	13.1	12.8
B *10^{-7}	0.760	**0.809**	0.812	0.809	0.754	K_L (L^1mg^{-1})	0.473	**0.417**	0.360	0.381	0.388
	Dubinin-Radushkevich - 12 wt.% Na_2SO_4						*Langmuir - 12 wt.% Na_2SO_4*				
SSE	**16.5**	18.3	26.6	18.3	20.4	SSE	**6.4**	7.3	11.5	9.3	7.7
HYBRID	7.1	**5.6**	7.0	5.6	6.0	HYBRID	7.8	**6.6**	9.0	7.4	12.9
ARE	8.6	5.6	**4.8**	5.6	5.6	ARE	10.1	8.7	**7.9**	8.2	12.0
MPSD	0.3	0.2	0.3	**0.2**	0.2	MPSD	0.1	0.1	0.1	**0.1**	0.2
EABS	16.0	14.6	14.9	14.6	**14.2**	EABS	9.2	9.5	10.8	10.2	**9.1**
SNE	5.23	**4.35**	4.86	4.35	4.49	SNE	3.58	**3.31**	3.90	3.52	4.51
q_m (g^1kg^{-1} resin)	24.0	**24.7**	26.1	24.5	25.3	q_m (g^1kg^{-1} resin)	13.0	**13.3**	13.8	13.6	12.7
B *10^{-7}	0.996	**1.058**	1.108	0.809	1.067	K_L (L^1mg^{-1})	0.477	**0.416**	0.340	0.370	0.561
	Dubinin-Radushkevich - 24 wt.% Na_2SO_4						*Langmuir - 24 wt.% Na_2SO_4*				
SSE	**15.5**	17.5	23.7	17.5	22.9	SSE	**4.3**	4.6	5.2	5.3	4.7
HYBRID	7.2	**5.6**	6.7	5.6	6.6	HYBRID	5.1	**4.6**	4.8	4.9	4.7
ARE	8.8	5.9	**5.2**	5.9	5.4	ARE	7.4	6.3	**6.0**	6.1	6.3
MPSD	0.3	0.2	0.3	**0.2**	0.3	MPSD	0.1	0.1	0.1	**0.1**	0.1
EABS	16.5	15.2	13.4	15.2	**13.4**	EABS	7.1	6.9	6.9	7.0	**6.7**
SNE	5.32	**4.49**	4.77	4.49	4.74	SNE	4.80	**4.42**	4.48	4.56	4.43
q_m (g^1kg^{-1} resin)	25.2	**26.0**	27.3	26.0	27.2	q_m (g^1kg^{-1} resin)	13.6	**13.7**	14.0	14.0	13.9
B *10^{-7}	1.199	**1.275**	1.315	1.275	1.304	K_L (L^1mg^{-1})	0.452	**0.346**	0.321	0.317	0.343

Table A. 4 Non-linear least square (NLLS) analysis of D-R and Langmuir model for F^- equilibrium isotherm profiles in temperature of 303 – 333 K with Al^{3+} and Zr^{4+} pre-loaded Lewatit Monoplus TP 260 resin. Minimum error values are indicated with bold numbers. (12 wt.% Na_2SO_4; Initial conc. ~25 ppm F^-; pH 7)

Aluminum						Zirconium					
	SSE	HYBRID	ARE	MPSD	EABS		SSE	HYBRID	ARE	MPSD	EABS
	Dubinin-Radushkevich - 30◦C						***Langmuir - 30◦C***				
SSE	**16.5**	18.3	26.6	18.3	20.4	SSE	6.4	7.3	11.5	9.3	7.7
HYBRID	7.061627	**5.6**	7.0	5.6	6.0	HYBRID	7.8	**6.6**	9.0	7.4	12.9
ARE	8.6	5.6	**4.8**	5.6	5.6	ARE	10.1	8.7	**7.9**	8.2	12.0
MPSD	0.3	0.2	0.3	**0.2**	0.2	MPSD	0.1	0.1	0.1	**0.1**	0.2
EABS	16.0	14.6	14.9	14.6	**14.2**	EABS	9.2	9.5	10.8	10.2	**9.1**
SNE	5.23	**4.35**	4.86	4.35	4.49	SNE	3.58	**3.31**	3.90	3.52	4.51
q_m (g^1kg^{-1} resin)	24.0	**24.7**	26.1	24.5	25.3	q_m (g^1kg^{-1} resin)	13.0	**13.3**	13.8	13.6	12.7
B $*10^{-7}$	0.996	**1.058**	1.108	0.809	1.067	K_L (L^1mg^{-1})	0.477	**0.416**	0.340	0.370	0.561
	Dubinin-Radushkevich - 45◦C						***Langmuir - 45◦C***				
SSE	**7.7**	8.7	10.1	8.7	8.6	SSE	**1.4**	1.4	1.5	1.5	1.4
HYBRID	3.7	**2.9**	3.1	2.9	3.1	HYBRID	1.8	**1.7**	1.9	1.8	2.1
ARE	5.9	4.2	**3.9**	4.2	4.5	ARE	4.5	4.5	**4.5**	4.6	4.7
MPSD	0.2	0.2	0.2	**0.2**	0.2	MPSD	0.1	0.1	0.1	**0.1**	0.1
EABS	10.7	9.6	9.9	9.6	**9.3**	EABS	3.9	4.1	3.9	4.3	**3.9**
SNE	5.42	**4.16**	4.36	4.16	4.23	SNE	4.50	**4.47**	4.59	4.61	4.84
q_m (g^1kg^{-1} resin)	21.9	**22.3**	22.7	22.3	22.4	q_m (g^1kg^{-1} resin)	9.3	**9.4**	9.4	9.4	9.2
B $*10^{-7}$	0.551	**0.577**	0.591	0.577	0.570	K_L (L^1mg^{-1})	0.588	**0.558**	0.579	0.534	0.623
	Dubinin-Radushkevich - 60◦C						***Langmuir - 60◦C***				
SSE						SSE	**11.8**	12.3	12.5	13.5	14.3
HYBRID						HYBRID	18.1	**17.5**	17.6	18.1	23.4
ARE						ARE	14.4	13.7	**13.5**	13.9	14.3
MPSD						MPSD	0.2	0.2	0.2	**0.2**	0.2
EABS						EABS	10.9	10.8	10.8	11.4	**10.7**
SNE						SNE	4.43	4.33	**4.33**	4.49	4.93
q_m (g^1kg^{-1} resin)						q_m (g^1kg^{-1} resin)	6.3	6.2	**6.2**	6.0	7.0
B $*10^{-7}$						K_L (L^1mg^{-1})	0.863	0.844	**0.699**	0.846	0.607